

March 2012 - Vol:2 No:1

# International JOURNAL of SEWVC

— Structural Engineers World Congress —





# HISTORY OF STRUCTURAL ENGINEERS WORLD CONGRESS Inc. ( SEWC Inc.)

Here are a few important points taken from the paper on “ Structural Engineers World Congress Idea to Reality” by Roland L. Sharpe, Founding President SEWC Inc.

Informal discussions in the mid 1980s between U.S. and Japanese structural engineers and researchers raised questions about the role of the structural engineer, required capabilities, and how the SE public image could be improved. Further informal meetings and mail correspondence over several years examined in some detail how this interaction could best be accomplished. These interactions led to small meetings at American Society of Civil Engineers (ASCE) Congresses in the U.S. which culminated in 1994 when six professional organizations agreed to form a coalition to sponsor and organize the first Structural Engineers World Congress (July 18 to 23, 1998) in San Francisco.

Recognition of the need for a worldwide SE Congress, need for interaction between SEs worldwide, scope and impact of SE services and effects on society, the need to improve the image and credibility of the SE grew over the next few years.

## **Range of SE Activities**

Although several international organizations exist that serve structural engineers needs in specific areas such as bridges and buildings (IABCE), tall buildings, earthquake engineering, they do not serve many aspects of SE concerns. A consensus developed in the Task Committee that the WSC should include the full range of SE issues - technical, professional, ethics, education, legal, construction, products, and other related issues. There should be exhibits along with

sessions on these topics. It also became apparent that the WSC should be “people” oriented with the theme of getting to know each other better. It was estimated that there are about 50,000 structural engineers in the U.S. and perhaps 200,000 or more in the world.

The question of who is a structural engineer was examined. As noted previously, in Japan civil engineers design bridges and other structures associated with infrastructure and mostly work for the government. This appears to be true for some other countries. It was recommended that all engineers designing and constructing structures are considered structural engineers and should be included in WSC. The Committee felt strongly that the WSC should not become a membership organization and should not compete with existing international SE organizations.

In the 1998 congress in San Francisco, there were about 1800 participants from 49 different countries. A large number of exhibitors presented their products. Subsequently in 2002, it was held in Yokohama, Japan and in 2007 in Bangalore, India. Each of the congresses in Japan and India attracted more than 1300 delegates.

The Structural Engineering World Congress (SEWC) is dedicated to the Art, Science and Practice of Structural Engineering. SEWC Congress brings all the structural engineers on a common platform at-least once in 4 years

SEWC presents excellent opportunities for Structural Engineering professionals to interact with each other and to learn more about what is happening in the World of Structural Engineering now and about the trends for the future.

Founding Member Organisations	<b>2</b>
SEWC Board Members	<b>2</b>
Editorial Board	<b>2</b>
Members	<b>2</b>
Guidelines to Authors	<b>2</b>
President's Message	<b>3</b>
Editorial	<b>4</b>

---

## Journal Section

---

- 5** Our Fifty Year Experience in Shell Design  
Giuliani Gian Carlo and Giuliani Mauro Eugenio
- 12** Structural Design and Construction of Diagrids for Complex-shaped Tall Buildings  
Kyoung Sun Moon
- 17** Dynamic Elasto-plastic Time-history Analysis for Out-of-codes High-rise Structure  
Wanli Xue
- 22** An Overview on Diagrid Structures for Tall Buildings  
Maurizio Toreno, Raffaele Arpino, Elena Mele, Giuseppe Brandonisio and Antonello De Luca
- 29** Development of Typical Ceiling System Seismic Fragilities  
Giacomo Paganotti, Rajesh P. Dhakal and Gregory A. MacRae
- 34** On the Accuracy of Response Spectrum Analysis in Seismic Design of Concrete Structures  
Fabio Biondini, Andrea Titi and Giandomenico Toniolo
- 42** Stainless Steel: A Structural Anti-seismic and Fire Resistant Material  
V. Boneschi
- 47** Numerical Study on the Seismic Interaction between 2D Seismic Resisting Frames and Claddings  
Riccardo Diaferia, Andrew Baird, Stefano Pampanin and Alessandro Palermo
- 56** Testing of Recycled Aggregate Concrete by Non-Destructive Tests  
M. Chakrathara Rao, S.K. Bhattacharyya and S.V. Barai

---

## Magazine Section

---

- 63** The Spanish Fortress in l'Aquila: Emergency Actions, Investigations and Monitoring  
F. Casarin, F. Lorenzoni, L. Cantini, S. Munda, L. Binda, C. Modena, R. Ciabattoni and C. Cacace
- 71** News
- 77** Events

Published by: Vidyashankar Hoskere on behalf of SEWC Society, INSTRUCT, 1st Floor, UVCE Alumni Association Building, K.R. Circle, Bangalore - 560 001. Email: sewcsociety@gmail.com. Designed and Printed by: 'The Masterbuilder', 102/11, Tripti Apartments, Marshalls Road, Egmore, Chennai - 600 008, Tamil Nadu, India. Email: editor@masterbuilder.co.in

Disclaimer: All rights reserved. Reproduction in whole or part without prior written permission prohibited.  
The views expressed in this journal are those of the authors and do not reflect those of the publisher.

# Founding Member Organisations



American Concrete Institute



International Association of Shell and Spatial Structures



Japan Structural Consultants Association

**NCSEA**

National Council of Structural Engineers Associations



Structural Engineering Institute of ASCE

**SEAOC**

Structural Engineers Association of California

## Editorial Board



### Raghu Prasad B.K

Editor-in-Chief  
Advisor, Indian Institute of Science, Bangalore,  
Prof. [Retd.], Dept. of Civil Engg.,  
Indian Institute of Science, Bangalore  
SEWC India G.C. Member



### Pradeep K.P

Editor  
SEWC India G.C. Member  
Editor-in-Chief, The Masterbuilder,  
Secretary: ASCE IS Southern Region.  
ICI GC Member

## Members

### Qilin Zhang, China

Prof. of Civil Engineering, Tongji University, Shanghai, China.

### Airong CHEN, China

Bridge Engineering, Tongji University, China.

### Gorun Arun, Turkey

Architecture Faculty, Yildiz Technical University, Istanbul, Turkey.  
On the Editorial Board of International Journal of Architectural Heritage.  
Chair, IASS Working Group WG 17 Historical Structures of International Association for Shell & Spatial Structures.

### Rene Motro, France

Editor : International Journal of Space Structures, Universite Montpellier 2, France.  
International Association for Shell & Spatial Structures.

### Mehrotra S.C, India

He is a founder member and fellow member of Indian Association of Structural Engineers. He is the first Indian and first South Asian Elected as Executive Committee member of FIDIC (International Federation of Consulting Engineers) for the period of 2005-2009.

### Manamohan R Kalgal, India

SEWC India G.C. Member,  
Actively associated with Association of Consulting Civil Engineers, India,  
Indian Concrete Institute etc.

### Ron E. Shaeffer, USA

Member - Tensioned Fabric Structures Task Committee of ASCE. Secretary Air Supported Structures Standards of SEI Codes & Standards Activities Division Executive Committee of ASCE.

## Guidelines to Authors

Contributions resulting from original research in the area of structural Engineering, analysis, design, structural materials and other related topics in the form of technical papers to be published in the International Journal of Structural Engineers World Congress (SEWC) are welcome.

Prospective authors are free to prepare the manuscripts in their own convenient format and

submit in MS Word file. The publisher will modify the format according to the standard format of the journal before printing.

The authors are requested to particularly not to miss mentioning the page number of the paper / book in the list of reference.

The manuscript submitted will be peer reviewed and the comment will be made known to the author.

# SEWC Board Members

### Sundaram R, India

President- Structural Engineers World Congress (SEWC) - India  
Chairman & Managing Director,  
Sundaram Architects Pvt. Ltd  
Advisory Board Member - IASS  
No. 19, Kumarakrupa Road,  
Bangalore - 560 001. INDIA  
Email : edp@sundaramarchitects.com

### Roland L Sharpe, USA

Immediate Past Founding President  
Founder President of the Structural Engineers World Congress ( SEWC)  
Consultant with Stanford Linear Accelerator Center,  
R. Sharpe Consulting Engineers, 10320 Rolly Road, STE-1, Los Altos Hill, California, USA  
Email : rsharpe3@mindspring.com

### Narendra K Srivastava, Canada

Working Vice President  
Member of International Journal Editorial Boards,  
Vice President of the IASS  
Adjunct Research Professor at the University of Waterloo, Canada  
Email : srivasn@gmail.com

### Enzo Siviero, Italy

Working Vice President  
Prof.eng., structural consulting engineer in Padova  
Teacher Bridge Theory and Design at IUAV University in Venice  
Vice President, National University Council - Civil Engineering and Architecture PROGEEST Srl  
Via E. degli Scrovegni, 29, 35131 - Padova Italy  
Email : enzo.siviero@progeest.com

### Toshio Okoshi, Japan

Vice President  
Past president of the Japan Structural Consultants Association, a technical adviser in Nihon Sekkei and a Professor in Waseda University.  
Member of ASCE, IABSE, JIA, JCI and JSSC  
Email : okoshi\_t@ion.ocn.ne.jp

### James R. Cagley

Principal, Cagley & Associates Inc.  
6141 Executive Blvd, Rockville, MD 20852  
Email : Jim@cagley.com

### A. H-S. Ang, USA

Research Professor, University of California, Irvine, Email : Ahang2@aol.com

### Sung Pil Chang, South Korea

Email: spchang@snu.ac.kr

### Gian Carlo Giuliani, Italy

Dr.eng, structural professional engineer in Milano Italy),  
Alberta (Canada) and Cyprus  
Advisory Board member IASS, fellow member ASCE, IABSE, Member ACI, fib, PCI, GLIS  
Email : gc.giuliani@redesco.it

### Prof. Jiemin DING, Shanghai, China

Head of Tongji Architectural Design and Research Institute,  
Tongji Architectural Design (Group) Co., Ltd.

# President's Message



**Sundaram R**

President Structural Engineers World Congress, Worldwide  
Member, Advisory Board, IASS

I am happy to inform you that the response received for the last two SEWC Journals is overwhelming. We are now releasing the third SEWC Journal.

We have to continue to ensure the overall quality of the publication.

The success of the last two SEWC Journals instils confidence in us to strive hard for covering many more subjects related to structural engineering, which will help disseminate knowledge and information among the structural engineering fraternity.

SEWC India is organising an International Colloquium in New Delhi on the subject on 'Architecture-Structure' Interaction during November 25-27, 2013 in New Delhi and many top-notch Architects and Structural Engineers from different parts of the world have already confirmed their participation to deliver Keynote speeches to share their knowledge.

My congratulations to Dr. B.K. Raghunath Prasad, Editor-in-Chief and Mr. K.P. Pradeep, Editor of the Journal of SEWC for bringing out this latest Journal on time.

# Editorial

**Prof. Raghu Prasad B.K**

Editor-in-Chief

**T**he Journal is stepping in to 3rd issue. The first two issues were well received. The first issue depended entirely on the articles presented at SEWC, Como, Italy. In due course, it is the hope of the publishers to receive as many papers as possible so that the Editorial Committee can go through and recommend for publication.

We have started issuing e-copies instead of the hard copies of the proceedings so that the papers can reach quickly all the readers.

SEWC Journal is getting recognized all over the world. We encourage many to send papers for publication in the SEWC Journal.

Our aim is to make it to reach and maintain international standards.

# Our Fifty Year Experience in Shell Design

**Giuliani Gian Carlo<sup>1</sup> and  
Giuliani Mauro Eugenio<sup>2</sup>**

## Summary

The concrete shells are nowadays seldom used because of the cost of the forms and of the labor which are necessary for the construction; at the date, the precasting, which could raise a new interest for these very efficient structures, is not taken in due consideration by the construction firms.

Some examples of these structures which were designed

by the authors along with the relevant precasting and erection system are illustrated, with the aim of disseminating the advantages of the precast shell solution

A selection of shells with double curvature (positive and negative), as well as barrel vaults, and folded plates units is illustrated and summarize a more 50 than year personal experience in this field.

JOB	SHAPE	PREFABRICATION	PRESTRESSING	CASTING	ASSEMBLING	ERECTION	UNIT DIMENSIONS
AERITALIA	barrel vault	in plant	pretensioning	wet concrete	on site * $\Delta$	lifting	30.00 by 30.00 m
ALFA ROMEO	barrel vault	on site	post-tensioning	wet concrete	no	hoisting	16.00 by 5.33 m
BORDIGHERA	conical	no	post-tensioning	wet concrete	no	direct casting $\Delta$	
BOX HOUSE	box	in plant	no	wet concrete	on site * $\Delta$	hoisting	-
FACTORY	folded plate	on site	pretensioning	shot crete	no	lifting	30.00 by 6.00 m
MALAGA TWR	folded plate	no	post-tensioning	wet concrete	no	direct casting	
PIO X	free form	no	no	shot crete	no	direct casting	-
PO BRIDGE	folded plate	on site	post-tensioning	shot crete	on site $\Delta$	launching	1120.00 by ....
SACE	folded plate	on site	pretensioning	wet concrete	on site * $\Delta$	lifting	20.00 by 20.00 m
SILO	conical	on site	post-tensioning	wet concrete	no	liftin g	d = 46.00 m
WAREHOUSES	velaroid	on site	pretensioning	wet concrete	no	lifting	16.00 by 16.00 m
					* = epoxy $\Delta$ = posttensioning		



The construction methods, which were studied and decided in the design step, range from in place casting by using shot crete to the on site and in factory prefabrication, on ground assembly and lifting to the final position.

In many cases pretension or posttension were used.

The methods of analysis which were used range from the manual solving of the shell theory equations to the use of structural models and finally to the finite elements techniques.

**Keywords**

Shells - Design - Construction - Erection

**1. General classification of the illustrated shells**

The characteristics of the shells can be defined by the shape, the size, the construction method and so on; in the following table the above said characteristics are enlisted in order to allow for an easy reference to the particular features of all the jobs which are illustrated.

**2. The shell roof for the Pio X church in Bolzano - Italy**

The roof is composed of four shells with negative curvatures which bear on contour walls leaning outwards; the shells intersect each other on space lines edges over the altar (figures 1-2)

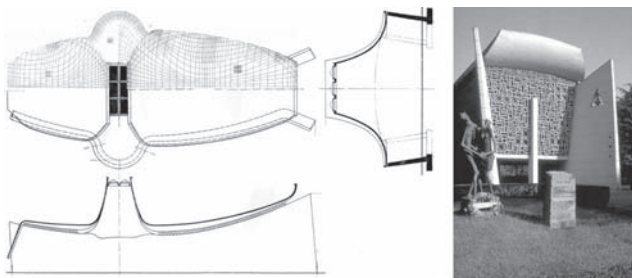


Figure 1. Plan and sections of the church (main reinforcement shown in the upper half of the plan) and the main facade



Figure 2. Outside and inside view of the church

The shell thickness of 8 cm in the middle is increased to 12 cm towards the edges. the main dimensions are 55.50 m in the longitudinal direction and 26.30 in the transversal one.

At the time of the design (1961) the structural analysis by means of finite elements was not available and therefore a model was used, mainly to detect the stresses on the shell edges, while for the inner parts the general shell theory was

used for checking the reliability of the results obtained from the model.

Double welded meshes were used as general reinforcement while additional rebars were added where necessary for resisting the membrane stresses; these bars were given a pattern following in an approximate way the principal directions of the tensile stresses.

Because of the steep surfaces of the shells, the shot-crete technique was selected as the method of casting.

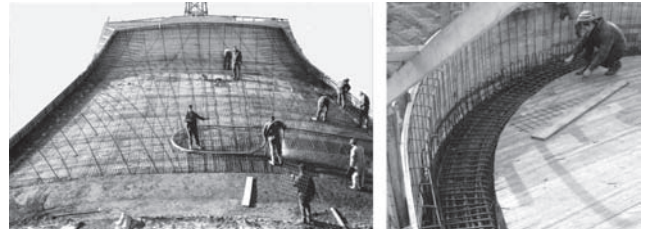


Figure 3. Shot-crete being applied over the reinforcing meshes and bars and a detail of the edge reinforcement

**3. The roof over the hall of Hotel del Mare in Bordighera - Italy**

The roof is composed of a truncated cone shell which features a crown hole and bears a garden on top; a post-tensioned ring beam supports the shells and restrains the horizontal forces which are transmitted by means of 36 horizontal steel hinges thus eliminating bending moments on the shell edge.

Slender and sculptured steel columns with a hinge at mid height transfer the loads to the foundations.

The outer diameter is 25.90 m, while the one of the crown hole is 8.00 m

The lower surface of the shell is ribbed in order to better resist the radial bending moments (figure 4); the thickness ranges from 16 cm to 8 cm in the valleys and from 36 cm to 16 cm in the ridges.

The structural analysis was performed according to the shell theory, taking into account the compliance of the radial deformations of the shell and the ring beam.

The structure was cast in place over a wood form which was prepared for obtaining a pleasant finishing of the concrete which remains in sight.

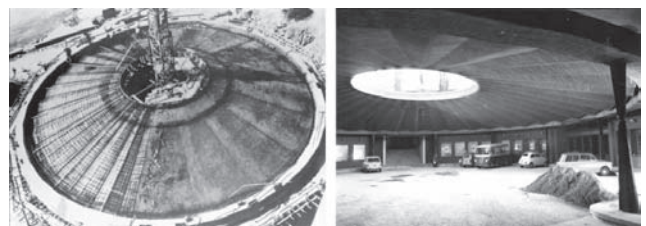


Figure 4. Outer and inner view of the shell



#### 4. North light shells for the Alfa Romeo car factory in Arese - Italy

These shells were designed for on site prefabrication to cover the car assembly building on columns grid lines located at 16.00 centers in both directions.

The plan dimensions of each shell are 14.80 m by 5,33m, while the thickness is 6 cm with an increasing to 14 cm at the longitudinal edges; a lower valley beam and an upper rib add stiffness to the shell.

End diaphragms laying along the shorter dimension close the pattern of the membrane actions and transfer the vertical loads to a box beam, precast also.

Longitudinal prestress was used to resist the longitudinal tensile stresses and, thanks to the relevant curvilinear pattern to reduce the bending moments acting in the radial direction of the shell.

In addition to the dead and the live loads, the shells were design to support the load of 10.0 kN/m transferred by the suspensions of the assembly devices.



Figure 5. View of the construction of the assembly building

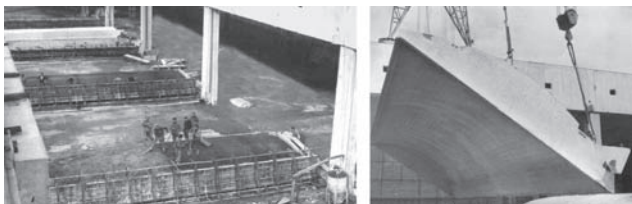


Figure 5. Casting of the shells and hoisting by means of a gantry crane moving over the box beams

The structural analysis was performed according to the barrel vault theory taking into account the compliance of the displacements of the longitudinal edges of the shell with the ones of the stiffening rib and valley beam.

The box beams were prefabricated also in two halves which

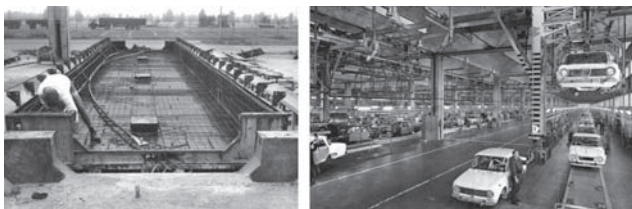


Figure 5. Formwork and reinforcement of an half of the box beam and an internal view of the building

feature a folded plate shell behavior; post tensioned cables allowed for the balance of all the tensile stresses.

#### 5. Warehouses - precast shells for roofing 16m by 16m bays - several sites in Italy

These shells were designed for on site prefabrication to cover a warehouse with columns grid lines located at 16.00 centers in both directions.

The shell features a positive curvature with edge stiffening beams which were prestressed by strands provisionally anchored to the self stressing form.

The raise of the shell is 0.85 m and the thickness is 0.05 m only; the edge beams are 0.60 m. deep and 0.20 m wide

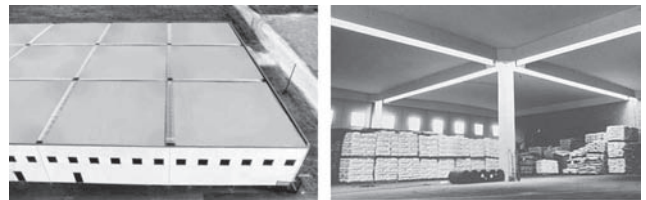


Figure 6. Outer and inner views of the shells

The unit was precast on site and lifted to the top of the columns by means of hydraulic jacks pulling strands anchored to the shell; the final connection was given by high grade tension bars.

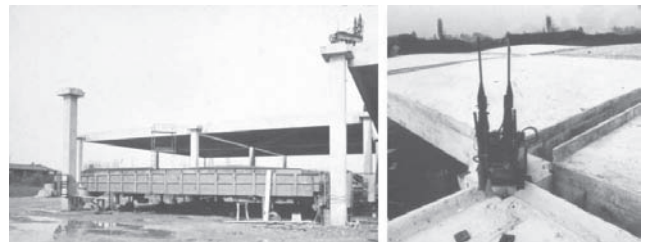


Figure 7. View of the construction site with self stressing form and a detail of the lifting equipment.

At the time of the design (1971) the structural analysis by means of finite elements was not available and therefore a model was used, mainly to detect the stresses on the shell edges, while for the inner parts the general shell theory was used for checking the reliability of the results obtained from the model.

The model allowed for the detection of the buckling also; the first mode was a complete reversal of the curvature; we were able to observe this change of shape, without collapse, for a shell which was exposed to a severe accidental fire.

By overloading the model and evaluating in a simplified way the reduction of the effective concrete modulus which can be produced by the long time effects of the concrete shrinkage and creep we approximately checked the safety factor of the shell against this kind of buckling.

## 6. Factories - precast pre stressed folded plate shells - several sites in Italy

These shells were designed for on site prefabrication to cover a factory with columns grid lines located at 24.00 m by 6.00 m centers; the wall thickness is 0.06m...

The folded plate shape was not prismatic but was adjusted by deforming the surfaces for achieving a longitudinal broken line shape which was very effective for exploiting the load bearing action of the straight line prestress.

The shells were precast on self stressing forms, moved by means of special carts and lifted at the top of the columns by means of hydraulic jacks pulling strands anchored to the shell; the final connection was given by high grade tension bars.



Figure 8. View of a factory under construction and of an unit being moved from the casting position

Many other shells of this kind were designed also for different lengths and widths and with slightly different shapes.

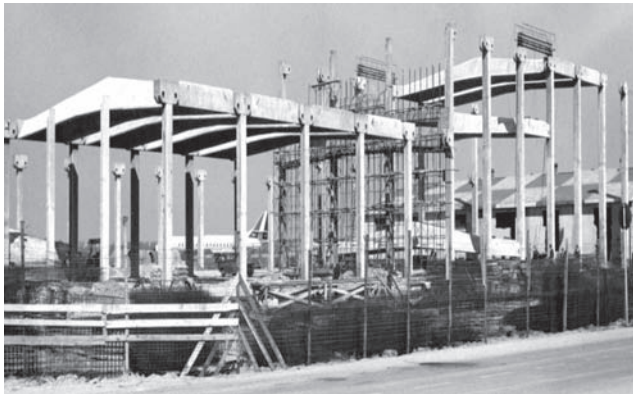


Figure 9. View of another factory under construction

The on site construction method was always the same; the inclined plates were cast with shotcrete.

The analysis was performed by using the plate theory for determining the influence displacement coefficients of the actions on the strip edges and finally by writing the relevant compliance equations which solve the problem.

We designed the ad hoc equipment for moving and hoisting the units also.

### 7. A 20m by 20 m roof unit for a factory in Dalmine. (Italy)

These units were designed for on site assembling of pre-



Figure 10. Views of the lifting equipment and of the use of the shotcrete

cast folded plates to cover several factory halls with columns grid lines located at 20.00 m centers in both directions.

The folded plates were on site precast and are built in with [shaped end diaphragms which constitute a segment of the unit main beam; pretensioned strands are located at both the longitudinal edges of the shell, inside stiffening ribs; the wall thickness is 0.06m.

A template was used for aligning the shells and grouting of the joints between the diaphragms was effected; strands were pulled inside the ducts left in the diaphragms and were post tensioned.

At the end, the unit was lifted at the top of the columns by means of hydraulic jacks pulling strands anchored to the main beam; the final connection was given by a strand cable.

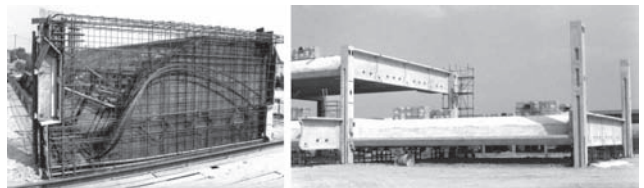


Figure 11. Views of the folded plate prefabricated cage and of the assembling and erection procedure



Figure 12. View of the connection at the top of the columns and of the factory bays

## 8. Prefabricated box houses (Region Friuli Venezia Giulia - Italy)

Two types of box units are used for construction of the two story houses; the end ones with three walls, and two floors, and the intermediate ones and the composed of with two walls, and two floors.

The walls feature a sandwich section which include the insulation in between the inner vertical load bearing panel and the outer architectural panel.



Both the floors are built in with the edge panels and therefore the structural behavior is the one of a 3D shell.

The analysis was performed by means of the general plate theory equations taking into account the common edge displacement compliance of the horizontal and the vertical panels.

The units are completely in factory prefabricated and equipped with all the wirings, the plumbing, partitions, doors, windows, floors and so on.

The on site assembling was performed by means of epoxy grouting and post-tensioning, allowing for a full seismic resistance of the completed house.

The whole system got the full approval of the French Body C.S.T.B.

Sun panels are applied to the South-West facades for producing hot water to be used in the house services and for the winter heating system

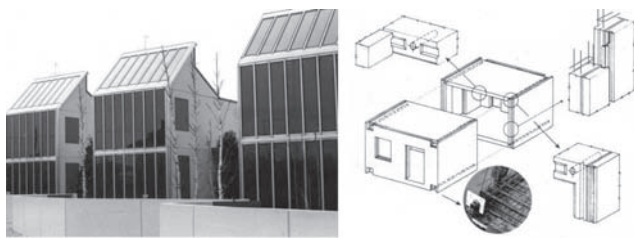


Figure 12 . View of a row of completed houses and scheme of the unit assembling



Figure 13. The form for the in the plan casting and the erection of an unit

### 9. Huge silos in Portoscuso (Italy)

N. 3 huge silos (diameter 42 m, height 36 m) with thin walls (0.25 m thick) which were pre stressed by means of circumferential cables; the thin shell roof (0.12-0.08 m thick) was cast at ground level inside the walls, pre stressed and lifted to the design height.

The analysis was performed by means of the general conical shell theory equations taking into account the common edge displacement compliance of the sequential elements.

### 10. A 30m by 30 m roof unit for the Aeritalia hangar in the Turin airport. (Italy)

These units were designed for on site assembling of pre-cast shells to cover an hangar with columns grid lines located at 30.00 m centers in both directions.

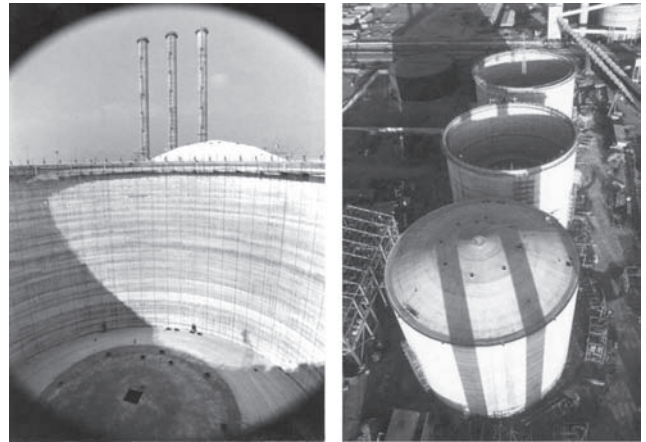


Figure 14. Views of the shell roof during the lifting and of the in progress construction of the silos

The shells were in factory precast and are built in with [shaped end diaphragms which constitute a segment of the unit main beam; pretensioned strands are located at both the longitudinal edges of the shell, inside stiffening ribs; the wall thickness is 0.06m.

A tilt casting position was selected for avoiding a double form; after the demoulding the shells were rotated in the final position and transported to the erection site.

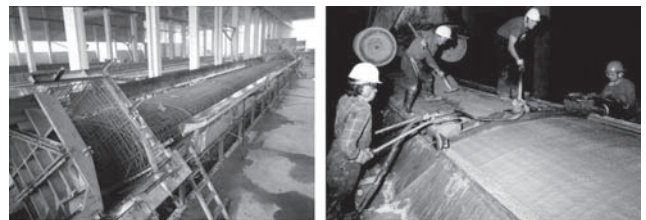


Figure 8. View of the reinforcement and of the casting of the shell in the factory



Figure 9. View of the demoulding and rotation of the shell and of the on site assembly of the roof unit

A template was used for aligning the shells and grouting of the joints between the diaphragms was effected; strands were pulled inside the ducts left in the diaphragms and were post tensioned.

At the end, the unit was lifted at the top of the columns by means of hydraulic jacks pulling strands anchored to the main beam; the final connection was given by a strand cable.

The rails of an overhead crane, capable of a 200 kN lift, were suspended from the main beams.

The preliminary analysis was performed according to the barrel vault theory taking into account the compliance of

the displacements of the longitudinal edges of the shell with the ones of the stiffening rib and valley beam; in order to evaluate the safety factor against buckling, a non linear finite element analysis was performed for the final design.



Figure 8. Inner and outer views of the hangar

### 11. Folded plate shells for the base building of the Malaga Airport control tower (Spain) and precast negative curvature shells for the shaft ribs (\*)

These shells constitute the two different level roof of the tower base service building; each shell is replicated 12 times following a circular symmetry around the vertical axe of the tower (figure 9).

The supports are constituted by vertical columns located on the polygonal inner edge and by X shaped struts on the outer edge; these struts are erected in an inclined position with the lower vertex connected to a spherical bearing.

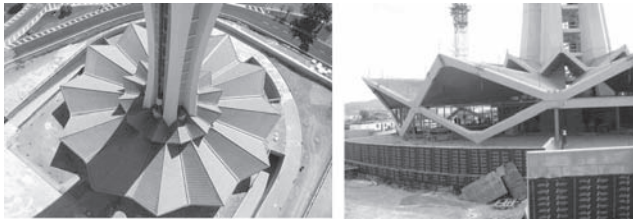


Figure 9. A bird's eye view of the completed shells and the facade X shaped struts

Because of the flat surfaces, the reinforcement was composed of a double welded wire mesh with additional rebars located close to the valleys and the ridges; at the connection of the upper and lower shells, where the contact surfaces are narrow, postensioned cables were used instead of the rebars.



Figure 10. Scaffolding and forms for the shells and inside view of a lower one with the ball bearing detail

Although the shells were designed for a segmental circular casting which required one formwork only, the construction firm had to proceed with a complete round scaffolding and form in order to reduce the construction time (figure (10)).

The shot-crete technique was used for the casting of the shells.

The X facade struts were constructed by jointing two pre-fabricated V shaped members by means of postensioned threaded bars.

The tower shaft has a strong visual impact and is composed of three-dimensional shell precast elements for the segments of the six wide body ribs which constitute the structure, supports the vertical loads and resist the seismic and the wind actions.

The above said shells were constructed by using the "matching concrete" technology (figure 11), i.e. casting each element in a form next to another already cast one, to allow for a "dry" joint erection with a thin layer of epoxy resin and reinforced by post-tensioned bars.

(\*) structural design by M.E. Giuliani architect B. Fairbanks



Figure 11. "Matching Concrete" casting technique for the ribs and element being hoisted

### 12. Folded plate girders for a bridge on the Po river (Italy)

The bridge features continuous pre stressed girders with an inverted omega folded plate section, to carry two pipelines and to contain and drain any oil leakage.

The spans are 36.00 m wide and the post-tensioned girders are continuous over 7 or 8 columns; the 1370 m long bridge was divided in 6 independent sections (figure 12).

For the erection system the self launching was selected; this bridge constitutes the first Italian example of the use of this technology.

Provisional front and rear steel gantries as well as additional, external post tensioning cables were used during the launching.

The casting of the inclined webs was performed by using shot-crete; reinforcing bars and post tensioning cables were used (figure 13).

The analysis was performed by using the plate theory for determining the influence displacement coefficients of the actions on the strip edges and finally by writing the relevant compliance equations which solve the problem.

We designed the ad hoc equipment for the bridge launching also.



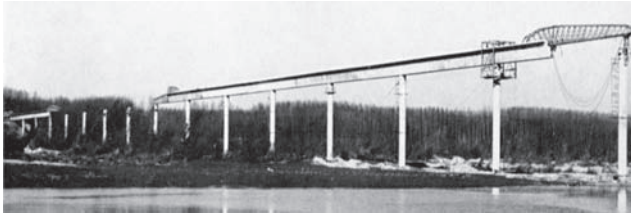


Figure 12 View of the bridge during the launching

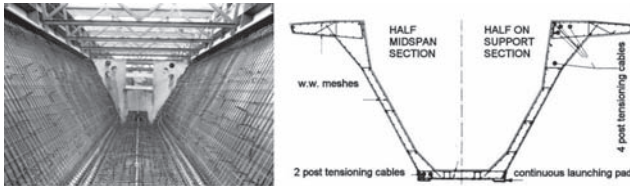


Figure 13. View of the assembled reinforcement and of the relevant design scheme

### 13. Conclusions

Although the common opinion is that concrete shells should no longer be used, the architectural elegance and the structural efficiency which can be exploited by studying and designing these elements, including the relevant construction methods can not be dropped, even at the date, without any, at least preliminary investigation.

According to the design and construction experience earned with the illustrated examples, precast solutions are very often highly cost effective if the constructor has the suitable level of expertise required.

In many cases, while it may be far more exacting in terms of engineering, precasting is the only available choice because it is far more competitive than on site conventional construction with regard to price, the quality of the work and construction time.

The coupling of the shell load bearing capacity and the precasting technique results in a very high structural efficiency, as well as in a low construction price and in the

minimum material consumption, and therefore in a more sustainable construction.

As a recommendation, it is necessary to stress that precasting is one of the basic choices that needs to be made at the very beginning of the design process; the conversion of a conventional structure into a precast one very rarely turns out to be the best choice or completely free of compromises.

One needs to decide on precasting straightaway, evaluating the pros and cons before adopting it or, on the contrary, deciding to go for a conventional structure.

When major buildings are dealt with, all aspects of decision about precasting must be carefully considered again at the design stage, because the system and method of assembly and erection generate temporary actions which may require changes of the structural sizing. Not to mention the technical/cost effectiveness of such a decision.

We should, however, point out that the opportunities to gain and implement considerable skill and mastery in the field of shell concrete constructions are becoming fewer and fewer and those companies operating in the field of precasting are often the safe-keepers of the remaining experience and the necessary aptitudes

New-concepts in the load-bearing system are needed to optimize the construction system and therefore:

long live the shell!

### Author Affiliation

Giuliani Gian Carlo<sup>1</sup> and Giuliani Mauro Eugenio<sup>2</sup>

<sup>1</sup> Dr.Eng., Exclusive Consultant Redesco Progetti srl Milano/Italy gc.giuliani@redesco.it

<sup>2</sup> Dr.Eng., General Manager and Consultant Redesco Progetti srl Milano/Italy gc.giuliani@redesco.it

# Structural Design and Construction of Diagrids for Complex-shaped Tall Buildings

**Kyoung Sun Moon**

## Summary

Early design of tall buildings culminated with the emergence of the International Style, which produced many Miesian towers all over the world for decades. Today's diverse design directions prevalent for tall buildings, however, have produced various building forms, such as freeform and other non-Miesian forms such as twisted and tilted forms. This paper investigates performance-based structural design solutions for various complex-shaped tall buildings. Among many different structural systems developed for tall buildings, an emphasis is placed on the study of diagrid systems, which are very widely used for today's tall buildings due to their structural efficiency and distinctive architectural aesthetics.

For each complex form category, tall buildings are designed with diagrid systems, and their structural efficiency is studied in conjunction with building forms. In order to investigate the impacts of various important geometric configurations of complex-shaped tall buildings, such as the degree of fluctuation of freeform, rate of twisting and angle of tilting, parametric models are generated using appropriate computer programs. The models are then exported to structural engineering software for design and analyses. Based on the study results, design considerations as well as construction issues are discussed for more efficient use of diagrids for complex-shaped tall buildings.

## Keywords

diagrids, tall buildings, steel structures, complex-shape.

## Theme

tall buildings – structural design – wind loads

## 1. Introduction

Since the application of the diagrid structural system for major tall buildings, such as the 30 St Mary Axe of 2004 in London and the Hearst Headquarters Tower of 2006 in New York, its use, especially for tall buildings, has continuously been increased. The diagrid system, with its diagonals' axial actions, provides very efficient structures for tall buildings, the design of which is generally governed by lateral stiff-

ness. With no vertical perimeter members in general, diagrid structures produce very unique and distinguished architectural aesthetics in any existing urban context.

Today, as is true of other buildings types, many different design directions and consequently produced various building forms are prevalently found in tall buildings. The structural efficiency of diagrids for tall buildings of conventional prismatic building forms has already been well proven by researchers and engineers. This paper studies the structural efficiency of diagrid systems employed for tall buildings of complex forms including freeform and other non-prismatic forms such as twisted and tilted forms. While an emphasis is placed on the study of diagrid structures, other alternative structural systems such as braced tubes and outrigger systems are also discussed comparatively.

In order to investigate the impacts of variation of important geometric configurations of complex-shaped tall buildings, such as the degree of fluctuation of freeform, rate of twisting and angle of tilting, parametric structural models are generated using Rhino/Grasshopper. The models are exported to structural engineering software such as SAP 2000 for design and analyses. Based on the study results, design considerations are discussed for more efficient and integrative use of diagrids for complex-shaped tall buildings.

## 2. Fundamentals of structural design of diagrids for tall buildings

A diagrid structure is modeled as a vertical cantilever beam on the ground, and subdivided longitudinally into modules according to the repetitive diagrid pattern. Each module is defined by a single level of diagrids that extend over multiple stories. Figure 1 illustrates the case of a 6-story module. In order to more accurately estimate the lateral rigidity provided by diagrids, all the required lateral stiffness is allocated to the perimeter diagrids, and core structures, omitted in Figure 1, are only gravity systems.

Depending on the direction of loading, the faces act as either web planes (i.e., planes parallel to wind) or flange planes (i.e., planes perpendicular to wind). The diagonal members are assumed to be pin-ended, and therefore resist the transverse shear and moment through axial action only. With this

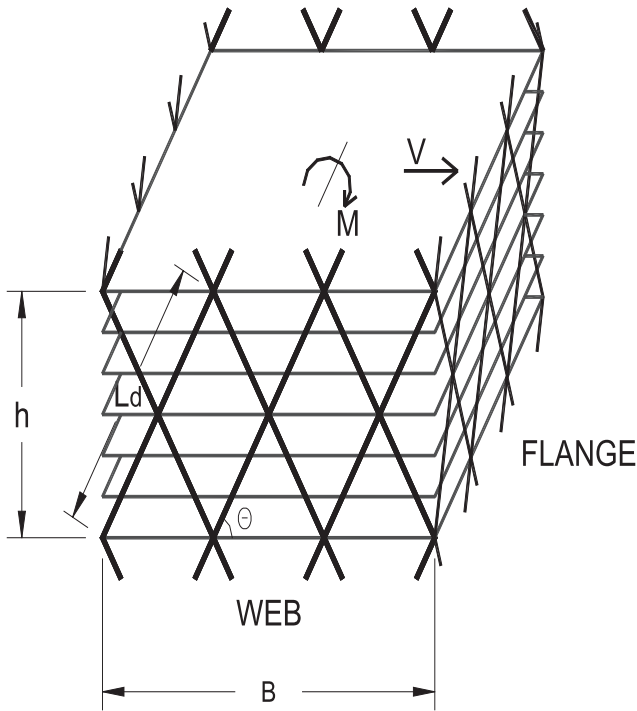


Figure 1. Typical diagrid module

idealization, the design problem reduces to determining the cross-sectional area of typical web and flange members for each module. Following the design methodology developed by Moon et al. (2007), Equation 1 and 2 expresses the diagrid module's shear and bending stiffness based on the web and flange plane members respectively.

$$K_t = 2N_w \left( \frac{A_{d,w} E}{L_d} \cos^2 \theta \right) \quad (1)$$

$$K_b = N_f \left( \frac{B^2 A_{d,w} E}{2L_d} \right) \sin^2 \theta \quad (2)$$

Member sizes for the modules can be computed using Equations (3) and (4) customized for each design case.

$$A_{d,w} = \frac{VL_d}{2N_{d,w} E_d \gamma \cos^2 \theta} \quad (3)$$

$$A_{d,f} = \frac{2ML_d}{(N_{d,f} + \delta) B^2 E_d x h \sin^2 \theta} \quad (4)$$

$A_{d,w}$  is the area of each diagonal on the web;  $A_{d,f}$  is the area of each diagonal on the flange;  $V$  is shear force;  $M$  is moment;  $L_d$  is the length of diagonal;  $E_d$  is the modulus of elasticity of steel;  $\theta$  is the angle of diagonal members;  $\gamma$  is transverse shear strain;  $x$  is curvature;  $N_{d,w}$  is the number of diagonals on each web plane;  $N_{d,f}$  is the number of diago-

nals on each flange plane;  $\delta$  is the contribution of web diagonals for bending rigidity;  $B$  is the building width in the direction of applied force.

### 3. Freeform diagrid tall buildings

As a building's form becomes more irregular, finding an appropriate structural system for better performance and constructability is essential to successfully carry out the project. The diagrid structural system has great potential to be developed as one of the most appropriate structural solutions for irregular freeform towers. It is a very challenging task to accurately define and construct any freeform tower due to its complex geometry. If a freeform tower's geometry is defined by polygons other than triangles, its originally designed form is more vulnerable to distortion during construction. Triangular structural geometric units naturally defined by diagrid structural systems can specify any irregular freeform tower more accurately without distortion.

Diagrid systems are employed for 60-story freeform tall buildings to investigate their structural performance. Freeform geometries are generated using sine curves of various amplitudes and frequencies. For the purpose of comparison, preliminary member sizes for the 60-story conventional rectangular box form diagrid tall building shown in Figure 2 are generated first to satisfy the maximum lateral displacement requirement of a five hundredth of the building height.

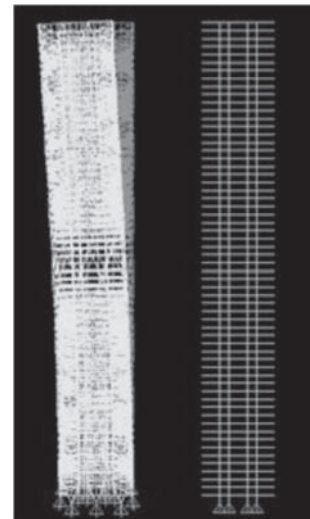


Figure 2. 60-story diagrid tower's deformed shape in 3D (left) and undeformed section through core in 2D (right)

The building's plan dimensions are 36 x 36 meters with an 18 x 18-meter gravity core at the center and typical story heights of 3.9 meters. The SEI/ASCE Minimum Design Loads for Buildings and Other Structures is used to establish the wind load. The structures are assumed to be in Chicago and within category III, which implies that there is a substantial hazard to human life in the event of failure. Based on the code, the basic wind speed is 40.2 meters per second (90 mile per hour). One percent damping is

assumed for the calculation of the gust effect factor.

Once the conventional rectangular box form diagrid structure is designed using Equations 3 and 4 and analyzed, three different freeform diagrid cases shown in Figure 3 are comparatively studied. In order to estimate the lateral stiffness of diagrid structures employed for freeform structures, the member sizes used for the straight rectangular box form tower are also used for the freeform towers. Thus, each structure is designed with very similar amount of structural materials. Compared to the rectangular box form diagrid structure, which has 36 x 36 meter square plan on each floor, the first freeform case's floor plans fluctuate within the plus/minus 1.5 meter boundaries of the original square. The second and third cases' floor plans fluctuate within the plus/minus 3 and 4.5 meter boundaries of the original square respectively. Despite these geometry changes, total floor area of each case is kept to be the same.

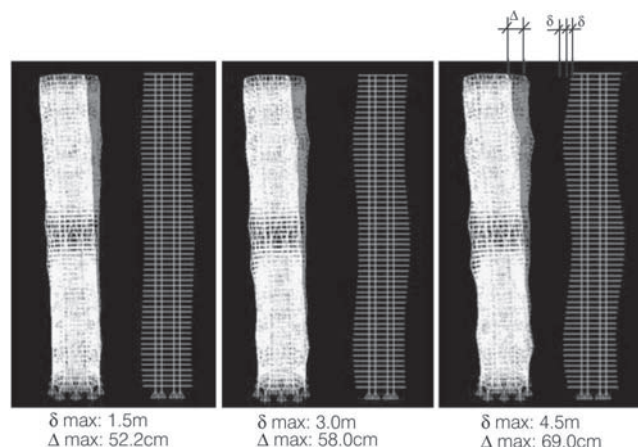


Figure 3. 60-story freeform diagrids' deformed shape in 3D (left), undeformed section through core in 2D (right)

As can be seen in Figure 3 which shows the deformed shape of each diagrid structure in a scale factor of 20, the lateral displacement of the structure becomes larger as the freeform shape deviates more from its original rectangular box form. The maximum deflection at the top of the structure of the first, second and third case is 52.5 cm, 58.0 cm and 69.0 cm, respectively, compared to 46.6 cm in the case of the straight tower. This is very much related to the change of the diagrid angle caused by the freeform of the tower. The straight tower designed first for the comparison is configured with the optimal diagrid angle of about 70 degrees. As the degree of fluctuation of freeform increases, the diagrid angle deviates more from its original optimal condition, which results in substantial reduction of the lateral stiffness of the tower. Therefore, freeform shapes should be determined with careful consideration of their not only architectural but also structural performance.

#### 4. Twisted diagrid towers

Twisted forms are often employed for tall buildings such as the Chicago Spire in Chicago, Infinity Tower in Dubai and Shanghai Tower in Shanghai. While none of these twisted

towers were designed with diagrid structures, this section investigates the structural performance of diagrids for twisted towers. Sixty-story towers of different twisted rates are designed with diagrid structures. The member sizes used for the straight diagrid tower in the previous section are also used for the twisted diagrids. Design conditions are the same as before.

Figure 4 illustrates three different cases studied. The first case is the diagrid tower with a twisted rate of 1 degree per floor. The second and third case is another twisted version of the tower with a twisted rate of 2 and 3 degrees per floor, respectively. The maximum deflection at the top of the structure of the first, second and third case is 47.5 cm, 51.2 cm and 57.0 cm, respectively. As the rate of twisting increases, the building's lateral stiffness decreases, and, consequently, its deflection increases. As in the freeform towers, this phenomenon is also very much related to the change of the diagrid angle, now caused by twisting the tower. As the rate of twisting increases, the diagrid angle deviates more from its original optimal condition, which results in substantial reduction of the lateral stiffness of the tower.

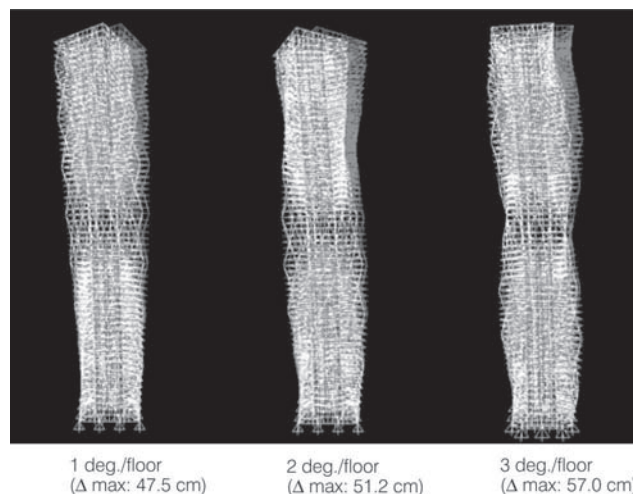


Figure 4. 60-story diagrid structures of various twisted rates

The braced tube, which also carries lateral loads by its primary structural members' axial actions, is another very efficient structural system for tall buildings. Similar studies were performed with braced tube structures. When the braced tube is employed for twisted towers, its structural performance is similar to that of the diagrid system. As the rate of twist increases, the lateral stiffness of the system is decreased. The difference between diagrids and braced tubes employed for twisted towers is that the rate of stiffness reduction is more accelerated with the increased rate of twist in braced tube structures. Figure 5 summarizes the maximum deflections of twisted towers of diagrids and braced tubes comparatively.

With regard to the across-wind direction dynamic response due to vortex shedding, however, a twisted or free form tower generally performs better than a straight one because a complex-shaped tall building better disturbs the formation



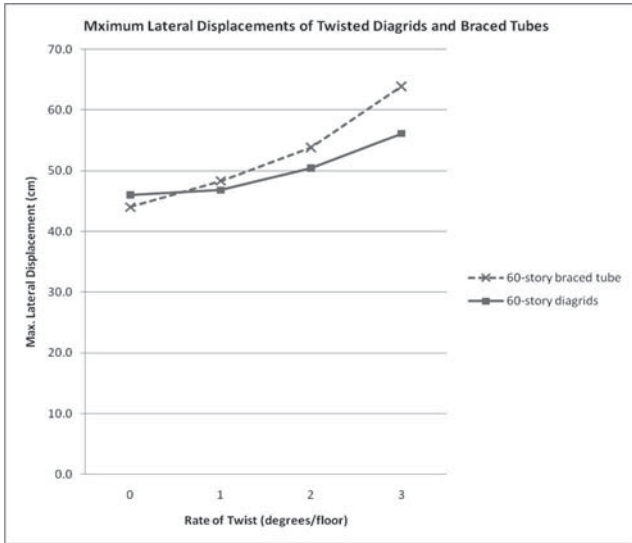


Figure 5. Maximum lateral displacements of 60-story twisted diagrids and braced tubes

of organized alternating vortices around it. Therefore, a tall building's geometry should be determined with very careful consideration of its dynamic performance as well. For example, the total 120 degree twisting of the Shanghai tower was determined based on the wind tunnel tests with multiple models of various twisted rates ranging from 90 to 210 degrees (Gensler, 2009). Another important issue to be considered for twisted or free form towers is their constructability. As the complexity of building form becomes greater, construction of the tower becomes more challenging. Indeed, many aspects should be considered in an integrative way with multidisciplinary collaboration to successfully carry out complex-shaped tall building projects.

### 5. Tilted diagrid towers

This section investigates the structural performance of diagrid structural systems employed for tilted towers. The 60-story straight diagrid tower designed earlier is now tilted in three different ways shown in Figure 6. The first case tilting, with 12 floor offset, results in a tilted angle of 7 degrees. The second and third case tilting, with 16 and 20 floor offset, results in a tilted angle of 9 and 13 degrees, respectively. These configurations are similar to that of the Signature Towers (formerly known as Dancing Towers) designed by Zaha Hadid. While these towers do not employ diagrids as their structural systems, this section employs diagrids for tilted towers and investigates their structural performance.

This section investigates the structural performance of diagrid structural systems employed for tilted towers. The 60-story straight diagrid tower designed earlier is now tilted in three different ways shown in Figure 6. The first case tilting, with 12 floor offset, results in a tilted angle of 7 degrees. The second and third case tilting, with 16 and 20 floor offset, results in a tilted angle of 9 and 13 degrees, respectively. These configurations are similar to that of the

Signature Towers (formerly known as Dancing Towers) designed by Zaha Hadid. While these towers do not employ diagrids as their structural systems, this section employs diagrids for tilted towers and investigates their structural performance.

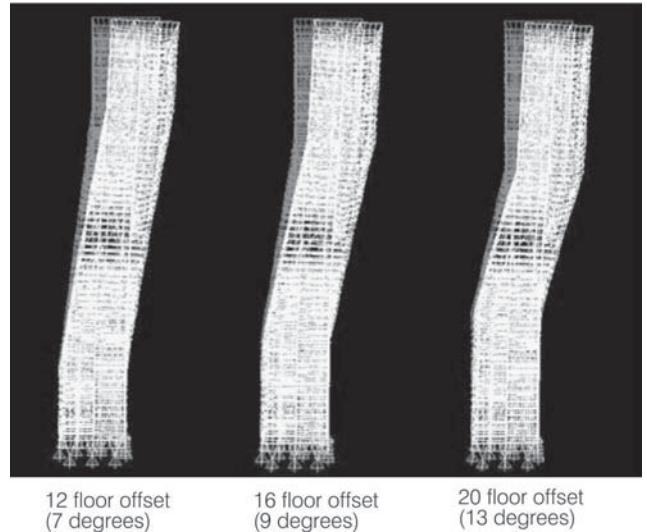


Figure 6. 60-story tilted diagrid structures of different configurations

Even though dead and live load induced deformations are large, they can be adjusted during the construction process if planned carefully. Therefore, if other non-structural design requirements can be met successfully by diagrid structures, they can be a feasible option for tilted towers.

	Lateral Displacement due to Dead & Live Load	Lateral Displacement due to Wind Load	Total Displacement due to Dead, Live & Wind Load
Case 1	55.1cm	46.2 cm	101.3 cm
Case 2	59.4 cm	46.3 cm	105.7 cm
Case 3	62.5 cm	46.5 cm	109.0 cm

Table 1. Lateral displacements of tilted towers

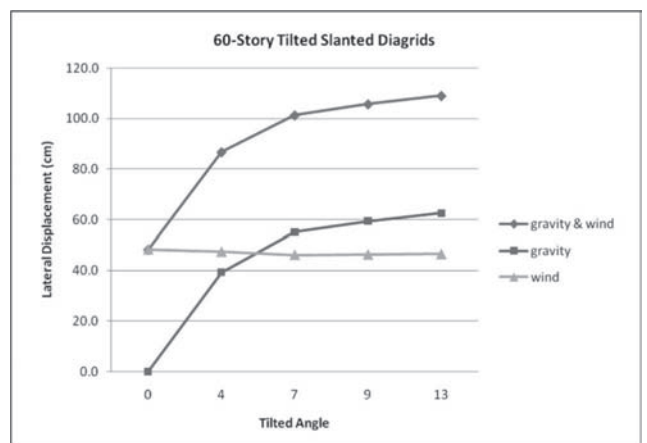


Figure 7. Maximum lateral displacements of 60-story tilted diagrid structures of different configurations

Similar studies were performed using braced tubes and outrigger systems. The structural performance of braced tubes employed for tilted towers were found to be similar to that of diagrids, while the performance of outrigger systems was better than that of diagrids or braced tubes.

## 6. Conclusions

Diagrid structures are prevalently used for tall buildings worldwide. The unique compositional characteristics of diagrids provide great structural efficiency and aesthetic potential as an accentuating element in any existing urban context generally composed of buildings of orthogonal components. This paper presented structural performance and constructability issues of diagrid structures employed for complex-shaped tall buildings. Though widely used today, application of diagrid structures for tall buildings is still relatively new. With abundant emergence of complex-shaped tall buildings, more studies on their potential structural systems and multidisciplinary collaboration are very much required to construct built environments of higher performance.

## 7. Acknowledgement

This research was supported by a grant (Code# '09 R&D A01) from Cutting-edge Urban Development Program funded by Ministry of Land, Transport and Maritime Affairs of Korean government.

## Author Affiliation

Kyoung Sun Moon

Ph.D., Assistant Professor, Yale University, New Haven/  
USA kyoung.moon@yale.edu

## References

- [1] Ali, M. M. and Moon K. (2007). Structural Developments in Tall Buildings: Currents Trends and Future Prospects. *Architectural Science Review*, 50.3, pp 205-223.
- [2] Connor, J.J. (2003). *Introduction to Structural Motion Control*. New York: Prentice Hall.
- [3] Gensler, M. A. (2009). Completing a Supertall Trio, Council on Tall Buildings and Urban Habitat 2009 Chicago Conference: New Challenges in a World of Global Warming and Recession, October 22-23, Chicago.
- [4] Moon, K. (2008). Optimal Grid Geometry of Diagrid Structures for Tall Buildings, *Architectural Science Review*, Vol. 51.3, pp 239-251.
- [5] Moon, K., Connor, J. J. and Fernandez, J. E. (2007). Diagrid Structural Systems for Tall Buildings: Characteristics and Methodology for Preliminary Design, *The Structural Design of Tall and Special Buildings*, Vol. 16.2, pp 205-230.

# Dynamic Elasto-plastic Time-history Analysis for Out-of-codes High-rise Structure

Wanli Xue

## Summary

Seismic response of a high rise building under rare earthquake is numerically investigated in the paper. The Height of the building is 266m, including 62 stories, which goes beyond the limit of 180m in Chinese standard. The structural system of steel frame-concrete core tube structure is adopted and CFT members are used for the exterior frame columns. The typical floor plane of the building is oval shaped with the portion of 2:1 between two axes, and obviously, the lateral stiffness in the direction of minor axis is far less than that in the direction of major axis. Therefore, to strengthen the lateral stiffness in the direction of minor direction and decrease lateral displacement, 3 steel-truss strengthened stories are set at the 25F, 41F and 56F, respectively. Dynamic time-history analysis is performed to investigate its elasto-plastic behaviors under severe earthquake excitations. Beam-column members of the structure are simulated by beam elements, while the core tube is simulated by shell elements. The concrete damage plasticity model is used for the elasto-plastic material of core tube members, while the kinematic hardening rule is defined for steel beam-column members and a RC constitutive rule is self-programmed for concrete beam-column members. The input motions of 3 sets of strong earthquake records and 1 set of artificial wave are adopted in the analysis. The displacement performances and the stress performances of the structure are all examined in the analysis, such as plastic damage development of the core tube, the storey deformation and the storey drift angle of the building and the floor stress development at the strengthened floors, etc. The results show that, under severe earthquakes, steel frame members and steel truss members in the strengthened floors can keep elastic. Severe damages are detected in almost all coupling beams in the core tube, as well as shear-walls near strengthened stories, where lateral stiffness would decrease seriously. Through the investigation, it is also found that the largest story drift is less than the maximum allowable value in the Chinese code for seismic design of buildings. Based on the analysis, it is concluded that the high-rise building will not collapse when the place is subjected to severe earthquakes and some design suggestions are proposed in the paper.

## Keywords

Out-of-codes, high-rise structure, dynamic elasto-plastic analysis.

## Theme

Structural Design –action engineering /earthquake –composite

## 1. Structure survey

The total height of the building is 266m, including 62 stories on top of the ground and 3 stories underground (Figure 1 shows structure overground). The structural system of sparse outer steel frame and concrete core tube and extension-arm truss is adopted. CFT members are used for the exterior frame columns. Steel girders are used for both



Figure 1. The whole structure

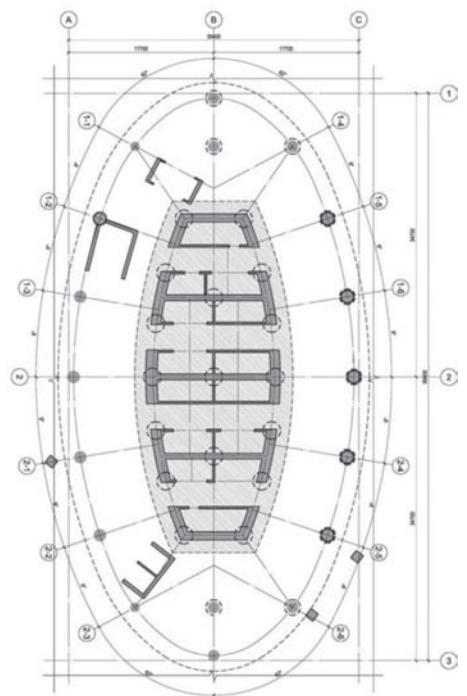


Figure 2. floor plan

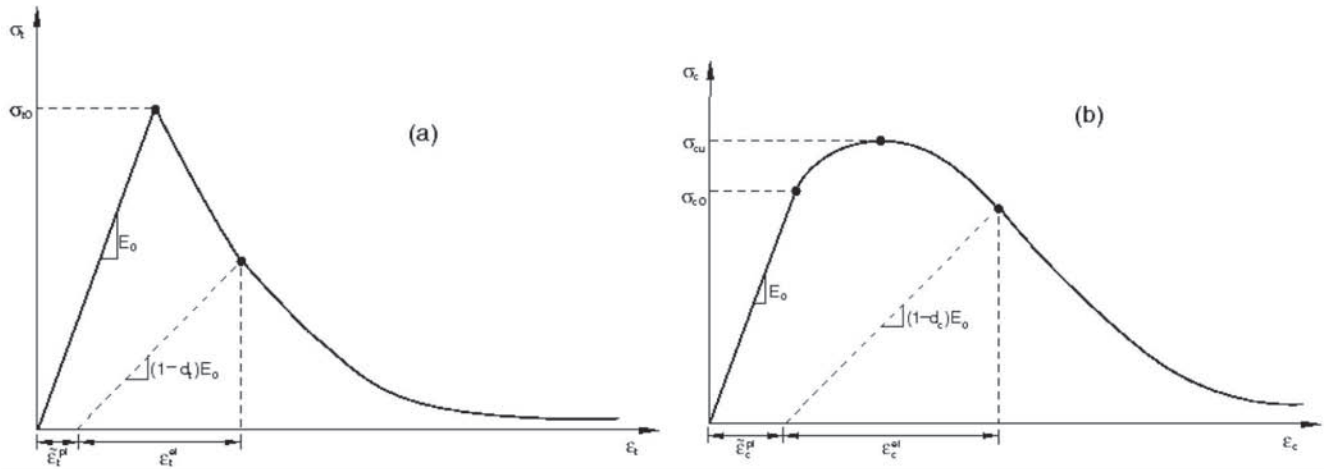


Figure 3. tension and compression stress-strain behavior

the frame beam and the secondary beam. The typical floor plan of the building is oval shaped with the portion of 2:1 between two axes (as shown in Figure 2), and obviously, the lateral stiffness in the direction of minor axis is far less than that in the direction of major axis. Therefore, to strengthen the lateral stiffness in the direction of minor direction and decrease lateral displacement, 3 steel-truss are set at the 25F, 41F and 56F in minor direction, respectively.

According to the Chinese code, the highest applicable height for concrete frame-core tube at B rank is 180m and this building exceeds the limit. For building out of code, it is proposed that Elasto-plastic analysis should be performed to verify that the structure meets the earthquake design requirements: "standing upright in severe earthquake". The deformation between floors of structure should be checked and the extent of yielding and damage of the major members should be verified.

## 2. The finite element model

The following assumptions are made for elasto-plastic analysis model:

- 1) Underground structure is ignored, and the structure is assumed to be embedded at the ground surface.
- 2) Slabs of the strengthened floors and the neighbor floors are simulated by shell element, while slabs of other floors are simulated with rigid floor assumption.

### 2.1 Elements

Shell element is employed to simulate both wall and coupling beams with wall element size 1~2m and coupling beam element size 0.4m. Shell element is also applied to concrete slab with element size 1.5m. Beam element is used to simulate both beam and column. Concrete-filled steel tubular is composite members and is simulated by two beam elements with the same nodes. One element is to simulate the concrete; the other is to simulate the steel tube. Truss at the strengthened floor is simulated with truss ele-

ment. Besides, longitude rebar of shear wall boundary member and coupling beams are also simulated with truss element, while other distributing rebar is simulated with rebar layer.

## 2.2 Material constitutive model

### (1) Concrete material

The constitutive model of concrete material for shear wall and slab uses the elasto-plastic damage model. This model can accurately simulate the hysteretic behavior of concrete under the dynamic loading and consider the degradation of stiffness and strength in combination with the nature of stiffness recovery due to crack and closure under tension and compression cycles. The standard value of concrete axial compressive and axial tensile strength as well as the elastic modulus is chosen according to code. The constitutive curve of concrete is shown in Figure 3, (a) for tension stress behavior, (b) for compressive stress behavior.

The compressive stiffness is recovered upon crack closure as the load changes from tension to compression. On the other hand, the tensile stiffness is not recovered as the load changes from compression to tension once crushing micro-cracks have developed. Figure 4 illustrates a uniaxial load cycle assuming the default behavior.

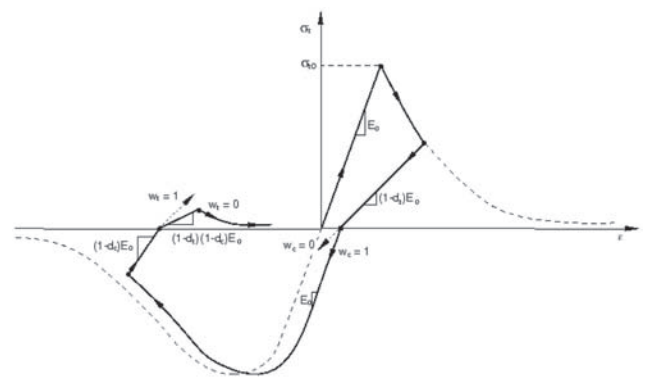


Figure 4: Stiffness recovery



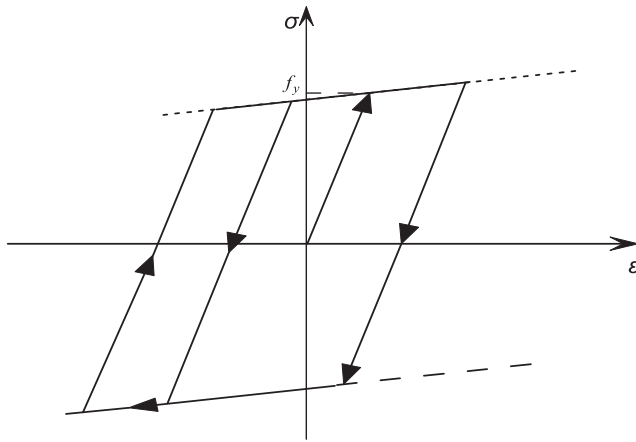


Figure 5. Bilinear kinematic hardening model

However, concrete beams use fiber element, and material constitutive model is imported with user material subroutine.

**(2) Steel material**

Steel material employs bilinear kinematic hardening model (shown in Figure 5). In the load cycle, the Bauschinger effect is included and no stiffness degradation is considered. The initial plastic strain is  $f_y/E_s$ , in which  $f_y$  is yield stress and  $E_s$  is the elasticity of elastic stage. The limit strain at failure is 0.025. The elasticity modular of hardening stage is 0.01 $E_s$ .

**3. Seismic waves**

Four sets of seismic waves adopted in the analysis are provided by CABR. Among them, three sets are natural waves and one set is man-made wave. The main seismic direction is X or Y, and the minor seismic direction is Y or X correspondingly. The ratio of peak value of the main direction and minor direction is 1:0.85, and peak value of the main direction is 220gal. The duration of wave is 30s, which meets the requirement that duration time must be 5~10 times of structure natural vibration period. Structure damping is 5%.

**4. Analysis cases and results**

**4.1 Result of modal analysis**

Through modal analysis, structure dynamic performance can be obtained. Natural vibration periods and equivalent

Item	Midas Gen		ABAQUS	
Equivalent total gravity load (DL+0.5LLkN)	1706271		1716142	
T1(s)	6.02	Translation of Y direction	6.01	Translation of Y direction
T2(s)	4.58	Translation of X direction	4.47	Translation of X direction
T3(s)	3.97	torsion	3.96	torsion
T4(s)	1.65	Translation of Y direction	1.75	Translation of Y direction
T5(s)	1.55	Translation of X direction	1.55	Translation of X direction

Table 1: Periods and equivalent total gravity load

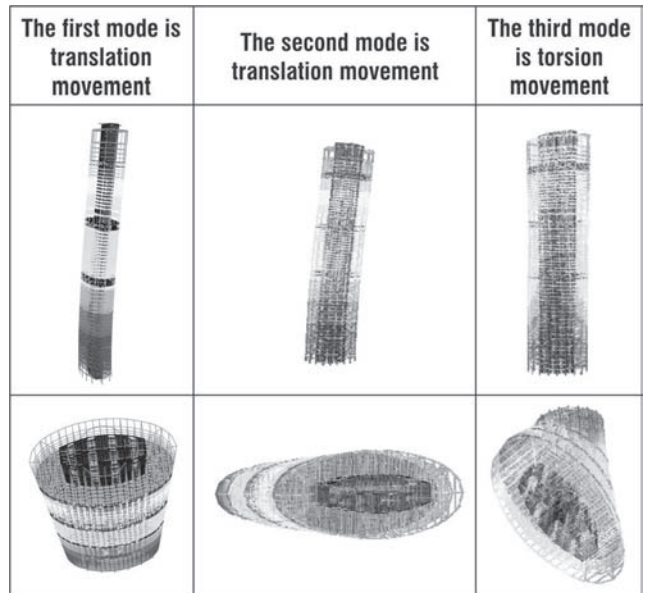


Figure 6. Mode shape

Construction Stage	Gravity load
1	Dead load of 1 <sup>th</sup> ~5 <sup>th</sup> storey activated
2	Dead load of 6 <sup>th</sup> ~10 <sup>th</sup> storey activated
3	Dead load of 11 <sup>th</sup> ~15 <sup>th</sup> storey activated
4	Dead load of 16 <sup>th</sup> ~20 <sup>th</sup> storey activated
5	Dead load of 21 <sup>th</sup> ~25 <sup>th</sup> storey activated
6	Dead load of 26 <sup>th</sup> ~30 <sup>th</sup> storey activated
7	Dead load of 31 <sup>th</sup> ~35 <sup>th</sup> storey activated
8	Dead load of 36 <sup>th</sup> ~40 <sup>th</sup> storey activated
9	Dead load of 41 <sup>th</sup> ~45 <sup>th</sup> storey activated
10	Dead load of 46 <sup>th</sup> ~50 <sup>th</sup> storey activated
11	Dead load of 51 <sup>th</sup> ~55 <sup>th</sup> storey activated
12	Dead load of 56 <sup>th</sup> ~62 <sup>th</sup> storey activated
13	50% of live load

Table 2: gravity load applied through construction stage

total gravity load of structure calculated from different software are compared in table 1. The difference of equivalent total gravity load and periods calculated from Midas Gen soft and ABAQUS soft is small, which verifies that the finite element model is accurate enough to calculate seismic response of structure.

The mode shape is shown in figure 6. The first and second mode is translation movement; the third mode is torsion movement. The period ratio of torsion mode and the first translation mode is 0.66, less than the limit of code 0.9.

**4.2 Construction stage analysis**

The building is so high that the application way of gravity load may influence the distribution of internal force and de-

Item \ wave	The max storey drift in X direction	Storey of the max drift	The max storey drift in Y direction	Storey of the max drift
XL741YL742	1/527	43	1/313	62

Table 3: the max elasto-plastic storey drift

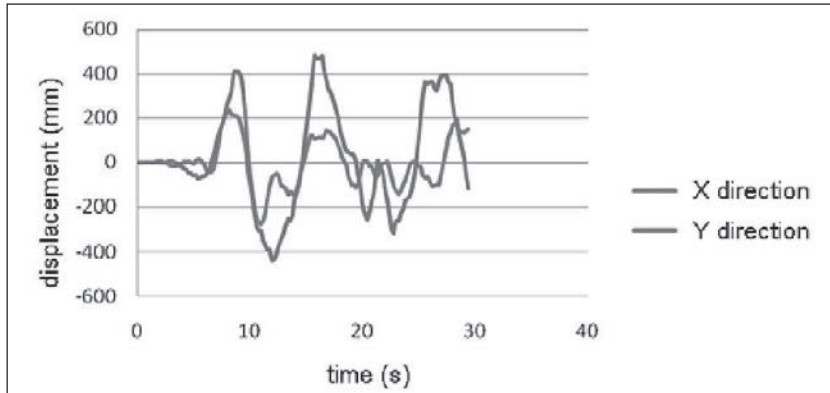


Figure 7. history displacement of structure vertex

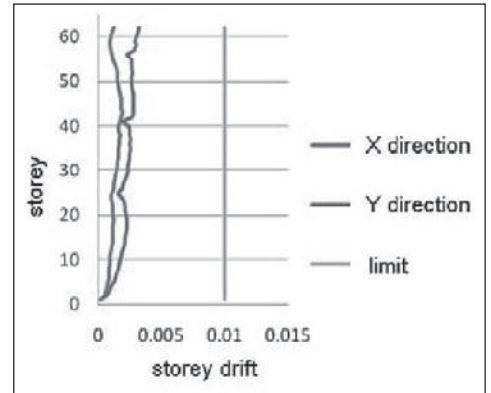


Figure 8. Storey drift

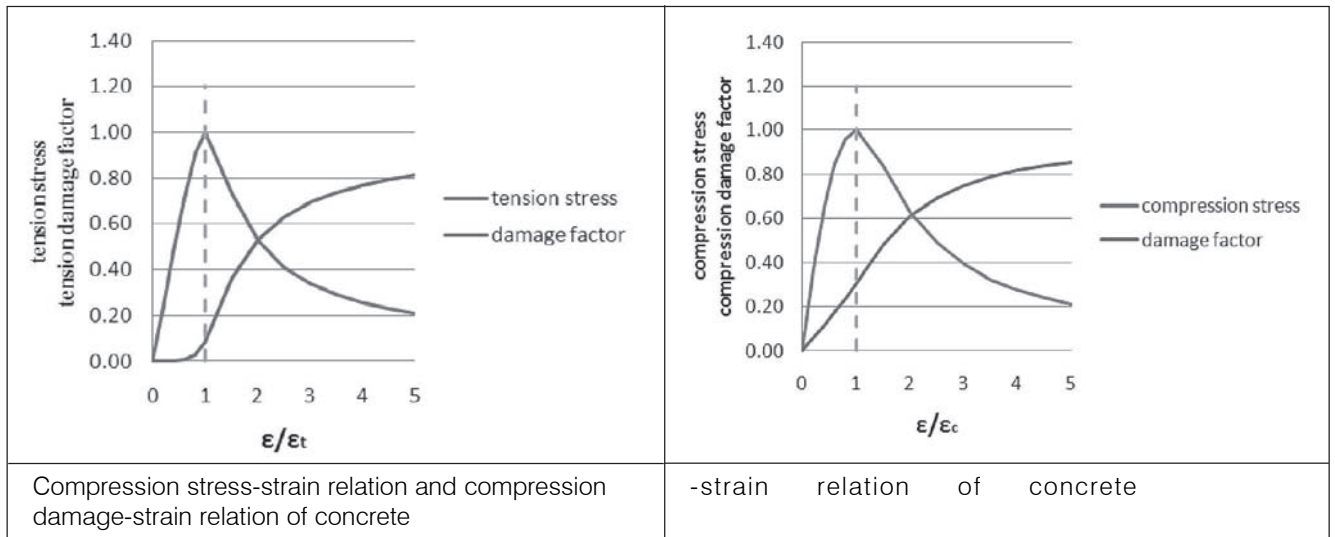


Figure 9: stress-strain relation and damage-strain relation

formation of structure. In the analysis, Gravity load is applied through simplified construction stage. Construction stage is divided into 13 stages and Gravity load of five storeys is applied in every stage. 50% of live load is applied at the last stage. The construction process is shown as table 2.

### 4.3 Seismic response under rare earthquake

For seismic analysis under rare earthquake, bidirectional waves are input and the damping of every mode is 5%. The damping matrix is formed based on Rayleigh damping theory. Limit to paper length, only the result of man-made wave is given in the paper.

#### (1) Structure displacement

History displacement of structure vertex under rare earthquake is shown in figure 7.

The max elasto-plastic storey drift is shown in table 3. Storey drifts of every storey are shown in figure 8.

#### (2) Damage of member

Figure 9 gives stress-strain relation and damage factor -

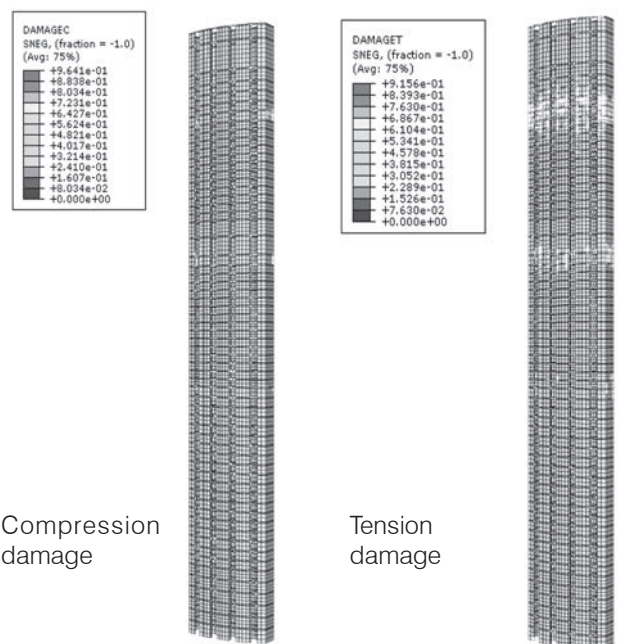


Figure 10. distribution of shear wall damage

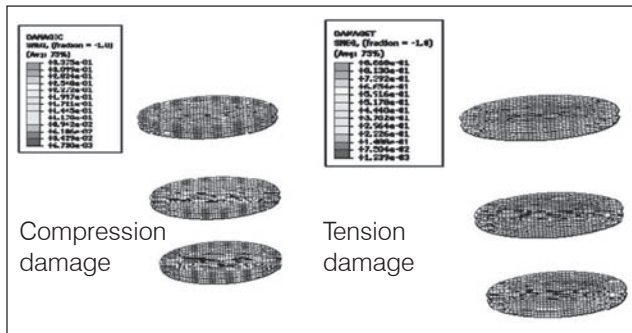


Figure 11. distribution of concrete slabs damage

strain relation of concrete material. It is concluded that if tension damage factor of concrete is less than 0.1 or compression damage factor is less than 0.3, concrete material can be considered to be undamaged.

The distribution of tension and compression damage factor under severe earthquake is shown in figure 10. It can be concluded from the figure 10 that compression damage factor of most of the wall concrete is less than 0.3, so wall concrete is rarely crushed. Tension damage factor of concrete wall of strengthened stories reaches 0.9, and concrete cracks seriously. Almost all coupling beams' tension damage factor reaches 0.9. Part of coupling beams' compression damage factors reaches 0.9. So most of coupling beams are destroyed by tension damage.

Figure 11 gives Tension damage and compression damage of strengthened storeys' concrete slab. The max compression damage factor is 0.3 and the max tension damage factor is 0.88. So strengthened stories' concrete slab is destroyed seriously and tension damage of concrete slab near truss is more serious. So it is proposed that some measures are taken to strengthen these concrete slabs.

Outer steel frame and truss of strengthened stories do not enter plastic stage. A proportion of longitude steel of shear wall enters plastic stage.

## Conclusions

From dynamic elasto-plastic analysis, it can be concluded that:

- 1) The max storey drift is less than limit of code. Structure meets the requirement "standing upright in severe earthquake"
- 2) Under rare earthquake, most of coupling beam is seriously damaged, while the damage of shear wall is relatively minor. This satisfies the structural design principle that coupling beam damages before the wall. But shear walls of strengthened stories damage seriously. It is proposed that strengthened stories' shear wall should be strengthened.
- 3) Strengthened stories' concrete slabs are seriously damaged. It is proposed that some measures should be taken to strengthen the concrete slab of strengthened stories.
- 4) Outside steel frame and truss of strengthened stories do not enter plastic stage under rare earthquake.

## Author Affiliation

Wanli Xue

Dr.Eng., general Manager China Construction Design International Shanghai/China xue.wanli@ccdi.com

## References

- [1] Feng Iijuan, Shang xiaojiang, Xu Ziguo, Static and dynamic elasto-plastic analysis of structures based on ABAQUS. Earthquake Resistant Engineering and Retrofitting, Vol 30, No.5, P 14-19, October 2008
- [2] Li Chengming, Li Zhishan, Wang Guojian, Study on elastic-plastic finite element analysis based on section fiber beam-column element. Building structure, Vol 37, No.12, P 33-35, December 2007
- [3] Lee,J., G.L. Fenves, Plastic-damage model for cyclic loading of concrete structures, Journal of Engineering Mechanics, Vol 124, No.8, P 892-900,1998

# An Overview on Diagrid Structures for Tall Buildings

**Maurizio Toreno<sup>1</sup>, Raffaele Arpino<sup>2</sup>,  
Elena Mele<sup>3</sup>, Giuseppe Brandonio<sup>4</sup>  
and Antonello De Luca<sup>5</sup>**

## Abstract

The originality of form is one of the new trends that can be identified in the current design of tall buildings. In this design trend, the so-called diagrid structures, which represent the latest mutation of tubular structures, play a major role due to their inherent aesthetic quality, structural efficiency and geometrical versatility.

In this paper an overview on application of such typology to high-rise building is carried out; in particular, in the first part of the paper, the peculiarities of diagrid systems are described, focusing attention on the structural behaviour under gravity and lateral load and reviewing strength-based and stiffness-based design criteria.

In the second part of the paper, a comparative analysis of the structural performance of some recent diagrid tall buildings, characterized by different number of stories and different geometries, is carried out, namely the Swiss Re Building in London, the Hearst Headquarters in New York and the West Tower in Guangzhou.

## Keywords

Diagrid system, Swiss Re Building, Hearst Headquarters, West Tower.

## Theme

Buildings - construction - non conventional architecture.

## 1. Introduction

Diagrids, or exodiagonal systems, are perimeter structural configurations characterized by a narrow grid of diagonal members which are involved both in gravity and in lateral load resistance. Diagonalized applications of structural steel members for providing efficient solutions both in terms of strength and stiffness are not new, and an earlier example to medium-rise buildings can be found in the IBM Pittsburgh building, "perhaps one of the first uses of diagrid" [1]. However nowadays a renewed interest in and a widespread application of diagrid is registered with reference to large span and high rise buildings, particularly when they are characterized by complex geometries and curved shapes, some times by completely free forms.

Among the large-span buildings some examples are represented by the Seattle Library, the London City Hall, the One Shelley Street in Sydney, and more recently by several outstanding Pavilions realized at the Shanghai 2010 Expo, (e.g. France, UAE) as well as by some dazzling projects like the Astana National library. Among tall buildings, noteworthy examples are the Swiss Re building in London, the Hearst tower in New York, the CCTV headquarters building in Beijing, the Mode Gakuen Spiral Tower in Aichi, the Cyclone Tower in Asan, the West tower in Guangzhou, the Lotte super tower in Seoul, the Capital Gate in Abu Dhabi, the Bow project in Calgary, the Building of Qatar Ministry of Foreign Affairs in Doha.

With specific reference to tall buildings, diagrids are increasingly employed due to their structural efficiency as well as architectural suggestion. In fact diagrid structures can be seen as the latest mutation of tube structures, which, starting from the frame tube configuration, have increased structural efficiency thanks to the introduction of exterior mega-diagonals in the braced tube solution, firstly suggested by Fazlur Khan in the impressive Chicago John Hancock building; in this case the significant improvement in terms of lateral stiffness and shear lag reduction also reflects in the building architecture, strongly connoted by the clear and disciplined structure ("the honesty of structure" - Bruce Graham). The diagrid systems are the evolution of braced tube structures, since the perimeter configuration still holds for preserving the maximum bending resistance and rigidity, while, with respect to the braced tube, the mega-diagonal members are diffusely spread over the façade, giving rise to closely spaced diagonal elements and allowing for the complete elimination of the conventional vertical columns.

Therefore the diagonal members in diagrid structures act both as inclined columns and as bracing elements, and carry gravity loads as well as lateral forces; due to their triangulated configuration, mainly internal axial forces arise in the members, thus minimizing shear racking effects.

In order to assess the behavior of diagrid structures, first of all the behavior of the elementary triangular unit, in the following appointed as "diagrid module", is analyzed both under gravity and lateral loads, and the effect of the module geometry on the structural behavior is discussed. Then



three significant case studies are examined through the evaluation and comparison of some structural performance parameters.

### 2. The triangle diagrid module

The analysis of the diagrid structures can be carried out in a preliminary stage by dividing the building elevation into a group of stacking floors, each corresponding to a diagrid module.

As shown in [2] [3], the diagrid module under gravity loads  $G$  is subjected to a downward vertical force,  $N_{G,mod}$ , causing the two diagonals being both in compression and the horizontal chord in tension (figure 1 a). Under horizontal load  $W$ , the overturning moment  $MW$  causes vertical forces in the apex joint of the diagrid modules,  $N_{W,mod}$ , with direction and intensity of this force depending on the position of the diagrid module, with upward / downward direction and maximum intensity in modules located on the windward / leeward façades, respectively, and gradually decreasing values in modules located on the web sides (figure 1 b). The global shear  $VW$  causes a horizontal force in the apex joint of the diagrid modules,  $V_{w,mod}$ , which intensity depends on the position of the module with respect to the direction of wind load, i.e. the shear force  $VW$  is mainly absorbed by the modules located on the web façades, i.e. parallel to the load direction (figure 1 c).

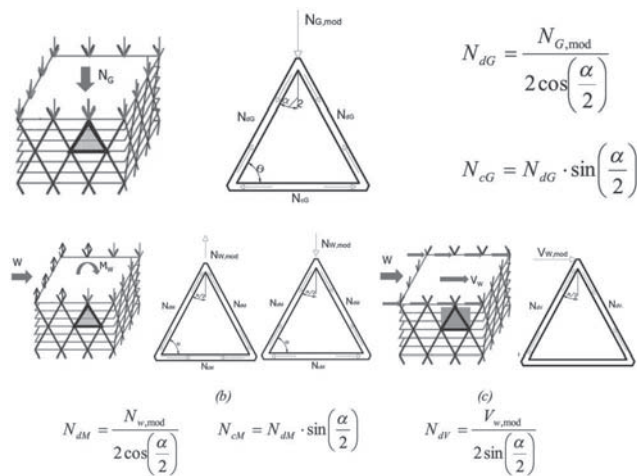


Figure 1. Diagrid module; a) Effect of vertical load; b) Effect of overturning moment; c) Effect of shear force

In the formulations provided in figure 1a; b; c; for deriving internal forces in the diagrid elements, it has been implicitly assumed that the external load is transferred to the diagrid module only at the apex node of the module itself. However, since the triangle module usually expands over a certain number of stories, transfer of loads to the module occurs at every floor level, thus also concentrated loads along the diagonal length are present (figure 2); as a consequence, bending moment and shear force are expected due to this load condition. However the introduction of a horizontal member at each floor girder to diagonal inter-

section (an intermediate chord, analogous to the secondary ties present in the braced tube system of John Hancock building), allows for the absorption of the force component orthogonal to the diagonal direction, thus preserving the prevailing axial force condition (figure 2).

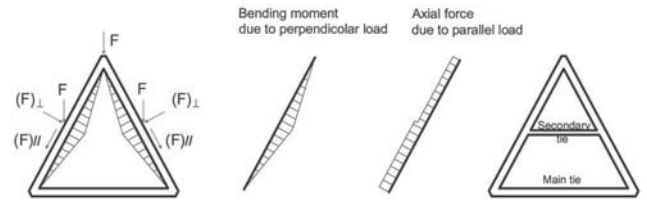


Figure 2. Diagrid module: Effect of gravity load along the diagonal length

Furthermore, the above simplified analysis of the diagrid module has been carried out implicitly assuming that the plane of the triangular module coincides with the vertical plane; however, recent applications often concern buildings characterized by curvilinear, non prismatic forms, which require the study of the diagrid curvature effect on the internal force distribution. In particular, by considering that the single module may be inclined of an angle  $\beta$  with respect to the vertical direction, the effect of both gravity loads and overturning moment gives rise to an additional horizontal force, in the direction orthogonal to the module plane. Therefore the chords of the diagrid modules, continuously connected each other along the building perimeter at the diagonal intersections, also act as hopping elements or ring beams, for absorbing these horizontal forces (figure 3). In addition, when the building has nonrectangular, rounded plans, similar effects due to this horizontal curvature develop under the action of lateral shear, and the ring beams also collect these outward forces arising in the horizontal plane (figure 4).

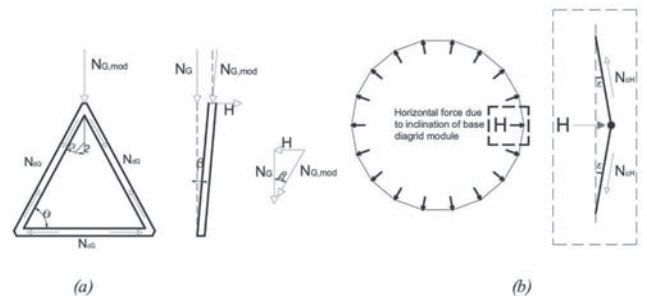


Figure 3. Diagrid module under vertical load - effect of vertical and horizontal curvature

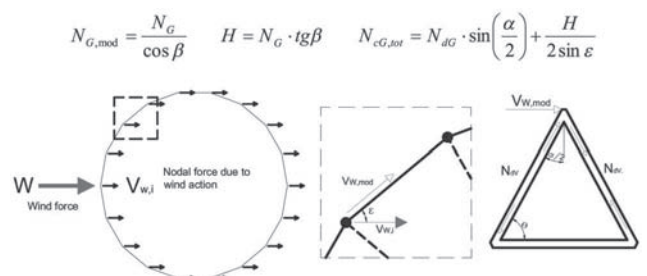


Figure 4. Diagrid module under horizontal load - effect of horizontal curvature

$$N_{G,mod} = \frac{N_G}{\cos \beta} \quad H = N_G \cdot \text{tg} \beta \quad N_{cG,mod} = N_{dG} \cdot \sin\left(\frac{\alpha}{2}\right) + \frac{H}{2 \sin \epsilon}$$

## Geometry

Diagrid structures, like all the tubular configurations, utilize the overall building plan dimension for counteracting overturning moment and providing flexural rigidity through axial action in the diagonals, which acts as inclined columns; however, this potential bending efficiency of tubular configuration is never fully achievable, due to shear deformations that arise in the building "webs"; with this regard, diagrid systems, which provide shear resistance and rigidity by means of axial action in the diagonal members, rather than bending moment in beams and columns, allows for a nearly full exploitation of the theoretical bending resistance.

Being the diagrid a triangulated configuration of structural members, the geometry of the single module plays a major role in the internal axial force distribution, as well as in conferring global shear and bending rigidity to the building structure. As shown in [2], while a module angle equal to  $35^\circ$  ensures the maximum shear rigidity to the diagrid system, the maximum engagement of diagonal members for bending stiffness corresponds to an angle value of  $90^\circ$ , i.e. vertical columns. Thus in diagrid systems, where vertical columns are completely eliminated and both shear and bending stiffness must be provided by diagonals, a balance between these two conflicting requirements should be searched for defining the optimal angle of the diagrid module. However, it is worth noticing that, varying the aspect ratio of the building, the demand for shear and bending stiffness also varies, being slender buildings more governed by a bending behavior than stocky buildings; therefore it is expected that increasing the building slenderness, also the optimal angle of the diagrid module should increase. Some useful indications on optimal angle values for buildings characterized by different aspect ratio are provided in [2] [3]. Furthermore for very tall buildings, i.e. buildings with aspect ratio of the order of 7 or more, the relative demand for shear and bending stiffness is not uniformly distributed along elevation, and a varying-angle diagrid configuration, with steeper angles towards the base, generates a more efficient design (with less material consumption) than uniform angle configurations [3], [4].

## 4. Case studies

In the following, some recent diagrid tall buildings, namely the Swiss Re Building in London, the Hearst Headquarters in New York, and the West Tower in Guangzhou (figure 5) are briefly presented and examined in comparative terms. In particular in table 1 the major building data are provided, while in the next subparagraphs some additional information on the structural system are presented for the three case studies. In the next paragraph a comparative analysis of the structural behavior under gravity and wind load is carried out for the three buildings, both by means of "hand calculations" based on the formulae provided in the previous paragraph 2, and by means of FEM computer modeling. Some conclusive remarks on the structural efficiency

of diagrid structures, as well as on the accuracy of simplified assessment of the structural behavior, are finally derived.

### 4.1. Swiss Re Building

30 St. Mary Axe - also known as the Swiss Re Building - in London, (figure 5 top left) is the first modern application and the most representative example of diagrid structure. Designed by Sir Norman Foster, with 40 stories and interstory height of 4.15 m, the tower is 180 meters tall. The building is circular in plan with diameter changing along elevation, equal to 56 m at its widest point, at the 20th story, reducing to 49 m at ground level, and to 30 m at the 38th level, where a steel and glass dome tops off the building. The double curvature of the building façade, both in the horizontal plane and along the vertical direction, gives rise to the effects which have been discussed in the paragraph 2. The diagrid structure is generated by a pattern of intersecting diagonals which follow the helical path of the so called light wells, created for enforcing natural light and air circulation. It is formed by a series of steel triangles, two-story high and 9 m wide, with an intermediate tie connecting the two diagonals, which gives to the module the aspect of a "A-shape frame". The diagonals are CHS members, with cross section between 508 x 40 mm at the lowest floors and 273 x 12.5 mm at the top, while the chord members have RHS, 250 x 300 mm with wall thickness of 25mm. The circular central core, which has constant diameter along elevation, does not contribute to the lateral resistance and rigidity, being a simple frame structure.

### 4.2. Hearst Tower

Also the Hearst Tower in New York was designed by Sir Norman Foster; the building, 46 stories and 183 meters tall, has a prismatic form and a rectangular floor plan, 48 x 37m and is built on an existent 6-storey building. The diagrid structure, creating the characteristic "diamond effect" in the façade, rises from 12 composite columns, which reach the tenth floor starting from the ground level. The diagrid module is 12.25 m wide and 16.54 m high, and covers four stories. The diagonal cross section are I shape, with maximum size W14x370 at the base of the diagrid (tenth level), while the megacolumns between the tenth and the ground level are concrete filled box section 1100 x 1100 x 10mm. [8]

### 4.3. Guangzhou West Tower

The Guangzhou West Tower, designed by Wilkinson Eyre architects, London with 103 stories and a height of 440m, is the tallest building in China and one of the tallest in the world. The building has a curvilinear shape along elevation and the floor plate is an equilateral triangle with round-corners, with side 65 m at the base, increasing to a maximum value of 65 m at approximately 1/3 of the way up the building, at which point the side begins to reduce, up to 43.5 m at the top. It has a composite structure, made by a central concrete core and perimeter diagrid structure, with the

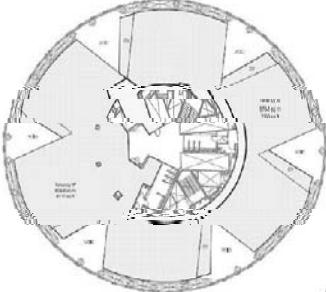

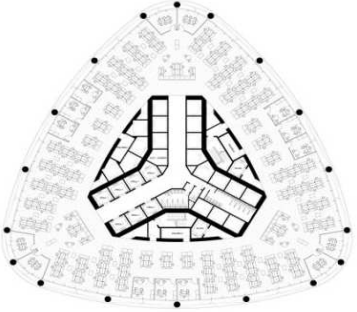
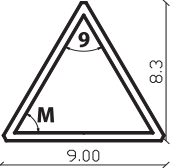
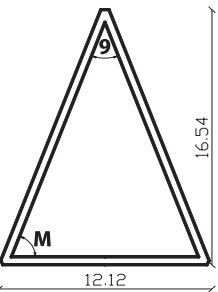
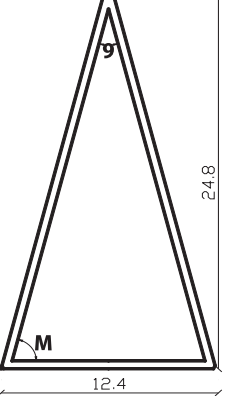
	Swiss Re		Hearst Tower		Guangzhou West Tower	
n° storey	40		46		103	
H [m]	180		183		440	
Plan shape						
L <sup>1</sup> <sub>max</sub> [m]	56		48		65	
L <sup>1</sup> <sub>min</sub> [m]	30		-		43.5	
L <sup>2</sup> <sub>max</sub> [m]	-		37		-	
L <sup>2</sup> <sub>min</sub> [m]	-		-		-	
H/L <sub>max</sub>	3.21		3.81		6.77	
H/L <sub>min</sub>	6.00		4.94		10.11	
H/L <sub>average</sub>	3.43		-		8.11	
A <sub>tot</sub> [m <sup>2</sup> ]	74300		79500		285000	
A <sub>l,max</sub> [m <sup>2</sup> ]	2476		1730		3074	
A <sub>l,min</sub> [m <sup>2</sup> ]	1885		1730		1580	
A <sub>core</sub> [m <sup>2</sup> ]	475	% A <sub>d</sub> /A <sub>max</sub> = 19% % A <sub>d</sub> /A <sub>min</sub> = 25%	350	% A <sub>d</sub> /A = 20%	880	% A <sub>d</sub> /A <sub>max</sub> = 29% % A <sub>d</sub> /A <sub>min</sub> = 55%
core – diagrid span [m]	d <sub>max</sub> = 31	d <sub>min</sub> = 24	d <sub>max</sub> = 31	d <sub>min</sub> = 24	d <sub>max</sub> = 16.6	d <sub>min</sub> = 6.8
Diagrid base module	 <p>H=8.3m L=9.0m θ=62° α=56°</p>		 <p>H=12..25m L=16.54m θ=70° α=40°</p>		 <p>H=24.8m L=12.4m θ=76° α=28°</p>	
Steel weight [t]	8358		10480		51310*	
Diagrid weight [t]	2423		3040*		14880*	
Unit steel weight [kN/m <sup>2</sup> ]	1.12		1.32		1.8	
Diagrid unit weight [kN/m <sup>2</sup> ]	0.32		0.38		0.52	

Table 1. Comparison among the three case studies - major data

	Swiss Re	Hearst Tower		Guangzhou West Tower
Dead load [kN/m <sup>2</sup> ]	4.45 [7]	4.45 (Assumed)		4.45 (Assumed)
Live load [kN/m <sup>2</sup> ]	Office: 3.00 [5] Store: 5.00 [5]	Office: 2.40 [6] Hall space: 4.80 [6] Mechanical space: 6.00[6]		Office: 3.0 [5] Hotel: 5.00 [5] Mechanical space: 6.00[5]
Code	Eurocode 1 [5]	ASCE 7-05 [6]		Eurocode 1 [5]
Wind base shear [MN]	31	x: 10	y: 14	140
Wind overturning moment [MNm]	2798	x:1042	y:1377	33234

Table 2. Loads assumed in the building analysis



Figure 5. Case studies; top left) Swiss Re; down left) Hearst Tower; right) Guangzhou West Tower

diagrid module expanding on six stories, 12.4 m wide and 24.8 m high. The diagonals are steel tubular members filled by concrete (CFST), with size ranging between 1080 x 55 mm at the first floor and 700 x 20mm at the top. The concrete core has a triangle shape with chamfered corners and fully participates to the lateral resistance up to the seventh floor, where it is eliminated, leaving place to a central giant atrium for the hotel which occupies the upper floors.

### 5. Analysis of the buildings

Both the formulae provided in paragraph 2 and finite element models have been utilized for assessing the structural behavior of the three buildings under gravity and wind loads.

In table 2 the values of dead, live and wind loads assumed in the analyses are provided. Due to lack of specific data, the equivalent static wind action has been computed according to Eurocode 1 [5] for the Swiss Re building and the West Tower, and according to ASCE 7-05 [6] for the Hearst

Tower. In the table, also the values of the global base shear and overturning moment due to wind action are provided.

In the following figures some comparisons between the FEM analysis results and the "hand calculation" results are given for the three case studies. For the sake of brevity, not all the analysis results are herein provided; in particular the following diagrams are reported: diagonal axial forces along the height due to gravity load, only for the Swiss Re building (figure 6a); diagonal stress level (i.e. axial demand to capacity ratio D/C) along the height due to gravity load for the three case studies (figure 6b, figure 7a, figure 8a); diagonals stress level at the base (z=0) due to combination of gravity and wind loads for the three case studies (figure 6d; figure 7b; figure 8b); lateral displacements along elevation for the three case studies (fig.9). From the first graphs (figures 6a, 6b, 7a, 8a) and from the comprehensive results reported in [9], it can be observed that the three structures under gravity load show diagonal stress levels ranging between 0.4 and 0.6, while under combined gravity plus wind loads (figures 6c, 6d, 7b, 8b) the diagonal stress levels at base are close to 1.0 for all the three buildings. In this load combination, the three towers assume a deformed configuration which suggests the prevailing cantilever behaviour, with top drift close to 1/500, thus confirming the high stiffness of this structural typology.

Finally, it is worth noticing that all the graphs reported in the above figures prove a very good correspondence between FEM and "hand calculation".

### 6. Conclusive remarks

In this paper an overview on the structural behavior of diagrid structures in tall buildings has been provided.

Starting from the evaluation of internal forces arising in the single triangle module under the effects of both gravity and wind loads, a discussion on the effects of the building form, as well as of the diagonal slope has been presented. The above considerations on the assessment of internal forces have been applied to three case studies, namely the Swiss Re Building in London, the Hearst Headquarters in New York, and the West Tower in Guangzhou, and the results have been compared to analogous results obtained through computer analyses. Some general conclusive remarks arise from (i) the assessment of the structural behavior, and (ii) the possibility of analyzing diagrid buildings, in a very pre-



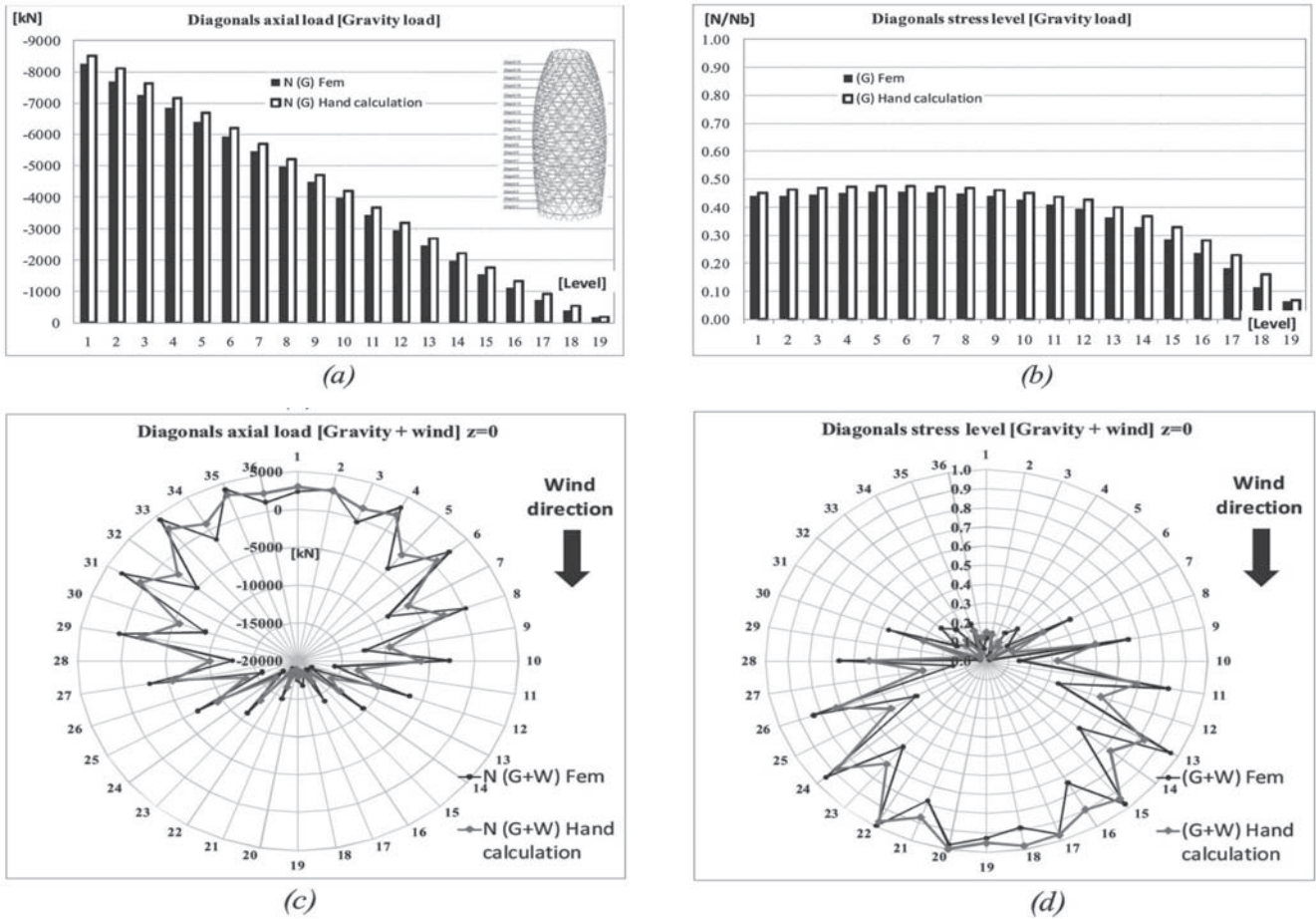


Figure 6. Swiss Re Building; a) Diagonals axial load due to G; b) Diagonals stress level due to G; c) diagonals axial load due to G+W; d) diagonals stress level due to G+W

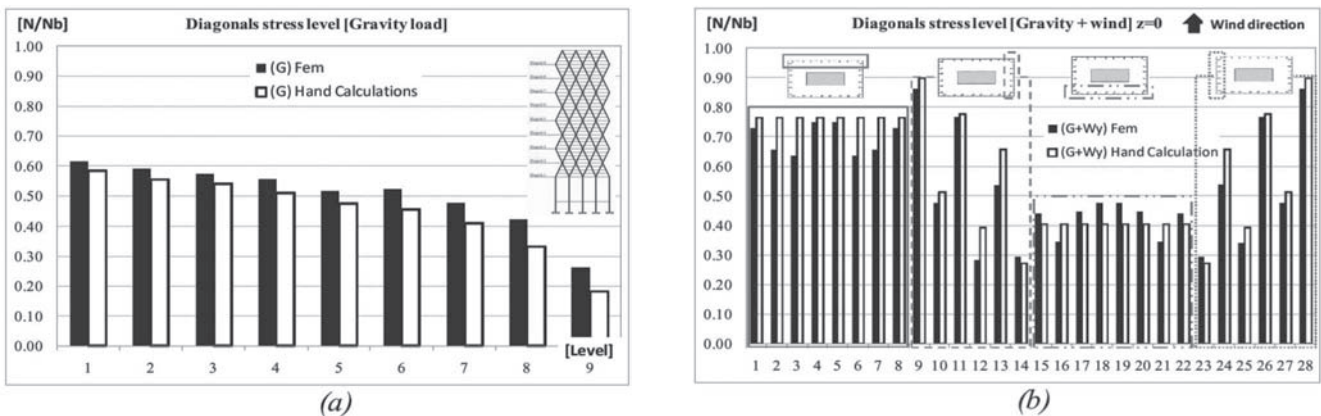


Figure 7. Hearst tower; a) Diagonals stress level due to G; b) Diagonals stress level due to G+W

liminary phase, through simple formulae.

Concerning the structural behaviour, three buildings show similar values of stress level in the diagonals (D/C ratio), both under gravity loads (around 0.50-0.60) and under gravity plus wind loads (close to 0.9-1.0). These values confirms that, thanks to the high rigidity of the diagonalised façade, the sizing of the steel members is mainly governed by strength criteria; as a matter of fact the total wind sway

is close the limit of  $H/500$ , quite universally assumed as a reference value in the design practice. This lateral stiffness, as well as the high torsional rigidity deriving from the tubular configuration of the building (i.e. the perimeter position of the diagrid system), also ensures a very good level of overall dynamic performance.

Other analysis results [9], not reported in this paper for the sake of brevity, suggest additional advantages of diagrid

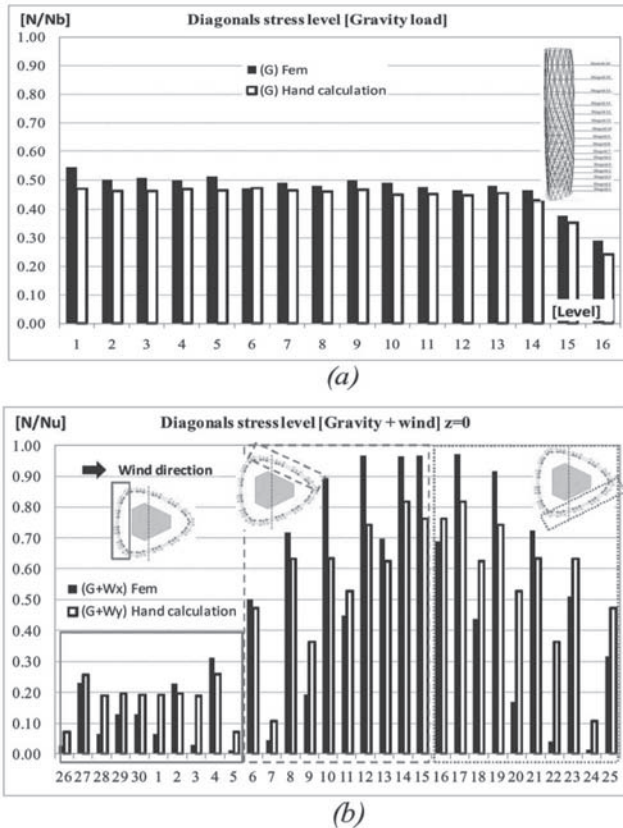


Figure 8. Guangzhou West tower; a) Diagonals stress level due to G; b) Diagonals stress level due to G+W

structures, mainly the high redundancy and resistance to progressive collapse. Such positive performance is coupled with a low unit steel weight of the diagrid system (in the range of 30 - 50 kg/sqm, for the three buildings), which confirms the great structural efficiency. The above aspects, as well as the possibility of adapting to nearly every building form, and of obtaining elegant façade appearances through an integrated architectural-structural design, are the main reasons for the increasing popularity of the diagrid systems.

Finally, the simplicity and straightforwardness of the structural system, made of triangulated frame units with members mainly working in axial force condition, allows for simplified "hand" analysis of the building with a good approximation level.

**Author Affiliation**

Maurizio Toreno<sup>1</sup>, Raffaele Arpino<sup>2</sup>, Elena Mele<sup>3</sup>, Giuseppe Brandonisio<sup>4</sup> and Antonello De Luca<sup>5</sup>

<sup>1</sup> Ph.D. Student, Department of Structural Engineering. University of Naples/Italy maurizio.toreno@unina.it

<sup>2</sup> Master Student, Department of Structural Engineering. University of Naples/Italy lello85@hotmail.it

<sup>3</sup> Professor, Department of Structural Engineering. University of Naples/Italy elenmele@unina.it

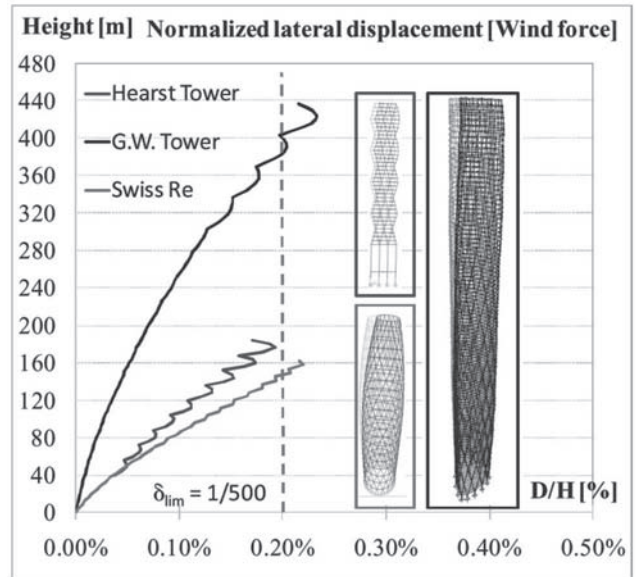


Figure 9. Normalized lateral displacement under wind force

<sup>4</sup> Ph.D., Department of Structural Engineering. University of Naples/Italy giuseppe.brandonisio@unina.it

<sup>5</sup> Professor, Department of Structural Engineering. University of Naples/Italy adeluca@unina.it

**References**

- [1] Weingardt R.G., Skyscraper Superstar - Leslie Earl Robertson, Structure magazine, p. 60-64 June 2007
- [2] Moon K.-S., Connor J.J., Fernandez J.E., Diagrid structural system for tall buildings: characteristics and methodology for preliminary design, The structural design of tall and special buildings N 16, p. 205-230 (2007)
- [3] Moon K.-S., Sustainable structural engineering strategies for tall buildings, The structural design of tall and special buildings (2008) N 17, p. 895-914 (2008)
- [4] Zhang C., Zhao F., Liu Y., Diagrid tube structures composed of straight diagonals with gradually varying angles, The structural design of tall and special buildings (2010), Article first published online: 11 Mar 2010
- [5] UNI ENV 1991 Eurocode 1, Basis of design and actions on structures (2004)
- [6] ASCE 7-05, American Society of Civil Engineers, Minimum design loads for buildings and other structures (2006)
- [7] Munro D., Swiss Re Building London, Nyheter om stålbyggnad N 3, p. 36-43 (2004)
- [8] Rahimian, A., Eilon, Y. Hearst Headquarters: Innovation and Heritage in Harmony. CTBUH 8th World Congress (2008)
- [9] Arpino R., Diagrid structures for tall buildings, Thesis (in Italian) (2010)

# Development of Typical Ceiling System Seismic Fragilities

Giacomo Paganotti<sup>1</sup>, Rajesh P. Dhakal<sup>2</sup>  
and Gregory A. MacRae<sup>3</sup>

## Summary

The failure of suspended ceiling systems has been one of the most widely reported types of nonstructural damage in past earthquakes. In order to understand this risk and develop mitigation strategies a small project on non-structural damage was recently funded by the FRST Natural Hazards Platform at the University of Canterbury. This particular project concentrates on two ceiling systems which are commonly used, or applicable, to NZ. This paper addresses the development of fragility functions for the ceiling systems based on component fragilities which have been obtained from experimental testing of USGTM ceiling components. The ceiling system fragility is obtained through Monte-Carlo analysis using in-plane finite element analysis. Demand parameters include absolute acceleration and displacement. The effect of rigid and flexible sprinklers is also investigated. It is shown that the acceleration resistance is dependent on the ceiling size. This information is being used directly to estimate both ceiling damage and loss to overall building structures.

## Keywords

Ceilings, experimental testing, fragility curves, Monte Carlo simulation.

## Theme

buildings – ceiling – earthquake – steel.

## 1. Introduction

Seismic damage to ceilings can cause significant downtime and economic loss in addition to life safety risk. In order to be prepared for such natural disasters, it becomes essential to reasonably estimate, predict and mitigate the risks associated with these potential losses. Figure 1 represents how an earthquake may affect a structure. Movement at a fault creates ground motion within the surrounding rock. This motion travels, as waves, to the site of the structure. These waves induce movement in the subsoil. Under large enough excitation all structures will undergo damage. As a result of the ensuing damage, decisions are based on the available information to minimise the effect of losses.

Extensive research has been carried out in the past on the seismic performance of structural elements including beams, columns, frames and floors. Although this is clearly important, in many cases for life safety and damage, significant loss can result from the seismic effects on non-structural components of major structures, a relatively untouched area of research.

Damage sustained to non-structural elements can often make up a substantial portion of the overall building losses. These losses, in terms of damage, death and downtime, can be measured in dollar terms (at least by the insurance industry). Non-structural damage includes damage to all contents, partition walls, ceilings and other components of the building, and can be caused by drift, acceleration and displacement. Of particular interest, for this project, is damage to ceilings and suspended ceiling systems as this can not only be expensive but very destructive to contents and dangerous for people in the building. Some ceilings, particularly suspended systems, demonstrate an intermediate degree of attachment to the structure meaning that they can be sensitive to drift, acceleration and displacement responses.

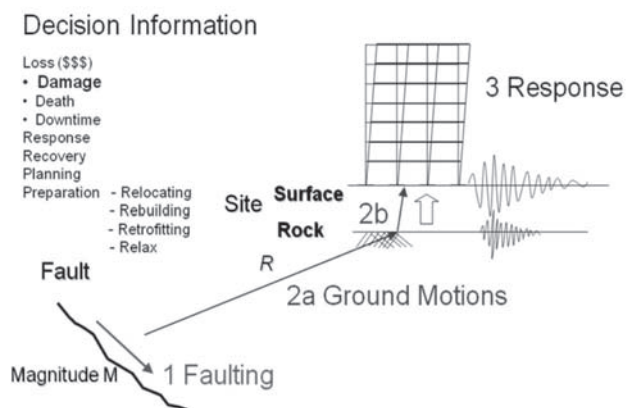


Figure 1. Earthquake Decision Information (MacRae, [8])

As shown in Figure 2, non-structural elements and building contents make up around 50%-70% of the total building cost in most buildings (Taghavi and Miranda [10]). Hence investigating earthquake effects on building non-structural elements is important. The 2010 Canterbury/Darfield earth-



quake has also shown that non-structural components and contents falling from height may threaten life safety. Also, Bradley [4] showed that for a 10 storey reinforced concrete office building, ceiling damage makes up 14 percent of the total damage costs. While research has been carried out on suspended ceilings, most of it has concentrated on testing of full suspended ceiling systems rather than ceiling system members. Additionally, existing research has not addressed methods for analyzing ceiling systems. As a result, there is no robust documentation showing the level of earthquake under which no damage is expected for a range of commonly used ceiling systems or a method for analysis of different suspended ceiling configurations.

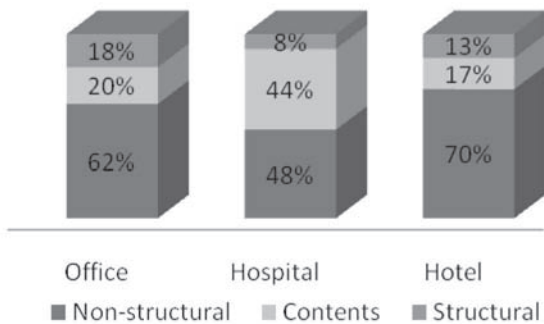


Figure 2. Building Type-Cost Breakdown (after Taghavi and Miranda [10])

The aims of this research are:

1. Evaluate capacities of USG(TM) ceiling components under different actions.
2. Develop a methodology for evaluation of ceiling fragility.
3. Assess the effect of sprinkler on ceiling fragility.

## 2. Typical suspended ceiling system construction

USG(TM) and Armstrong(TM) are two large manufacturers of suspended ceiling systems. Both of these manufacturers have carried out large scale testing on their products. This has led to the development of seismic resistant suspended ceiling systems and the publication of guidelines specific to their products. However, these tests conducted by the

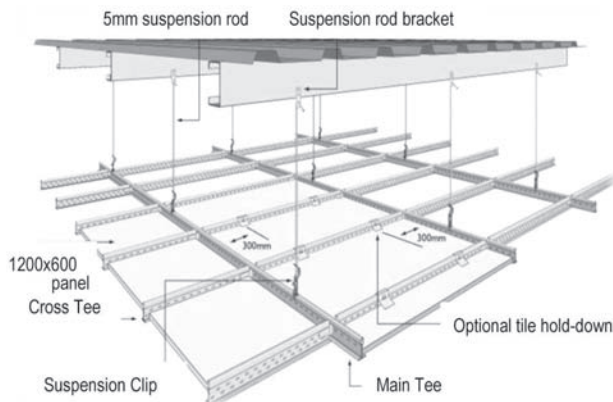


Figure 2. Typical ceiling configuration (based on Rondo, [09])

manufacturers and the results obtained have not been published. In this paper, the results for the USG(TM) Donn ceiling system are presented (USG Interiors [11]).

## 3. Tests

A series of tests devised to verify the strength of typical suspended ceiling components are described. They involve establishment of in-plane tension and compression capabilities of various section types, shapes and sizes. The availability of simple and reliable testing techniques suitable for seismic qualification of ceiling elements is likely to promote their continued and expanded use in buildings and industrial structures; potentially leading to less seismic damage than has been experienced in the past. Since analytical methods are generally not applicable to study suspended ceiling systems and data collected during past earthquakes are not suitable for fragility characterization, experimental methods represent the best and most reliable technique to obtain fragility curves for suspended ceiling systems. Hence, in this project it is decided to test different types of members and connections of a suspended USG(TM) ceiling system under monotonic loading. Table 1 presents a summary of all component tests conducted in this study. As can be seen in the table, each test is repeated 10 times so that the results could be statistically interpreted. From the tests, information on ceiling component strengths are gained, which are used to produce fragility curves for individual ceiling elements for various failure modes in terms of displacement/force.

No	Components	N° Tension	N° Compression	N° Shear
1	Cross Tee Members	10	10	
2	Cross Tee Members	10	10	
3	Wall Angle Members	10	10	
4	Hanger wide Membrs	10		
5	Hanging Connections	10		
6	Main Beam Splices	10	10	
7	Cross Tee Connection	10	10	10
8	Main Beam to Wall Angle	40		
9	Wall Angle to Wall	10		

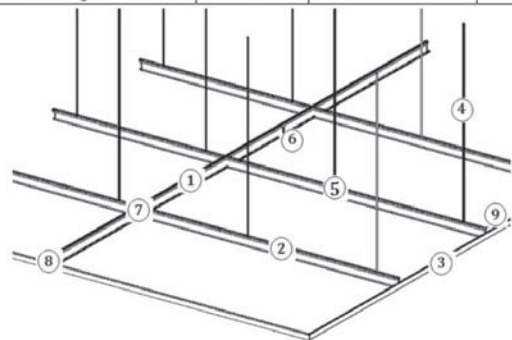


Table 1. Summary of Component Tests.

Efforts were made to use standard test methods. Unfortunately a code with test procedures for all types of components is not available. The tensile tests for the members are standardized by AS/2785:2009 [1] or C635-07 [02]. However there is no standard suggesting methods to test the



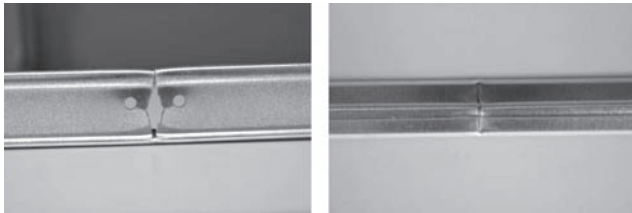


Figure 4. Member failure mode in tensile tests

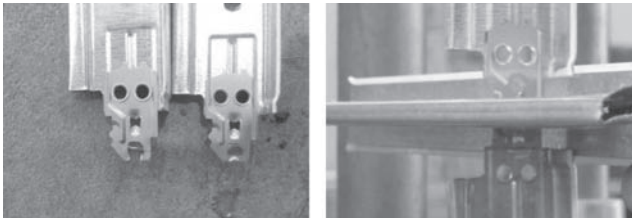


Figure 5. Failure mode of connection in the tensile test



Figure 6. Failure mode in a compression test specimen

connections, which are likely to be the weakest part of the ceiling system. Also for compression, there is no specific test Standard, and the design of the experiment is very important because the results could be very different with a different configuration. Hence, a rig was constructed which not only maintains the joint position during the test, but also allows for the compressive action to take place without restraining the system too greatly, as this would potentially give higher values. Typical failure modes observed in the tension (member and connection) and compression tests are shown in Figures 4-6.

During an earthquake the ceiling moves and the rivet connecting the grid to the wall angle is stressed. Due to this it is possible that the acceleration fractures the rivet, as shown in Figure 7, leading to collapse of tiles. The breaking of connections can cause the downfall of many tiles, as witnessed in the library at the University of Canterbury during the September 4 Darfield earthquake (MacRae and Dhakal, [9]).



Figure 7. Failure mode in the rivet connection between the main beam and the wall angle

According to Luco and Cornell ([6]), the “median<sub>x</sub>” and “dispersion  $\sigma(\ln x_i)$ ” are more reasonable measures to describe failure rather than the “average” and “standard deviation” Hence, results of the 10 tests were used to calculate the median and dispersion, which were used to obtain cumulative distribution function for the components, to be used in the analysis to follow. For instance, Figure 8 shows the fragility curves for the tension failure of the main beam and the cross tee based on the results of the tension tests. As can be seen in the figure, the median tensile capacity (i.e. 50% the probability of failure) is 8.5 kN for the cross-tee and 9.4 kN for the main beam. Similarly, for all the tests it is possible to plot a fragility curve like this.

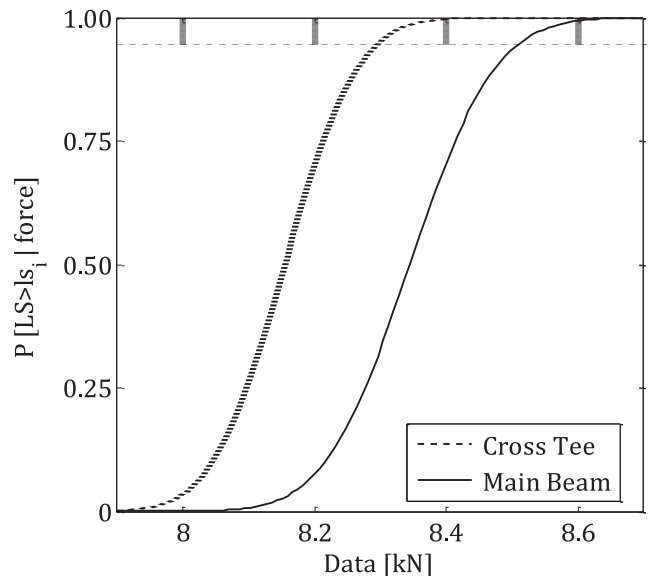


Figure 8. Member fragility curves obtained from the tensile tests.

#### 4. Analysis

The development of fragility curves generally involves the use of both mathematical modeling and physical observations. The likelihood of a ceiling failure can be probabilistically obtained if analyses are conducted using a suite of floor acceleration records. However, this is too complex for most designers. Also, it would be difficult to know if an error had been made in the analyses. For this reason, a different method is used in this study.

In parallel with laboratory tests, a Monte Carlo analysis is carried out to derive fragility curves for each component of the ceiling system. Monte-Carlo Simulation involves “sampling at random” to simulate a large number of experiments in order to statistically interpret the result.

The ceiling system is modelled as a two-dimensional grid subjected to monotonic loads to represent the effect of in-plane ceiling acceleration. A finite element analysis program, Ruamoko (Carr [5]), is used to carry out the modelling and analysis of the grid. The forces in the ceiling component are calculated and compared with the capacities deter-

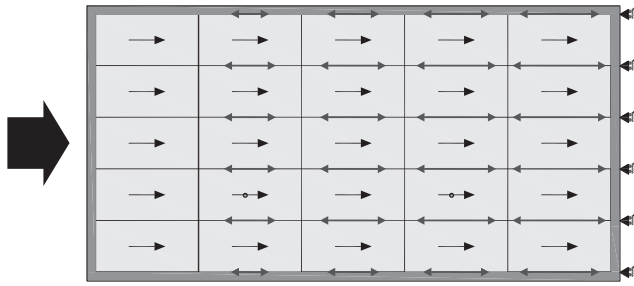
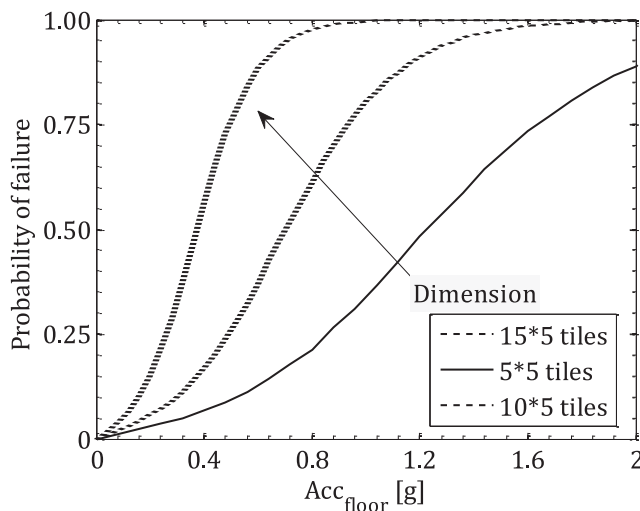


Figure 9. Model used to represent the ceiling

mined by testing. This allows the critical elements in different ceiling configurations to be identified. Monte-Carlo analysis is carried out on each case study ceiling using the strength distribution of the individual components and varying the applied loads. This analysis provides a spread of strengths for each ceiling, which provides the basis of fragility curves. In this study, fragility curves are prepared for USGTM ceiling system by plotting the probability of reaching or exceeding a limit state versus the corresponding median intensity measure.

The main steps of this analysis are:

- a) Choose a typical ceiling configuration;
- b) Obtain fragility curves for each component and connections by the tests;
- c) Perform a structural analysis for a specific value of intensity measure IM;
- d) Compute the force in all elements and connections for the IM selected;
- e) Generate a Monte Carlo analysis of strengths in all components;
- f) Compare strength and demand for each connection to see if any members fail;



- g) Repeat step e) many times to obtain the probability of failure for that IM;
- h) Repeat steps from d) to g) with different levels of IM to obtain a CDF, or ceiling fragility curve for failure.

Figure 9 shows a typical load path for this type of ceiling installation and the components/connection of this load path. Movement normal to the direction shown will be resisted in a similar manner to that shown. Thin green arrows represent induced inertial load from the drop in panels. These are actually applied to the cross beams beside the joints. The thick red arrows indicate load paths through the suspended ceiling members. The shear in the member perpendicular to the load is also considered. When sprinklers are present within some of the panels; the load path differs in the sense that the sprinklers will induce additional restraints once the gap between the sprinkler and the panel closes. In Ruaumoko, beam elements were used for modelling the cross tee and the main beam. The properties (i.e. Young Modulus, Shear Modulus) of these elements were assumed based on the material characteristics and the dimensions, area and moment of inertia were found by measurement and calculation. To model the sprinkler, contact elements were used, which takes into account the gap between the tile and the sprinkler. The stiffness of the contact elements is the same as that of the sprinkler perpendicular to the ceiling.

As explained previously, finite element analyses were conducted on a typical NZ ceiling system without and with sprinklers (with different gaps varying between 0 and 20mm). Comparing the resulting member/connection forces to their strengths as randomly picked through a Monte Carlo process allows evaluation if a member or connection will fail for that case. Repeating this for a large number of Monte Carlo simulations gives a probability of failure of the ceiling system. Fragility curves derived through this process for

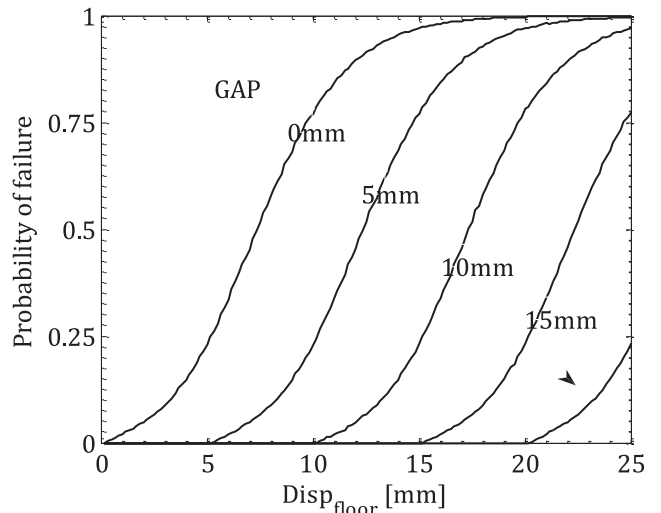


Figure 10. Fragility curves (i) (with the floor acceleration as IM) for different ceiling sizes and no sprinkler (Left); (ii) (with the displacement as IM) for different gaps between the sprinkler and the panel (Right).

three different ceiling sizes (without any sprinkler) are shown in Fig 10a. As expected, the bigger ceilings are more fragile; because the induced forces in members next to the restrained end increase with increasing number of panels whereas the strength remains the same; thereby resulting in a higher likelihood of failure. The effect of rigid sprinkler on the ceiling is expressed through fragility functions (in terms of floor displacement as the intensity measure) in Fig 10b. As can be seen, the gaps between a rigid sprinkler and the ceiling panel shift the fragility curves by the amount of the gap. It is shown that rigid sprinklers without sufficient gap cause poor ceiling performance. The effect of sprinkler flexibility is not investigated here, but it is obvious that a reasonably flexible sprinkler does not induce noticeable additional restraints to the ceiling system; and hence the fragility function of such ceilings is the same as that of the ceiling without any sprinkler.

## Conclusions

Tests were conducted and analyses were undertaken to obtain elements and ceiling seismic fragilities for the USG(TM) Donn ceiling system. In particular, it was shown that:

1. The most critical ceiling element was the compression connection at the ceiling boundary.
2. A methodology for developing seismic fragility was developed. It was shown that the median floor acceleration that caused ceiling failure was around 1g for a ceiling of dimension 5\*10 tiles. This acceleration decreases with an increase in ceiling size.
3. The presence of stiff sprinklers made other elements critical and significantly reduced the floor acceleration required to cause failure.

## 5. Acknowledgements

The authors gratefully acknowledge the financial support of the New Zealand Foundation for Research in Science in Technology who funded this work through their Natural Hazards Programme, the University of Canterbury New Zealand, as well as the Politecnico di Milano Italy which supported the first author. This paper is complementary to the paper presented in Auckland at the PCEE 2011 Conference in April 2011, on the performance of Armstrong(TM) ceiling system.

In particular special thanks to Tiziana Poli and Alessandro Palermo for the help given to the first author.

## Author Affiliation

Giacomo Paganotti<sup>1</sup>, Rajesh P. Dhakal<sup>2</sup> and Gregory A. MacRae<sup>3</sup>

<sup>1</sup>Master Student, Department of Building Environment Science & Technology, Politecnico di Milano, Milan, Italy. giacomo.paganotti@mail.polimi.it

<sup>2</sup>Associate Professor, Department of Civil and Natural Resources Engineering, University of Canterbury, Christchurch, New Zealand. rajesh.dhakal@canterbury.ac.nz

<sup>3</sup>Associate Professor, Department of Civil and Natural Resources Engineering, University of Canterbury, Christchurch, New Zealand. gregory.macrae@canterbury.ac.nz

## References

- [1] AS/NZS 2785:2000. Suspended Ceiling – Design and Installation.
- [2] ASTM C635-07. Standard Specification for the Manufacture, Performance, and Testing of Metal Suspension Systems for Acoustical Tile and Lay-in Panel Ceilings.
- [3] BS EN 13964:2004. Suspended Ceilings - Requirements and test methods.
- [4] Bradley B., 2009. "Structure-Specific Probabilistic Seismic Risk Assessment". PhD Thesis, University of Canterbury, New Zealand.
- [5] Carr A.J., 2004. RUAUMOKO: Inelastic Dynamic Computer Program, Computer Program Library, Department of Civil Engineering, University of Canterbury, Christchurch, New Zealand.
- [6] Luco, N., Cornell C. A., 1997. "Numerical Example of the Proposed SAC Procedure for Assessing the Annual Exceedance Probabilities of Specified Drift Demands and of Drift Capacity", Internal SAC Report.
- [7] MacRae G. A., 2006. "Decision Making Tools for Seismic Risk", Proceedings of the New Zealand Society of Earthquake Engineering Annual Conference, Paper 28, Napier.
- [8] MacRae G. A, Hair J. and Dhakal R. P., 2011. "Ceiling Damage In The 2010 Canterbury Earthquake", 8cucee Conference Proceedings, 8th International Conference on Urban Earthquake Engineering, March 7-8, 2011, Tokyo Institute of Technology, Tokyo, Japan
- [9] Rondo Key-Lock, 2009. Concealed Suspended Ceiling Systems, Auckland, New Zealand.
- [10] Taghavi, S. and Miranda, E., 2003. "Response Assessment of Nonstructural Building Elements". Report PEER 2003/05, Pacific Earthquake Engineering Research Center, University of California, Berkeley, 96 pp.
- [11] USG INTERIORS, 2009. Donn Brand Grid Suspension Systems, Chicago.

# On the Accuracy of Response Spectrum Analysis in Seismic Design of Concrete Structures

**Fabio Biondini<sup>1</sup>, Andrea Titi<sup>2</sup> and  
Giandomenico Toniolo<sup>3</sup>**

## Summary

The current seismic design of buildings is based on the use of response spectra, where the storey forces are evaluated through a linear dynamic modal analysis. SRSS or CQC combinations are used to represent the overall effects of the vibration modes, depending on the difference between adjacent periods. The results of this approach are assumed to be generally conservative and suitable for design. However, in this paper it is shown that for multi-storey buildings these considerations may not apply.

A precast three-storey building with different types of connections (hinged, hybrid and moment resisting) is studied in order to highlight the importance of the higher vibration modes for systems with different structural connections. The results show that storey forces obtained by modal analysis are significantly lower with respect to those predicted by non-linear time history dynamic analysis, even if the overall displacements are comparable.

This investigation has been developed during the design process of the structural prototype of a multi-storey precast building for pseudo-dynamic tests at ELSA Laboratory (JRC, Ispra), within the scope of FP7-SME-2007-2 "SAFECAST" project, to check the compatibility of the storey forces with the capacity of the testing equipment.

## Keywords

Modal analysis, nonlinear dynamic analysis, seismic design, reliability.

## Theme

Buildings – analysis – earthquake – concrete

## 1. Introduction

The seismic behavior of a structural system, as a multi-storey concrete frame, can be evaluated through different methods, with different computational cost and refinement. In particular, the current seismic design of structures is typically based on the dynamic modal analysis with response spectrum, where the contribution of each mode is evaluated through the solution of an eigenvalue problem, and

the overall effects are taken into account by means of modal combination, such as SRSS (square root of the sum of the squares) or CQC (complete quadratic combination), depending on the difference between adjacent periods. The estimation of storey forces allows the evaluation of the bending moments at the ends of columns and, consequently, the design of reinforcement.

In general this method has a low computational cost and it is considered conservative with respect to more refined methods of analysis such as nonlinear dynamic analysis. However, in this paper it is shown that for multi-storey buildings these considerations may not apply. This is shown with reference to a three storey precast building.

The study is supported by the European project Grant No. FP7-SME-2007-2 "SAFECAST", which aim is to investigate the seismic behavior of precast structures with different connections. Actual building codes, such as Eurocode 8 [CEN, 2004] and Italian National code (DM 14/01/2008) give the same importance to the different systems of connection, both hinged and emulative. This statement is justified after the results of past experimental and numerical investigations, carried out within the European research projects "ECOLEADER" and "GROWTH" [Biondini and Toniolo, 2009]. These studies are focused on the evaluation of the global ductility related to singlestorey precast industrial buildings with hinged connections, comparing it with the ductility related to cast-in-place structures.

"SAFECAST" project includes a pseudo-dynamic tests on a multistorey prototype that will be performed at the European Laboratory for Structural Assessment (ELSA), located at Ispra (Italy). The prototype represents a typical precast building. The aim of the experimental tests is the investigation of the seismic behavior of the structure for different systems of connections, considering the maximum capacity of the equipment. For the design of the structure and the sequence of pseudo-dynamic tests preliminary numerical analyses are performed to estimate storey displacements and forces.

The role of connections in the performance of the building is explored considering different structural schemes where the beam to column connections are hinged or moment resisting. The comparison between the results shows that,



even if storey displacements are comparable, storey forces evaluated through the dynamic modal analysis with response spectrum are significantly lower than those predicted by nonlinear dynamic analysis.

The results obtained highlights how the dynamic modal analysis with response spectrum, that is based on a linear elastic analysis where the energy dissipation is taken into account through a force-reducing behaviour factor  $q$ , is a conventional method not able to predict in a reliable way the actual seismic behaviour of the structure. This approach is however generally safe when the structural elements are assumed to have an appropriate ductility.

## 2. Description of the prototype

In the following the seismic performance of a three storey precast building subjected to pseudo-dynamic tests at the European Laboratory for Structural Assessment of the Joint Research Center of the European Community (ELSA) is investigated to explore the role of connections. Three structural schemes, namely Model 1 (frame system with connections), Model 2 (frame systems with emulative connections only at the top floor) and Model 3 (frame system with emulative connections) are considered. Different design solutions have been investigated with respect to the maximum capacity of the testing equipment. In particular the maximum capacity of the actuators, connected to the reaction wall at each storey of the building, is equal to 200 tons. In Figures 1-5 the original design of the prototype, calibrated with this value, is shown.

Different approaches have been used to estimate internal actions. First of all a simple translatory equilibrium is considered where the storey forces depend on the resisting moment at the base of the columns and have a linear growth. The design is then based on a dynamic modal analysis with response spectrum considering a peak ground acceleration  $a_g=0.25g$  (seismic zone 2 in the national design code). Storey forces so obtained are however significantly lower than those predicted by a subsequent nonlinear dynamic analysis. For this reason the original prototype has been reduced in size, considering different solutions and for each of them evaluating the corresponding storey forces. In the following the different solutions denoted Prototype A, Prototype B and Prototype C, are considered.

Prototype A (original scheme) has three bays in the main direction and two in the orthogonal one, with the same length equal to 7 m. This is a three storey building, with interstorey heights respectively equal to 3.3, 3.2 and 3.2 m. More details are shown in Figures 1-5. The cross-section of the columns is constant along the height, with size 50x50 cm and reinforced with 8Ø20. In the main direction there are hollow core beams, with a width of 2.25 m. Th two ribs of the beam have a thickness of 30 cm. The beams are supported by lateral corbels with the same thickness of the floor.

In the orthogonal direction there are prestressed slabs, different at each storey. At the first floor there are box ele-

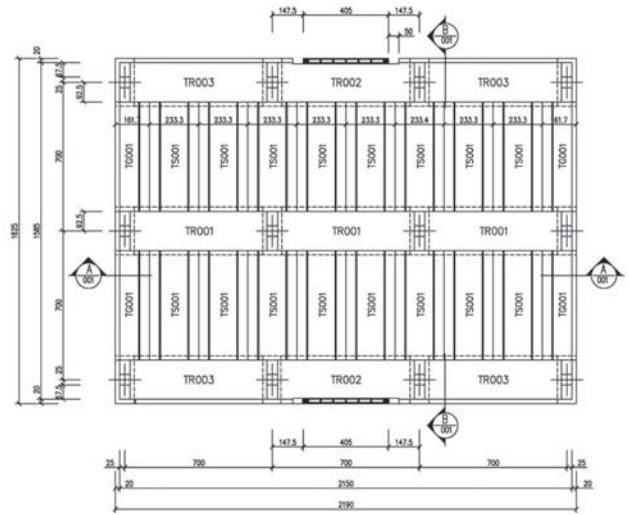


Figure 1: Plan view of the first floor, Prototype A

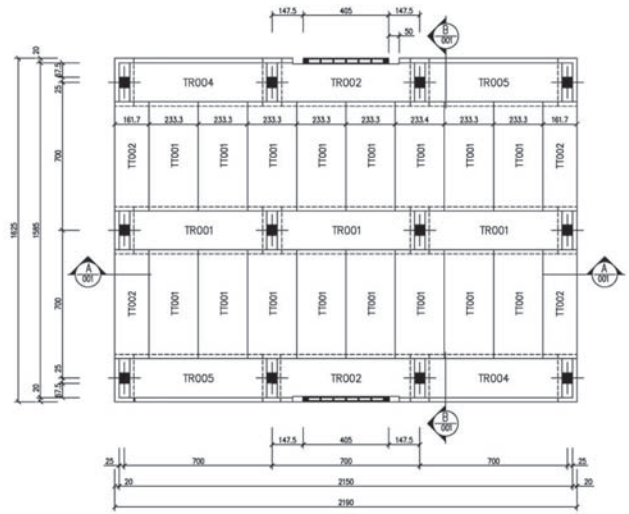


Figure 2: Plan view of the second floor, Prototype A

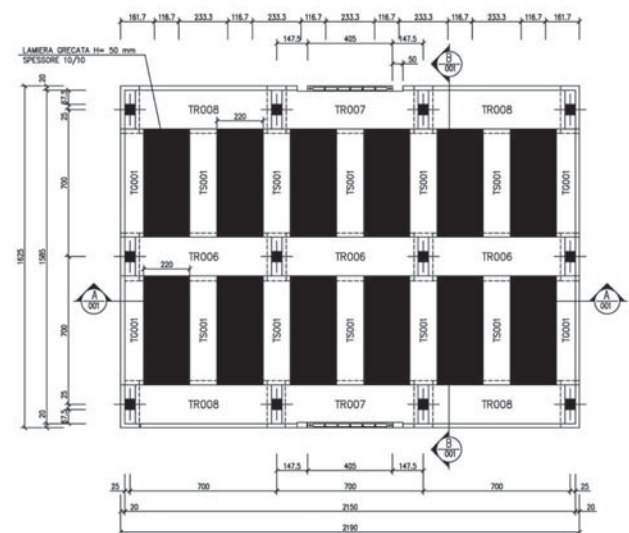


Figure 3: Plan view of the third floor, Prototype A

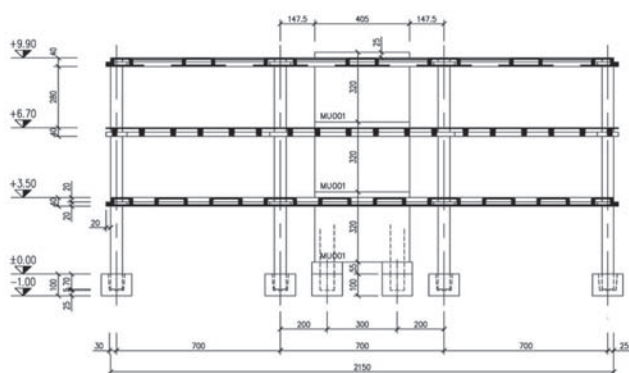


Figure 4. Elevation view, section A-A, Prototype A

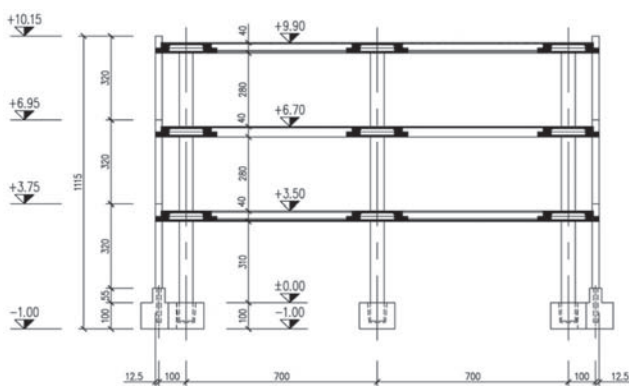


Figure 5. Elevation view, section B-B, Prototype A

ments connected one to each other with welded angles. At the second floor there are TT elements connected again with welded angles while at the top floor there are the same elements of the first storey but not connected.

Material used are concrete C45/55 and steel B450C, with strength equal to  $f_{ck}=45$  MPa and  $f_{yk}=450$  MPa.

In Prototype B the length of the beams and slabs is reduced from 7 to 6 m. In Prototype C one bay along the main direction is removed, with beams and slabs preserving the original length of 7 m. It was found that the latter solution satisfies with sufficient margin the limitations imposed by the maximum capacity of the actuators.

### 3. Experimental program

The prototype will be subjected to pseudo-dynamic tests at the European Laboratory for Structural Assessment (ELSA) [Donea et al., 1996]. The laboratory has a 16x21 m reaction wall, see Figure 6, able to impose high forces (~thousands of kN) appropriate to induce significant deformations and relevant damage on full-scale prototypes.

The methodology implemented to control the tests is based on a fully digitalized system, with distributed units connected to the main computer by fiber optics. The relevant parameters are measured by digital optic transducers while restoring forces are measured by load cells allocated within the actuators, which maximum capacity is 200 tons.

In this investigation seismic input is represented by the East-West component of the modified Tolmezzo accelerogram, Figure 7 (a), with a total duration of 12 s. The corresponding spectrum matches very well the EC8 response spectrum for a soil class B, Figure 7 (b). The selection of the accelerogram is based on an intensity index that measures the capacity of the earthquake to induce structural damage in the range of intermediate periods, [Fayfar et al., 1990].

For each structural scheme pseudo-dynamic tests will be performed. The first scheme (not presented here) has shear walls connected to the stories of the structure. The walls will be subsequently removed in order to test the frame structure, such as Model 1 (frame with hinged connections), Model 2 (frame with emulative connections at the top floor) and Model 3 (frame with emulative connections at each floor).

For the unbraced systems the level of acceleration is chosen in order to induce significant deformations but not excessive damage. The prototype is designed for a PGA equal to 0.25 g, related to the collapse limit state (or life preservation in the Italian code), for a soil class B with an amplification factor S equal to 1.2. The pseudodynamic tests will start with a level of acceleration equal to 0.12 g, considering it the threshold for the elastic behavior (or for a limited damage limit state). On the basis of these results the level of acceleration will be increased to fully activate the nonlinear behavior of the structure, without severe damage in order to perform the tests also on the other structural schemes. Finally on the last scheme (Model 3) the level of acceleration will be increased (approximately up to 0.25 g) in order to induce a severe damage on the structure. A series of cycle tests with increasing amplitude up to the collapse of the prototype will be finally carried out.

### 4. Numerical simulation

Numerical simulations are performed considering a 3D finite element model. Gravity loads are the only selfweights of structural elements. Seismic masses are instead simu-

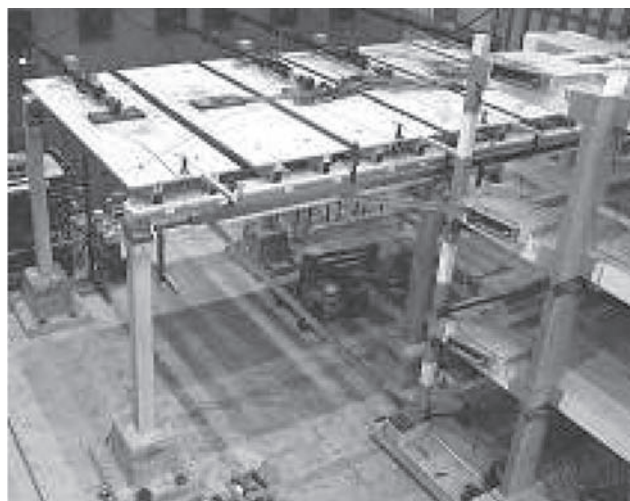


Figure 6. Reaction wall of ELSA laboratory (with the prototype of the research program GROWTH).

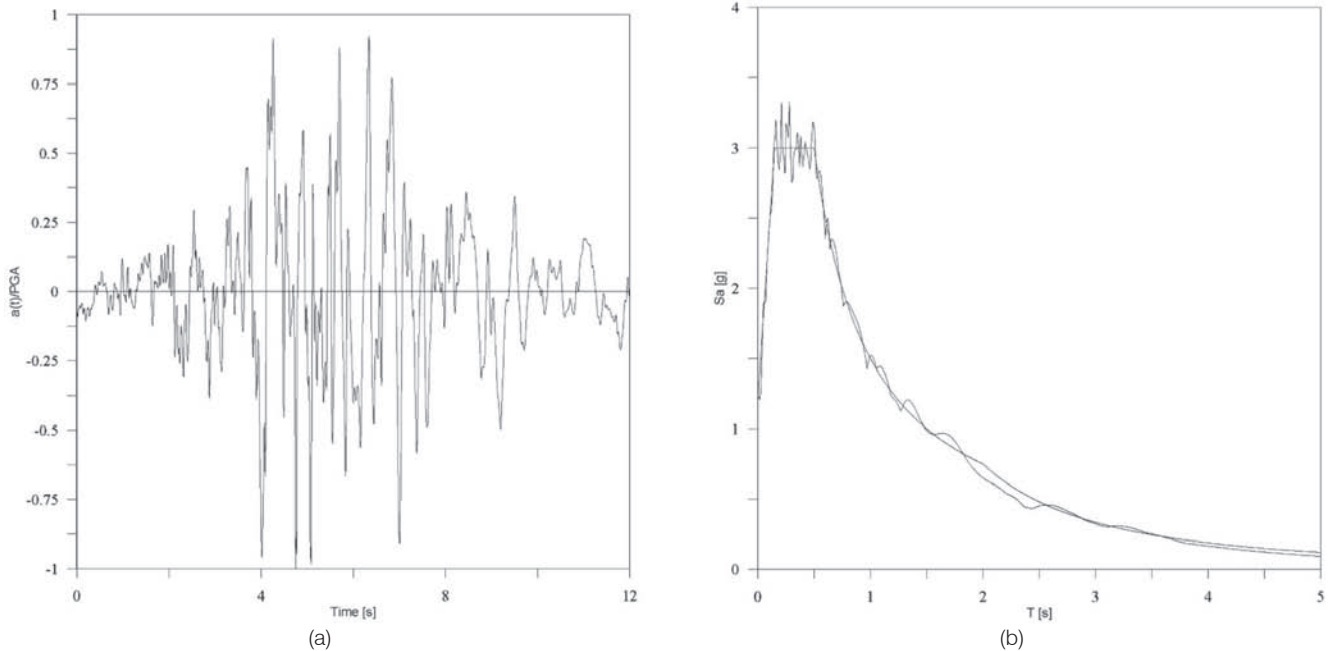


Figure 7. (a) Tolmezzo accelerogram, (b) response spectrum compared with EC8 spectrum for soil class B

lated in order to reproduce the dynamic properties of the structure in the actual service conditions. For this reason dead loads and part of the live loads are added. The following hypotheses hold:

- Rigid floor at each storey;
- Masses lumped in the centre of mass, overlaps to the centre of gravity of each floor. Each mass has two translational and one rotational degrees of freedom;
- Self-weight of slabs is distributed to the beams considering the corresponding influence areas;
- Beam to column connections are modeled as hinge connections or moment resisting connections, depending on the structural scheme;
- Columns are clamped to the ground.

#### 4.1 Modal analysis

For each prototype a modal analysis is performed, considering the three different structural schemes. Table 1 shows

periods and participating masses. As can be seen the contribution of higher modes is relevant, in particular for Model 1 (frame with hinged connections).

The evaluation of displacements and storey forces is based on a response spectrum for soil class B, soil factor  $S$  equal to 1.2 and 5% of viscous damping. The peak ground acceleration is 0.25 g and a behavior factor equal to 3 is chosen. To simulate in a roughly way the stiffness degradation due to concrete cracking the flexural stiffness of the columns is halved.

Displacements are evaluated in the center of mass and storey forces are expressed as follows:

$$F_{si} = \Gamma_j m \phi_j S_{ad}(T_j, \xi_j) g \quad (1)$$

where  $\Gamma_j$  is the participating factor,  $m$  is the mass matrix,  $\phi_j$  is the eigenvector of mode  $j$  e  $S_{ad}$  is the corresponding value of the design spectrum. The contribution of each mode is combined by means of the SRSS rule combination, since the periods of adjacent modes are sufficiently different.

	Mode	Prototype A		Prototype B		Prototype A	
		T [s]	Mass [%]	T [s]	Mass [%]	T [s]	Mass [%]
Model 1	I	1.71	71.2	1.51	71.2	1.57	71.3
	II	0.28	23.2	0.25	23.3	0.26	23.1
	III	0.11	5.5	0.10	5.6	0.10	5.5
Model 2	I	1.00	82.5	0.89	82.6	0.93	82.5
	II	0.19	14.8	0.17	14.8	0.18	14.7
	III	0.09	2.7	0.08	2.7	0.09	2.8
Model 3	I	0.43	89.1	0.37	89.4	0.40	88.7
	II	0.15	9.4	0.13	9.2	0.14	9.6
	III	0.09	1.5	0.08	1.4	0.09	1.6

Table 1. Periods and participating masses for all the prototypes

	Storey	Prototype A		Prototype B		Prototype A	
		$\Delta$ [cm]	V [kN]	$\Delta$ [cm]	V [kN]	$\Delta$ [cm]	V [kN]
Model 1	III	21.54	272	19.10	224	19.86	195
	II	11.63	333	10.31	253	10.72	233
	I	3.61	341	3.19	245	3.32	234
Model 2	III	11.98	342	10.58	292	11.10	250
	II	9.04	313	8.01	271	8.34	231
	I	3.41	322	3.03	259	3.14	223
Model 3	III	4.26	593	3.20	461	3.79	410
	II	3.37	570	2.54	450	2.99	395
	I	1.73	390	1.32	308	1.986	195

Table 2. Displacements and storey forces evaluated through modal analysis for all the prototypes

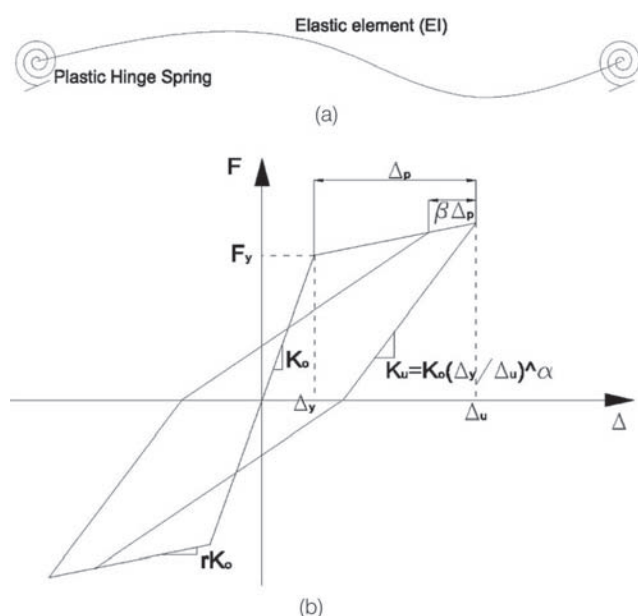


Figure 8. (a) Giberson model, (b) Takeda hysteretic law

Table 2 shows displacements and storey forces for all the prototypes. The amplitude of maximum displacements of the prototypes is similar, while significant differences can be found in terms of storey forces. Based on these results Prototype C represents the suitable choice to perform the experimental tests.

As already indicated by modal periods and participating masses, the results of modal analysis with response spectrum show, especially for Model 1, the relevant effects of

higher modes, because the distribution of forces along the height is different to that related to the fundamental mode.

### 4.2 Nonlinear dynamic analysis

The results of modal analysis with response spectrum are verified through nonlinear dynamic analyses. The maximum amplitude of the accelerogram is scaled to  $1.2 \times 0.25 = 0.3$  g.

Nonlinearity is concentrated at the ends of columns and beams, Figure 8 (a), using the model implemented in Ruamoko [Carr, 2001], where plastic hinges follows the Takeda hysteretic law, Figure 8 (b). The parameters  $\alpha$  e  $\beta$  are set respectively to 0.5 and 0.0 for columns and 0.0 and 0.6 for beams, [Lu and Silva, 2006]. Mander model is used for concrete, [Mander et al, 1988], which takes into account the increase in strength and ductility due to confinement. This effect is however considered negligible for the beams. For steel an elasto-plastic behavior with a hardening branch is adopted. The hysteretic behavior is calibrated through the momentcurvature diagrams of the critical sections, considering for each column the axial load coming from the static analysis. A bilinear approximation is assumed for these diagrams, and the yield strength is defined in a way that the area under the curves is equal.

The analysis are performed considering second-order effects.

Table 3 shows the maximum displacements and storey forces. As expected, displacements tend to decrease significantly considering schemes with hinged connections or emulative ones. However, the expected increase in terms of storey forces is not so evident coming from Model 1 to

	Storey	Prototype A		Prototype B		Prototype A	
		$\Delta$ [cm]	V [kN]	$\Delta$ [cm]	V [kN]	$\Delta$ [cm]	V [kN]
Model 1	III	16.51	1121	17.54	1006	16.48	722
	II	9.78	1427	10.68	1197	9.81	1047
	I	4.30	1782	4.60	1484	4.12	1384
Model 2	III	12.04	911	9.55	921	10.44	738
	II	8.86	988	7.26	962	7.16	747
	I	4.18	1116	3.49	1229	3.17	1143
Model 3	III	5.74	1323	5.36	1231	5.60	875
	II	4.48	1308	4.33	1100	4.38	1100
	I	2.58	1467	2.58	1286	2.44	982

Table 3. Maximum displacements and storey forces with nonlinear dynamic analysis for all the prototypes



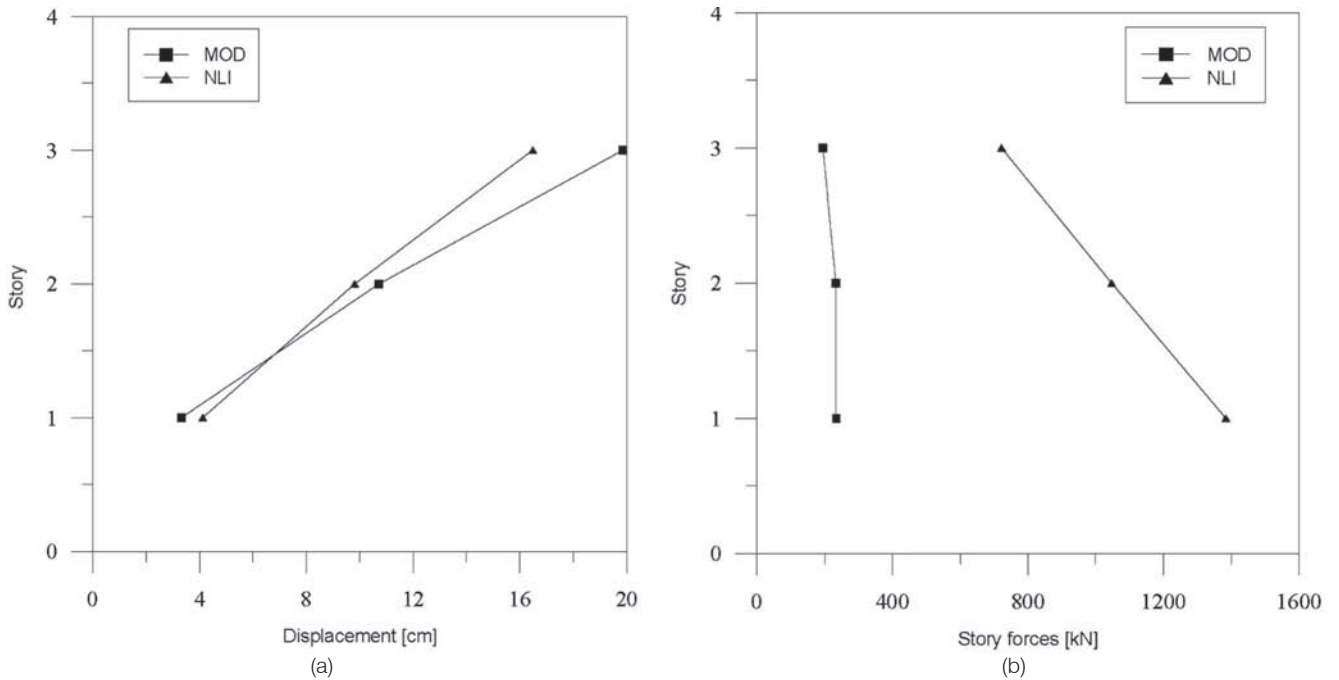


Figure 9. (a) Displacements, (b) storey forces for Model 1

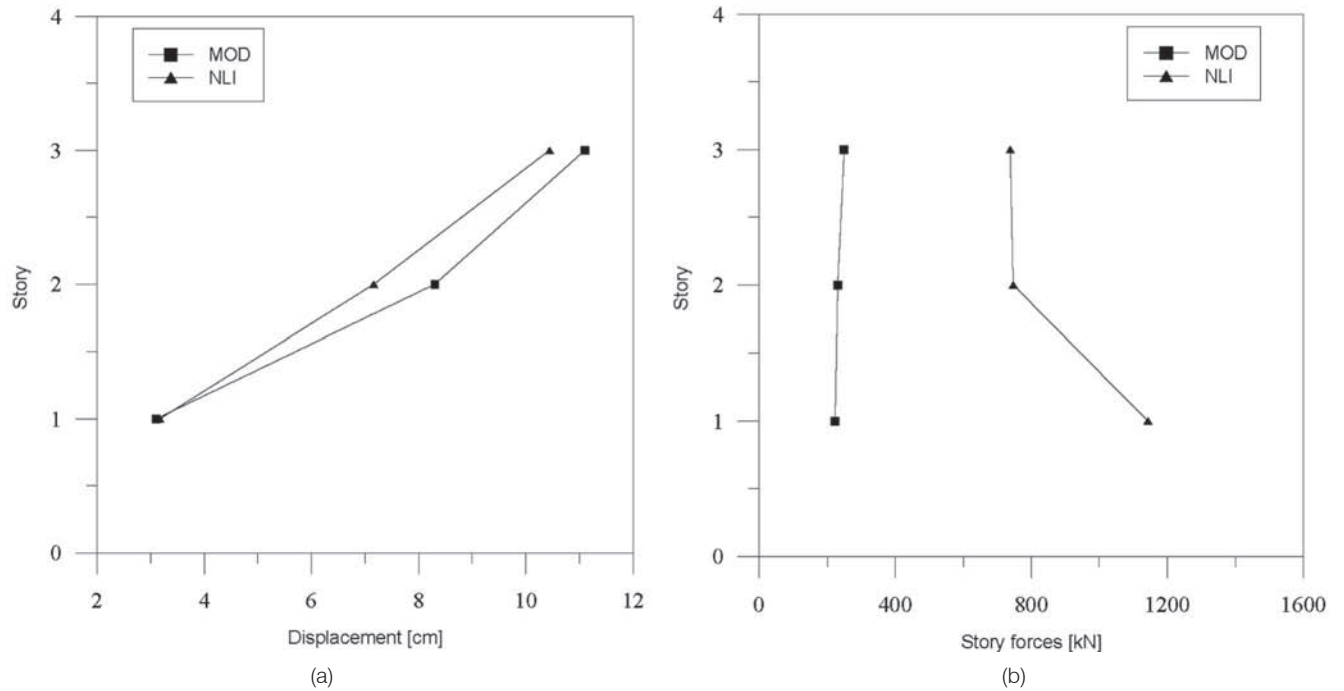


Figure 10. (a) Displacements, (b) storey forces for Model 2

Model 3. With reference to Prototype C, Table 3, all the storey forces are sufficiently lower than 2000 kN, allowing to perform the tests in safety.

### 5. Comparison between the results

For all the prototype analyzed the same considerations hold with regards to the effects of higher modes. For this reason only the results of prototype C (final choice) are presented and discussed. Nonlinear dynamic analyses are performed

neglecting viscous damping, supposing that all dissipation is included in the hysteretic behavior, while modal analysis is based on a 5% damped response spectrum.

Figures 9, 10 and 11 show maximum displacements and storey forces for each model. For Model 1 and 2 the displacements resulting from modal analysis (“MOD”) are slightly greater than those coming from nonlinear analysis (“NLI”), except for the first floor. Model 3 shows an opposite trend, but the difference is limited, not exceeding 2 cm.

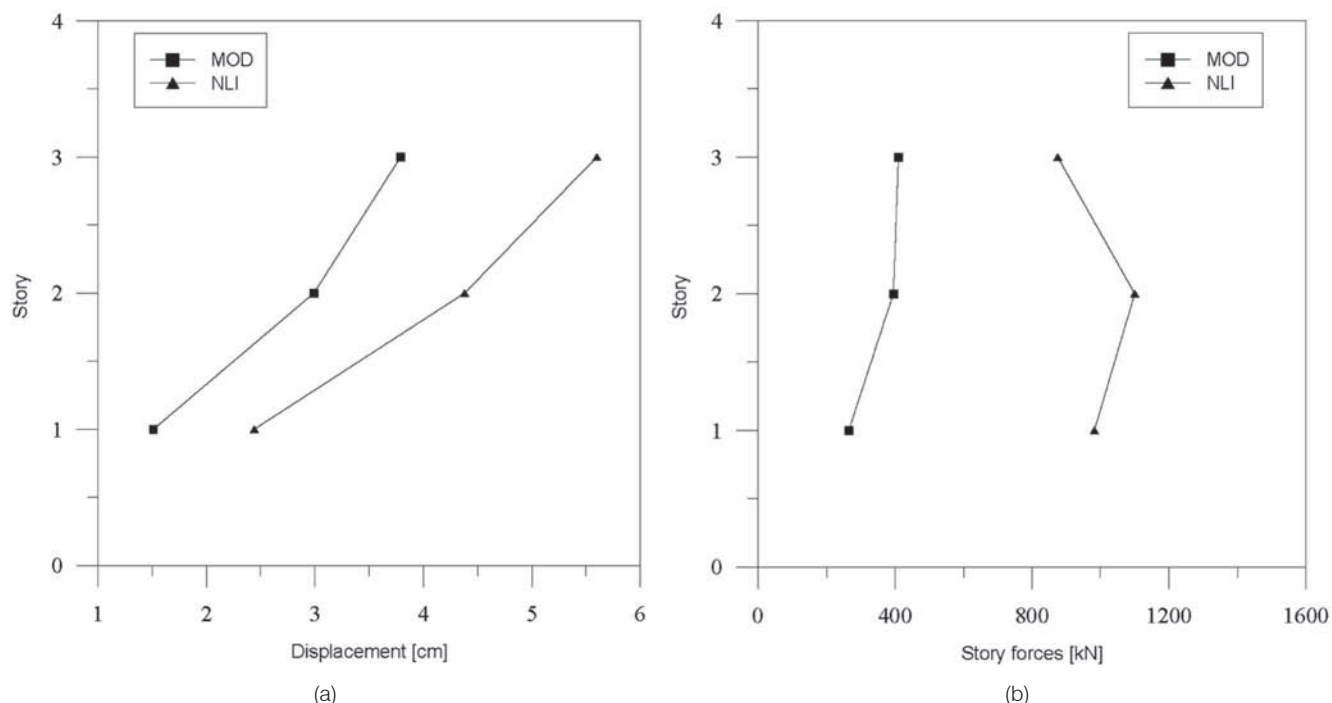


Figure 11. (a) Displacements, (b) storey forces for Model 3

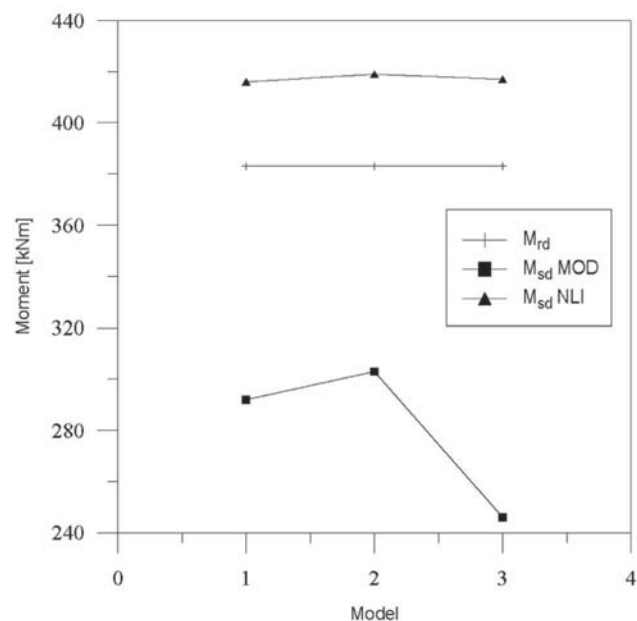


Figure 12: Resisting and acting moments at the base of the central column

Moment resisting connections allow to reduce the displacements, with values at the top floor decreasing from 17 to 6 cm.

These results are however indicative, because in real design the columns of the hinged solution would have a section increased. The good agreement found in terms of displacements is lost when storey forces are considered.

These differences are reflected in the estimation of the maximum bending moments at the base of the columns. In

particular Figure 12 shows the acting and the resisting moments at the base of the central column. In order to consider also in the modal analysis the second-order effects, the corresponding moments are amplified by the interstorey drift sensitivity coefficient  $\theta$  [CEN, 2004].

It is found that modal analysis predicts bending moments always lower than the resisting ones. Contrary, bending moments coming from nonlinear analysis tend to the ultimate strength of the corresponding moment-curvature diagrams of the section. This indicates that plastic hinges are developed at the ends of some columns. However, the activation of the dissipative mechanism allows to preserve the structure from the collapse.

### Conclusions

Seismic design of structures is typically based on the modal analysis with response spectrum, that is generally considered a conservative approach. The present investigation showed however that this statement has not a general validity. In particular a three storey building with different systems of connection, so different translational stiffness, has been studied, and displacements and storey forces have been evaluated. The results of the modal analysis with response spectrum have been compared with those coming from nonlinear dynamic analysis. The subsequent comparison is approximately satisfied in terms of displacements, while storey forces evaluated through the more refined method are significantly higher. This difference can be attributed to the role of higher vibration modes, indeed the opposing vibrations of the floors bring to higher storey forces, modifying the distribution of forces along the height of the structure.

To overcome the limitations due to the intrinsic approximations of the modal analysis with response spectrum the only reliable way seems to be the use of nonlinear dynamic analysis as indicated by recent codes [Model Code, 2010], even though it is not always straightforward in current design practice.

### Author Affiliation

Fabio Biondini<sup>1</sup>, Andrea Titi<sup>2</sup> and Giandomenico Toniolo<sup>3</sup>

<sup>1</sup>Associate Professor, Politecnico of Milan, Department of Structural Engineering, biondini@stru.polimi.it

<sup>2</sup>PhD student, Politecnico of Milan, Department of Structural Engineering, titi@stru.polimi.it

<sup>3</sup>Full Professor, Politecnico of Milan, Department of Structural Engineering, toniolo@stru.polimi.it

### References

- [1] CE de Normalization, Eurocode 8: Design of Structures for Earthquake Resistance. Part 1: General Rules, Seismic Actions and Rules for Buildings, European Standard NF EN, vol. 1, 2004
- [2] Biondini F., Toniolo G., Probabilistic Calibration and Experimental Validation of the Seismic Design Criteria for One-Story Concrete Frames, *Journal of Earthquake Engineering*, vol. 13, p. 426-462, 2009
- [3] Donea J., Magonette G., Negro P., Pegon P., Pinto A., Verzeletti G., Pseudodynamic capabilities of the ELSA laboratory for earthquake testing of large structures, *Earthquake Spectra*, vol. 12, 1996
- [4] Fayfar P., Vidic T., Fischinger M., A measure of earthquake motion capacity to damage medium-period structures, *Soil-Dynamics and Earthquake Engineering*, vol. 9., p. 236-242, 1990
- [5] Carr A.J., *Raumoko 3D Users Manual*, University of Canterbury, New Zealand, 2001
- [6] Lu B., Silva P.F., Estimating equivalent viscous damping ratio for RC members under seismic and blast loadings, *Mechanics Research Communications*, vol. 33, p. 786-795, 2006
- [7] Mander J.B., Priestley M.J.N. Park R., Theoretical stress-strain model for confined concrete, *Journal of Structural Engineering*, ASCE, vol. 14, p. 1804-1826, 1988
- [8] Model Code 2010, First complete draft, fib bulletin 56, vol. 2, 2010 Acknowledgements The present study is supported by the European research program SAFECAST, Grant agreement No. 218417

### Acknowledgements

The present study is supported by the European research program SAFECAST, Grant agreement No. 218417

# Stainless Steel: A Structural Anti-seismic and Fire Resistant Material

V. Boneschi

## Astract

Stainless steel is a material susceptible of many applications other than those involving its well-known resistance to corrosion. Worth of mention is its fire resistance and its capability to absorb impact energy, useful for application in anti-seismic construction.

Laboratory experiments showed that stainless steel could withstand high levels of alternate stresses as those induced by seismic events with increased performance in comparison with the traditional metallic materials used in construction.

Furthermore, numerical simulations based on the results of full-scale tests under anisothermal heating indicate that if the beam of EN 1.4301 is submitted to a load not exceeding 0.5 times the load inducing yield of the beam at room temperature, the time of resistance to fire is about 20-30 minutes, compared with only 10-15 minutes typical of carbon steel.

In addition, the intrinsic durability and resistance to corrosion of stainless steel guarantee that the characteristics of the component remain unaltered without any maintenance during its entire useful life cycle. In conclusion, stainless steel is not only a corrosion resistant material, but it is a safe structural material that moreover resists to corrosion.

## Keywords

stainless steel, fire resistance, seismic, toughness

## Introduction

The number of applications in building constructions where stainless steel is used as a structural material rather than for its intrinsic resistance to corrosion is increasing during the time [1].

Fire resistance and anti-seismic properties are becoming more and more important requirements for material selection in order to increase building safety.

The aim of this paper is to highlight these properties, in order to suggest to civil engineers to consider stainless steel as a structural steel that, moreover, it's corrosion resistant.

## 1. Stainless steel anti-seismic properties

It is well known that stainless steels, particularly the auste-

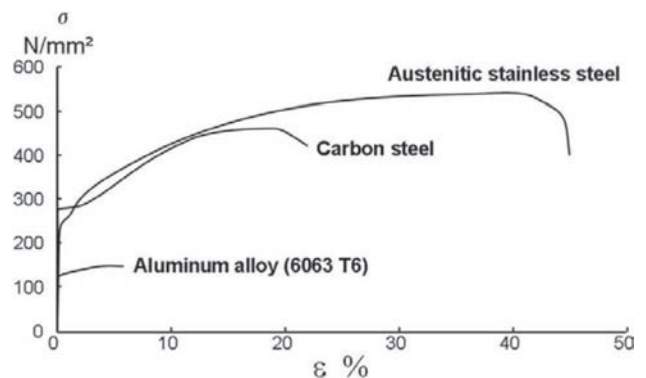


Figure 1. Qualitative stress-strain diagrams for austenitic stainless steel, carbon steel and aluminium alloy.

nitic ones, are characterised by high deformation ability, due to their outstanding elongation before fracture.

This is most evident looking at the stress-strain diagram of Figure 1: austenitic chromium-nickel stainless steels shows high elongation to rupture, while the behaviour of carbon steel, currently used for construction, or aluminium alloy is very much alike.

As the area delimited by the curves in Figure 1 is in direct proportion with the absorbed energy until fracture, the attractiveness of austenitic stainless steels is quite understandable.

No heat treatments can be used to increase mechanical properties of austenitic stainless steels, so the only feasible procedure is cold working. Of course, elongation ability decreases as a consequence of the cold working imparted to the material during processing, but the ductility of cold worked stainless steel is still so high to allow appreciable amounts of deformation.

The steel is also required to have so good toughness that no brittle fracture or important ductility loss occurred when subject to high deformation rates.

The high toughness of stainless steel is a key property for an anti-seismic material; in fact a good material should be able to dissipate the energy induced by the seismic waves.

In this sense, the very good properties of stainless steel has been shown by some studies on reinforcing steel by A.



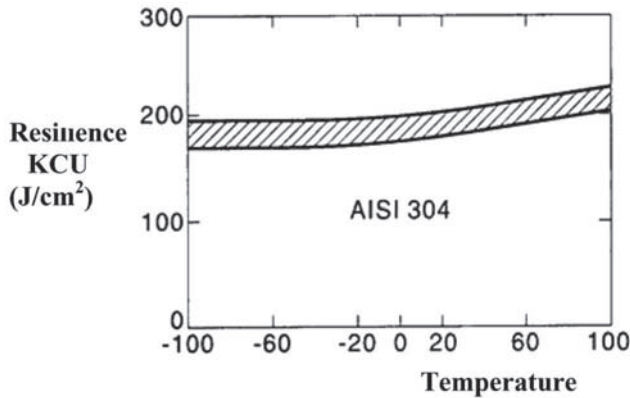


Figure 2. Toughness as a function of temperature: steel AISI 304 (1.4301).

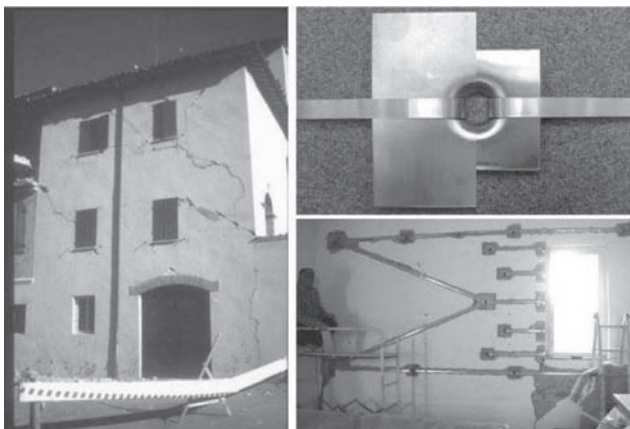


Figure 3. Toughness as a function of temperature: steel AISI 304 (1.4301).

Franchi- P. Crespi-A. Bennani [2]. Assuming that a low cycle fatigue laboratory test can simulate with sufficient accuracy and in a very simplified way the stress and the strain that a structural part must withstand during an earthquake, they pointed out that stainless steel rebar offers a higher total energy dissipation potential.

Austenitic stainless steel has very good toughness also at low temperatures without any abrupt ductile-to-brittle transition. The effects of low temperature and of high deformation rate are somehow similar, because both the situations lead to an increase of the yield strength, approaching ultimate strength, with the ensuing risk of fracture initiation. Austenitic stainless steels, having a large gap between yield and tensile strength, are less critical for temperature decrease or for events inducing high-rate stresses. As an example, Figure 2 illustrate the results of a Charpy impact test showing that these steels retain good toughness even at temperatures well below zero.

To conclude also one hint to the use of stainless as “consolidation” material after a seismic event; in Figure 3 it is shown an example of use of stainless steel strips to consolidate masonries of a building damaged by the earthquake.

## 2. Stainless steel fire resistance

As mentioned, the resistance to fire is an increasingly important parameter for construction materials. Experiences carried out by different European laboratories, Ala-Outinen (1996) [3], Baddoo & Gardner (2000) [4], Oksanen & Ala-Outinen (1997) [5], Zhao (2000) [6], highlighted the excellent performance of stainless steel. More recently, in 2009, the European Research Area of the European Commission published “Stainless steel in fire” [7], published an official report that summarises the findings of a European research project which studied the behaviour of a range of structural stainless steel solutions subject to fire loading.

In Italy too, in the past years, experiences have been performed, consisting in a finite-element modelling and then full scale testing on stainless steel welded beams at the Fire-Fighting Research Centre of the Fire Department in Rome; results in good accordance with each other were attained, useful to establish the excellent performance of stainless steel regarding fire resistance.

### 2.1 Finite-element study

Section typologies, marked by A and B, are reported in Figure 4.

The beams were stressed according to the 4-points bent beam configuration. Two models were developed, one for both the beam geometries. Beams were schematised with

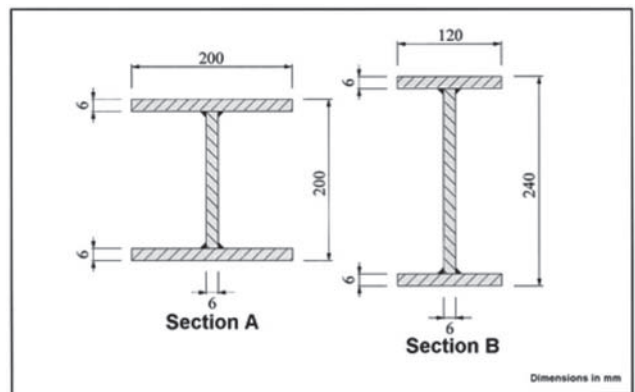


Figure 4. Sections of the tested beams.

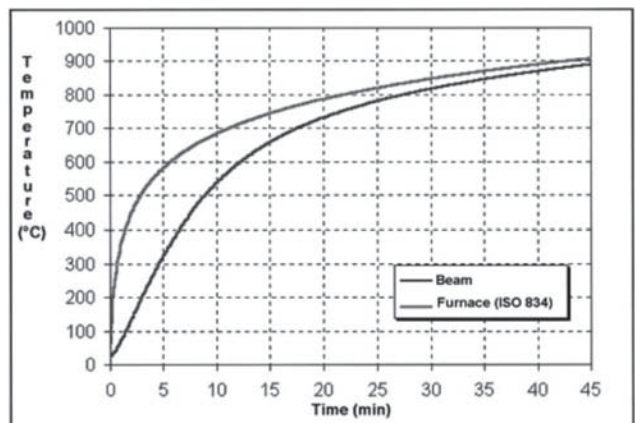


Figure 5. Imposed temperature slope.

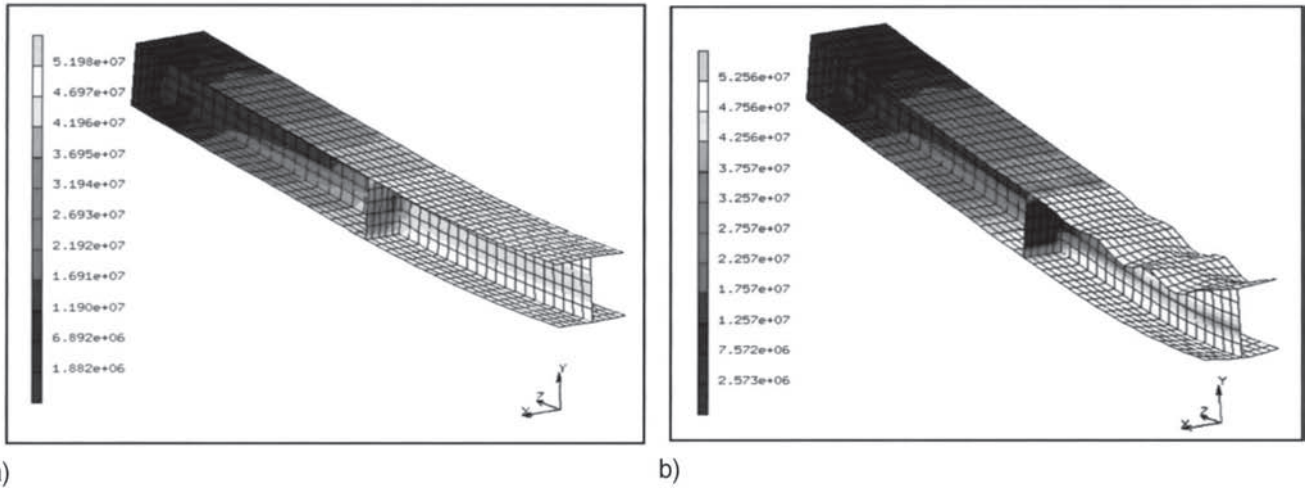


Figure 6. Beam type A – a): AISI 304, b): Fe 360.

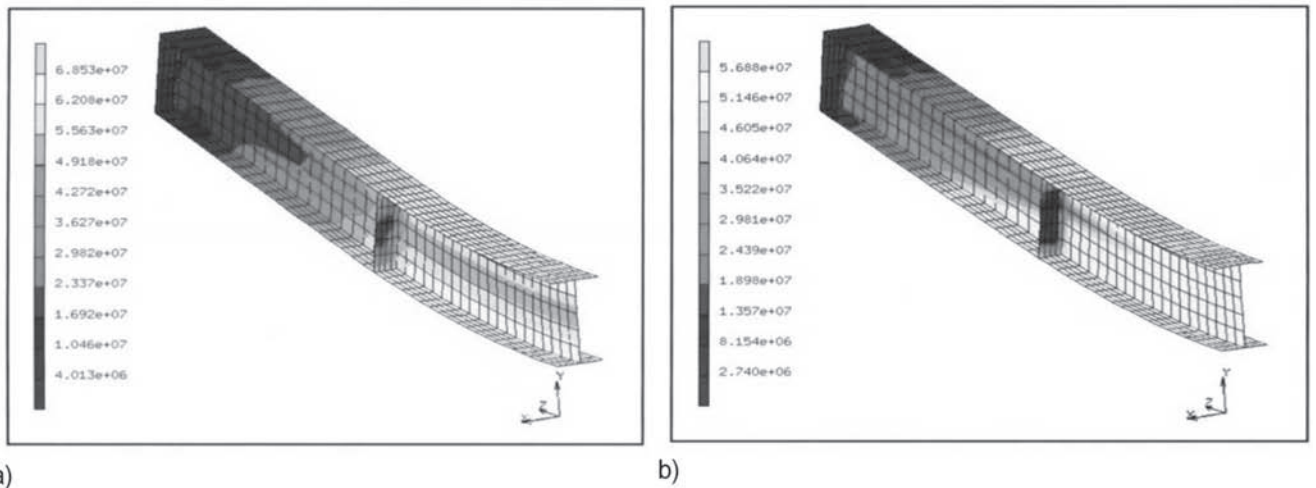


Figure 7. Beam type B – a): AISI 304, b): Fe 360.

shell type elements with four nodes. Due to geometric symmetry, only 1/4 of each structure has been schematised. Suitable boundary conditions have been imposed on the symmetry planes.

A progressive increase in temperature was applied to the section, starting from room temperature, with the particular slope given by ISO CD 834 Standard, establishing the incremental variation of the section temperature as a function of instantaneous furnace temperature and section geometry.

The temperature slope depends on the environment, on heat transfer, on the material and on its mass factor, i.e. the ratio between section surface exposed to fire and its volume.

The temperature increase with time imposed to the model was as shown in Figure 5.

Outlined material behaviour is elastic-plastic, with yield stress and work hardening depending on temperature. Data were worked out from the experimental curves by tensile tests for AISI 304 and from Eurocode 3 tables for Fe 360.

Material performance was evaluated in terms of stress distribution at collapse and of deflection variations during the time. Stress distribution at collapse for both the steels and both the beam geometries are shown in Figures 6 and 7.

Plastic yielding initiation of the beam was determined following BS 476 Standard, parts 20 and 21. The transition from elastic behaviour (safe structure) to plastic behaviour (formation of localised plasticization and the following achieving of structural instability) is determined by comparing the instant deformation rate of the beam (derivative of the deflection with respect to time) with a given value called “critical rate”.

When the instant deformation rate exceeds the critical value, the beam can no longer be considered as apt to withstand the load.

The time interval passing from the beginning of the exposure until the critical instant determines the so-called “fire resistance time”. From the temperature slope, also the critical temperature of the section is determined. With the same section geometry and exposure conditions, critical time and

temperature depend from the applied load and, of course, from material performance.

The ratio between the applied load and the load that in a full-scale testing induces yield on the beam at ambient temperature is defined as "loading factor": one can realise that this parameter is suitable to define the "severity" of the applied stress. It is therefore possible to draw the variations of critical time and temperature of the two materials taken into consideration (Fe360 and AISI 304) as a function of this parameter.

Different calculations were made for both the beam types (A and B) and for both the steels, imposing increasing loads: The results were elaborated according with BS 476 Standard to determine critical times and temperatures.

**2.2 Full-scale experimental testing**

Full scale testing was conducted at the laboratories of Fire-Fighting Research Centre of the Fire Department in Rome.

**2.2.1 Specimens**

The tested specimen beams have been obtained by welding from type 304 stainless steel plates. The nominal dimensions are those utilised for the finite element modelling.

**2.2.2 Testing**

Mechanical strength at room temperature and fire resistance tests were carried out on four AISI 304 stainless steel beams, according to ISO 834 Standard.

The test at room temperature was aimed at defining the threshold load for elastic behaviour.

Two jacks according to a four-point bending configuration gave stress. Heating slope was in accordance with UNI 7678 Standard. Eight thermocouples were positioned inside the furnace to control fire slope and 15 thermocouples were welded on the beam to obtain a thermal mapping.

Two transducers were placed in the middle of the beam to control deflection and deflection rate.

The tests were interrupted as soon as the deflection rate exceeded the threshold value, calculated by the formula:

$$V_{th} = L^2/(9000 \times h) \text{ mm/min}$$

Where L is the distance in mm between the supports and h the tested specimen height.

The time elapsed from exposure beginning until test end is the time-to-collapse.

The deflection test at room temperature highlighted that the top value of the load not inducing instability, in the static configuration of the test, was 30 kN for each jack.

The three tests of resistance to fire were carried out with the procedure as the static test, with jack loading 10, 15 and 30 kN respectively.

**2.2.3 Results**

The results of the full scale testing are reported in Figures 8 and 9, together with the results of the finite elements calculations.

In the figures, critical temperature and critical time to collapse for both the beam types examined are shown.

The comparison with the traditional carbon steel Fe 360 performance has been done only for the calculated values, as no experimental data were available on this latter steel.

The excellent agreement between numerical prediction and experimental values on 1.4301 steel is worth to note. This justifies the comparison between stainless steel and carbon steel, for which, as already mentioned only calculated values are available.

Diagrams show that the critical temperature decreases increasing loading. In fact, increasing the applied stress, a corresponding increase of the yield strength is needed, but this can be obtained only at decreasing temperatures. As a consequence, in presence of high loading factors (ratio between the applied load and the load that in a full-scale testing induces yield on the beam at ambient temperature),

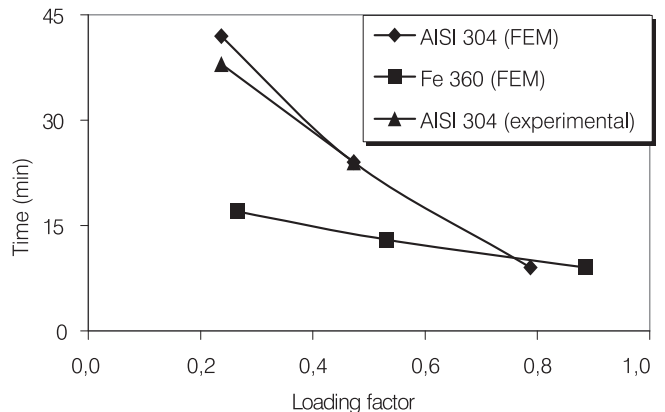
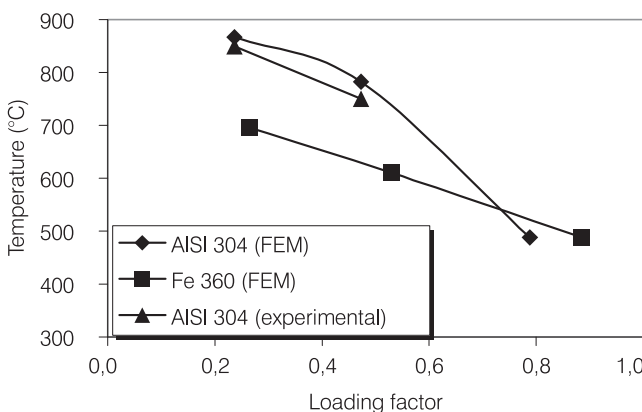


Figure 8. Beam A. Critical temperature and critical time.

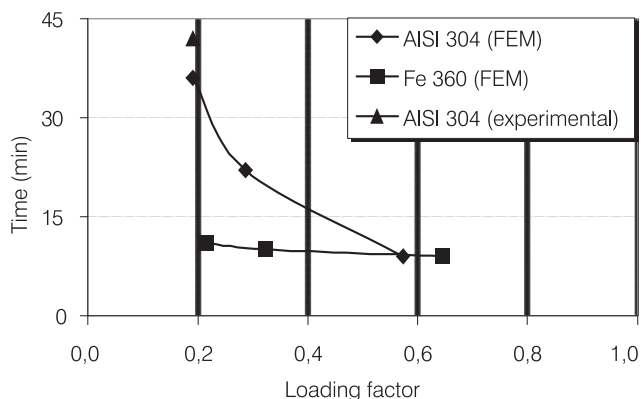
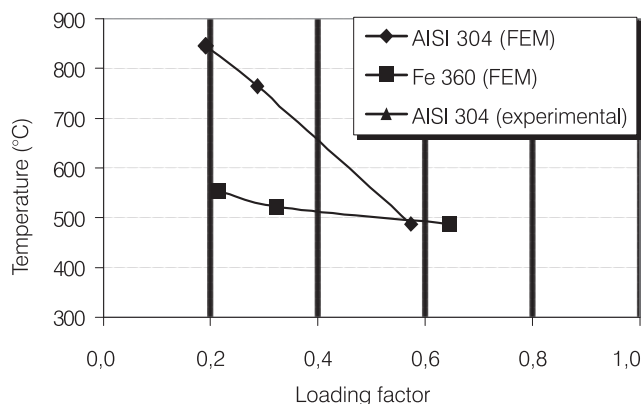


Figure 9. Beam B. Critical temperature and critical time

critical temperatures and times for the two steels tend to coincide; when very high yield strength are required, at temperatures not exceeding 400°C, both the materials behave almost the same. On the contrary, with loading factors below 0.5, it is possible to attain high temperature without collapse and in this case the use of EN 1.4301 is appreciably more convenient. In fact, the time of resistance to fire of 10–15 minutes, typical of Fe 360 increases up to 20–30 minutes for EN 1.4301, in a temperature range up to 650–800°C that is considered as the most critical for metallic structures during a fire accident. In this way, the time at disposal for the firemen intervention is in theory almost doubled and it is possible to operate on the structure in safe conditions.

On the base of these results, other simulations have been performed and all confirmed the great potential advantages offered by stainless steel structural components in the case of fire.

An interesting simulation [8] on a reticular structure under ISO 834 fire condition gave the following results:

Steel	Critical time (min.)	Critical temperature (°C)
Fe 360	10:32	478
AISI 304	15:19	603
AISI 316	28:53	796

**Conclusions**

The peculiarities making stainless steel a potential support to a design considering the possible occurrence of seismic events have been shortly illustrated:

- high mechanical strength;
- high deformation ability until fracture;
- ability to absorb high amount of energy;
- good toughness also at low temperatures.

Austenitic stainless steel showed a very good resistance to fire in the full scale testing. This material in some structural applications can be therefore a valid alternative to traditional carbon steel.

An important point to be considered is also its intrinsic durability and resistance to corrosion: stainless steel guarantees that these properties stay unaltered during the entire life cycle of the component, without any maintenance. This is much more important when the design takes into account also sustainability and LCA.

**Author Affiliation**

V. Boneschi,  
Centro Inox Milano/Italy, vittorio.boneschi@centroinox.it

**References**

- [1] M. Barteri and V. Boneschi. Structural Stainless Steel: fire resistant and Anti-seismic. 9th Nordic Steel Construction Conference – Helsinki 18-20 June 2001
- [2] A. Franchi, P. Crespi and A. Bennani “Stainless steel reinforcing bars for structural seismic applications”. XI National Congress “L’ingegneria Sismica in Italia” Genova 25-29 January 2004.
- [3] Ala-Outinen T.(1996) «Fire Resistance of Austenitic Stainless Steel Polarit 725 (EN 1.4301) and Polarit 761 (EN 1.4571)”. VTT Research Notes, 1760, Espoo, Finland.
- [4] Baddoo N. and Gardner L. (2000) “Member Behaviour at Elevated Temperatures” Final Report to the ECSC.
- [5] Oksanen T. and Ala-Outinen T. (1997) ”Stainless Steel Compression Members Exposed to Fire”. VTT Research Notes, 1864, Espoo, Finland.
- [6] Zhao B. (2000) “Material Behaviour at Elevated Temperatures”. Final Report to the ECSC.
- [7] European Commission, European Research Area EUR 23745. “Stainless Steel in Fire”, 2009.
- [8] M. Barteri, V. Boneschi, T. Coppola, C. Sciaboni “Stainless steel reticular structures: fire resistance finite element simulation”. Giornate Italiane della costruzione in acciaio. Isola di San Giorgio Maggiore, Venezia. 26-28 September 2001.



# Numerical Study on the Seismic Interaction between 2D Seismic Resisting Frames and Claddings

**Riccardo Diaferia<sup>1</sup>, Andrew Baird<sup>2</sup>, Stefano Pampanin<sup>3</sup> and Alessandro Palermo<sup>4</sup>**

## Summary

Damage to non-structural components during recent earthquake events, such as the Darfield earthquake in New Zealand (2010) have confirmed the need to better address the interaction between a structure and its non-structural components.

This paper aims to numerically investigate the seismic behaviour of a typical newly designed reinforced concrete multi-storey frame building with and without the interaction due to cladding panels. This interaction is investigated by means of non-linear static and dynamic analyses for common typologies of cladding systems. A seismic risk assessment analysis is also presented in order to develop fragility functions based on damage limit states for cladding connection. These are used for assessing the probability of damage of cladding systems after earthquake events of varying intensity.

Results confirm the high influence of cladding systems upon the seismic performance of multi-storey buildings. Also revealed is the significant variation in possible levels of cladding damage throughout a building. Further investigations are going to be developed, refining the use of fragility functions associated to innovative low damage cladding solutions.

## Keywords

numerical modelling, non-structural elements, facades, cladding, seismic design, fragility curves

## Theme

buildings – analysis – earthquake – concrete

## 1. Introduction

Reconnaissance following past earthquakes has shown that damage of non-structural elements during seismic events can cause significant economic losses and disruption to important or critical facilities. Furthermore, failures can result in potential hazards to pedestrians around the building. Recent earthquakes have further highlighted this concept, necessitating a detailed study in order to propose and develop innovative solutions able to reduce the risk of damage to non-structural elements. This work is part of an ongoing research effort with the aim of better understanding the interaction between facade systems and the structure.

Numerical models of cladding systems have been defined using previous experimental investigations and preliminary data from on-going experimental tests. A parametric analysis of a one-storey single bay frame clad with a precast concrete panel, fully presented in a companion paper (Baird et al. [1]), has been used as the foundation for this study on the seismic behaviour of multi-storey buildings with different cladding distributions. The interaction with the facade has been investigated by use of non-linear analyses utilizing both pushover and time-history analyses of typical cladding-structure systems.

In the first part of this paper, a parametric analysis has been performed, considering different distributions of precast concrete panels and structure heights. In the second part of the paper, a probabilistic risk assessment evaluation due to seismic hazard is presented for some of the claddings which compose the facade. This allows the development of fragility functions based on damage limit states previously identified in order to assess the probability of achieving defined damage levels of the cladding system.

Facade	Connection	Behaviour Characteristics	Strength	Stiffness	Ductility
Cladding Panel	Tie-Back (Partially Fixed)	Deform easily under lateral forces. Must withstand out-of-plane forces, e.g. wind	Low	Low	High
	Slotted/Sliding/Rotating	Disconnect the panel by allowing degree of freedom in one or more directions.	NA	NA	Medium
	Dissipative	Dissipate energy in connector body under lateral forces by yielding or friction.	Medium	Medium	Medium
	Fully Fixed (Bearing)	Transfer the self weight of the panel to the structure. No seismic characteristics.	High	High	Low

Table 1. Facade connection characteristics (Baird et al. [1])

## 2. Background

Recent studies on the interaction of cladding panels with the primary structure have underlined the need of understanding the influence of facades on the overall system (McMullin et al. [2], Baird et al. [1]). This behaviour is directly dependent on the cladding system analysed, in particular in relation to different connection types, as qualitatively presented in Table 1.

In order to assess the seismic response of multi-storey buildings with claddings, the solution of precast concrete panels attached to the beams by the use of tie-back (p. fixed) and fully fixed (bearing) connections has been herein adopted. Because of their low strength and stiffness with high ductility, the tie-back connections are the weakest level of the chain in the hierarchy of strength of the overall system. When this is the case it allows greater damping, strength and stiffness over many cycles as opposed to when damage occurs in the panel or frame. However this requires that the tie-back connections are designed to accommodate a large level of displacement demand or ductility (Baird et al. [1]).

Performance-based criteria for cladding connections are presented in this paper in order to determine the likely level of damage from varying earthquake intensity. This is in accordance with the shift towards a performance-based framework for both structural and non-structural system in newly designed buildings (Priestley [3]). The primary function of performance-based seismic design is the ability to achieve, through analytical tools, a building design that will reliably perform in a prescribed manner under one or more seismic hazard conditions (SEAOC [4]).

The in-plane performance of cladding panels are deemed to be sensitive to inter-storey drift (Taghavi and Miranda [5]) therefore the maximum drift of the connections is to be

monitored in order to compare damage limit states. It is important to note that the out-of-plane performance (as well as in-plane to some degree) of cladding panels is sensitive to acceleration, for this reason, this paper does not fully encompass all possible cladding panel damage and failure mechanisms. The probability of damage of the connections has been evaluated following the performance based earthquake engineering (PBEE) methodology used by Cornell et al. [6].

The use of the Incremental Dynamic Analysis (IDA) procedure proposed by Vamvatsikos and Cornell [7] is able to define the probability of different damage limit states being reached. This is done by subjecting a structure to a suite of earthquake accelerograms with the intensity level varied from a low to high level. This study builds on a defined procedure for such an analysis which is being extended and validated for non-structural elements (Stojadinovic and Hunt [8]).

## 3. Case study: multi-storey frame systems

The case study proposed is based on the Red Book building (New Zealand Concrete Society [9]) which acts as a design example of the New Zealand Concrete Code (NZS 3101 [10]). The building was originally designed for the city of Christchurch, but for this study the building has been assumed to be located in the higher seismicity site of Wellington in order to achieve larger damage. Figure 1 (left) illustrates the plan view of the structure, with the seismic frame analysed highlighted. The analyses have neglected the beam extensions that form the corner of the building since in 2D these do not affect the bare frame behaviour. The bottom floor has a storey height of 4m while the upper floors have a storey height of 3.6 m for a total of 10 levels. Design loads, forces and seismic masses have been calculated according to NZS1170:1 [11] and NZS1170: 5 [12] following Force Based Design (FBD) methodology.

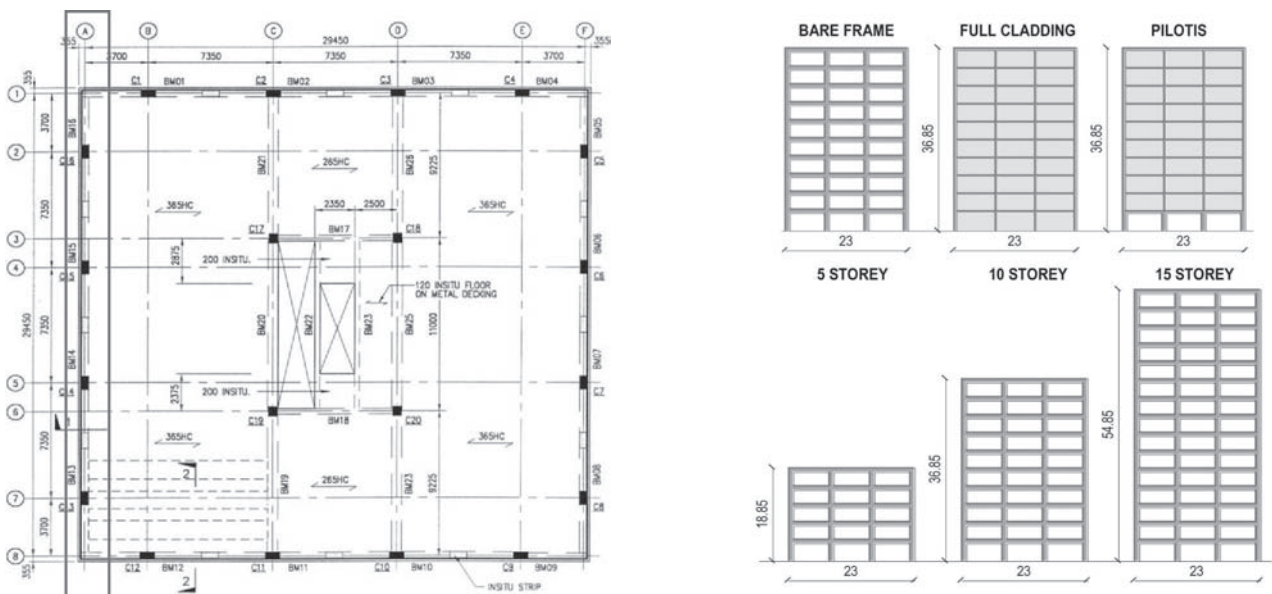
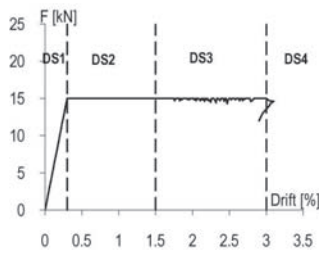


Figure 1. Plan view of the building (left, [9]) and claddings distribution/frames configurations (right)



	Damage state	Drift limit	Behaviour	Repair required	Outage
DS1	None	$< 0.3\%$	Pre-yielding	None	No
DS2	Minor/Moderate	$0.3\% \leq x < 1.5\%$	Post-yielding	Inspect, adjust	$< 3$ days
DS3	Major	$1.5\% \leq x < 3\%$	Local buckling	Repair elements	$< 3$ weeks
DS4	Failure	$> 3\%$	Collapse	Rebuild system	$> 3$ weeks

Figure 2. Propose damage limit states related to tie-back connections

In the first part of this paper (SECTION A) different distributions of precast concrete panels were considered as well as various heights of the frame (5-10-15 storeys). 5 and 15 storey buildings have been adapted using the same section properties of the 10 storey building. Two possible architectural cladding configurations have been considered: Full Cladding (FC) and Pilotis (PI), compared to the Bare Frame (BF), (Figure 1-right). Full cladding consists of cladding panels in every bay in every storey of the frame and pilotis is the same without panels at the first floor.

In the second part of the paper (SECTION B), a probabilistic risk assessment evaluation due to seismic hazard is presented for facade panels basing on the 10 storey cases (FC and PI) in relation to three cladding connections at different floor level.

### 3.1 Cladding characteristics

The cladding system is represented by precast concrete panels of 0.2 m thickness attached to the primary structure on the beam with tie-back connections at the top and with bearing connections at the bottom. The panels have been treated as not having any window openings for simplicity. However it can safely be assumed that correctly detailed panels with openings would behave nearly identically to the panels modelled since both provide large in-plane stiffness. The system has been designed considering a suggested drift of 0.3% (Baird et al. [1]). For this study, damage limit states are related to the behaviour of the tie-back connections based on various experimental behaviour (McMullin et al. [2], Stojadinovic and Hunt. [8]) and first outcomes from the experimental test which is currently taking place in the laboratory of Civil Engineering of University of Canterbury (New Zealand). The damage limit

states for the connections have been presented as the drift of the connection or "connection drift". The connection drift is defined as the relative displacement of the connection divided by inter-storey height. Four damage limit states are herein proposed and shown in Figure 2. Damage State 1 (DS1) represents elastic behaviour, it therefore concludes at the onset of damage which is best defined by the yield drift of the connection. Damage State 4 (DS4) is defined from the onset of collapse. The other damage stages (DS2, DS3) are more subjective in their definitions. It is suggested that the boundary separating DS2 and DS3 should be defined as a level of damage which would cause loss of function and repairs are needed to restore the full functionality of the structure. Below this boundary, damage (categorised as DS2) is considered to be slight and tolerable. Whereas damage suffered in DS3 is significant such that the elements are not likely to perform their function as evidenced by:

- excessive permanent drift at the end of the earthquake;
- excessive damage to connection due to effects such as local buckling

### 3.2 Modelling issues

The models have been implemented using the programme RUAUMOKO (Carr [13]). Beams and columns have been represented by elastic elements with inelastic behaviour concentrated in plastic hinge regions (Giberson model) and defined by the moment curvature hysteresis rule "Modified Takeda" (Otani and Sake [14]). Precast concrete panels have been modelled as quadrilateral elastic elements, while the connections have been considered as springs associated to a non-linear rule and attached directly to the beams

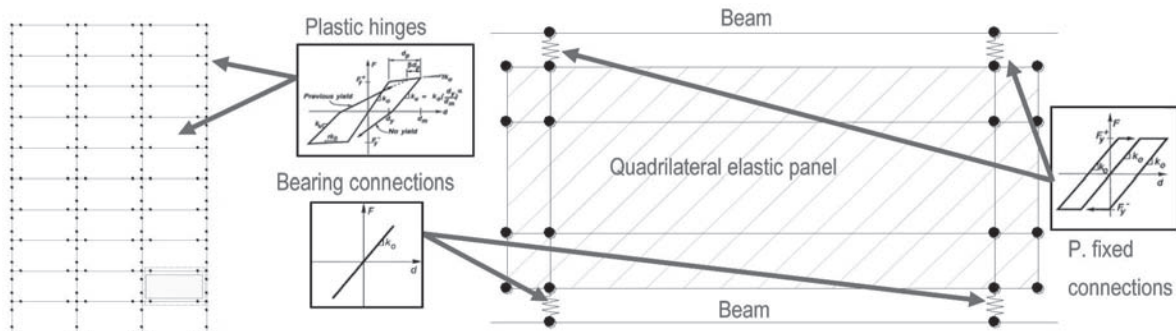


Figure 3. Modelling of the frame (10 storey case) and cladding panel with hysteretic rules used

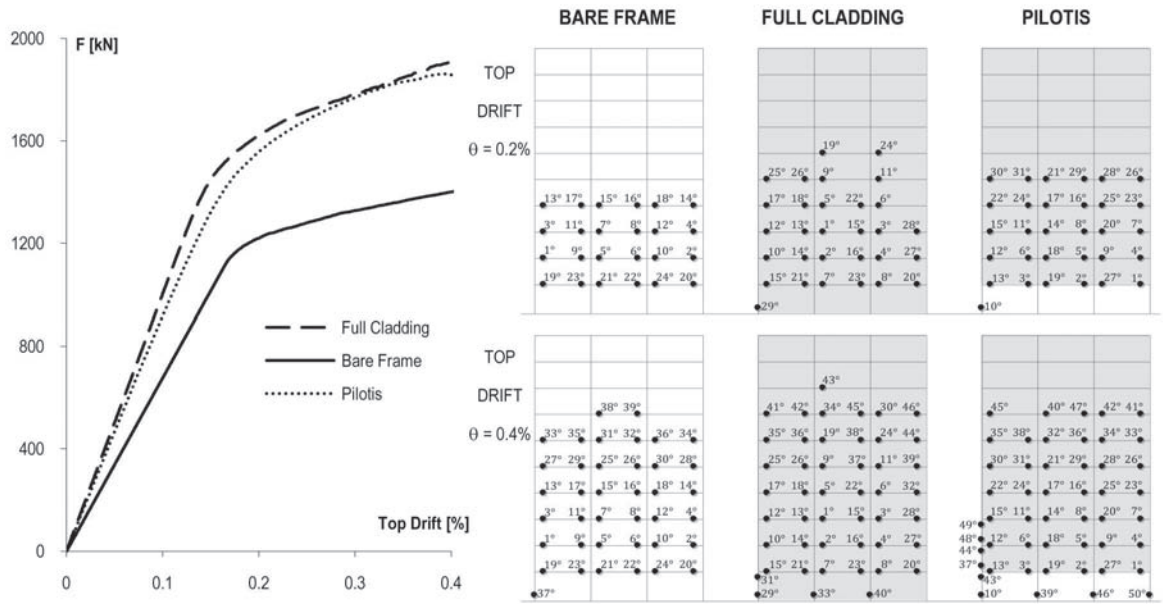


Figure 4. Pushover analysis (10 storey case) – monotonic response (left); comparison of the damage mechanism with activated plastic hinges at 0.2% and 0.4% top drift (right)

in two points, as shown in Figure 3. All the connections are characterised by a bi-linear elasto-plastic rule. The top (tie-back) connections have high ductility without strain hardening and the bottom (bearing) connections have high strength and high stiffness with the intention of them to remain elastic.

#### 4. SECTION A: numerical investigation

In the following paragraphs, the results from the non-linear pushover and time-history analyses are presented for the different configurations described in section 3.

##### 4.1 Pushover analyses

Static non-linear pushover analyses of the models were performed to investigate the lateral base shear and top displacement relationship of the building. The analyses compare the behaviour of the systems under a triangular distribution of the forces acting up the height of the building meant to represent earthquake demand. In Figure 4(left) the monotonic response of the 10 storey building case (base shear vs. top drift) is shown, representing the three different configurations analysed: Bare Frame, Full Cladding and Pilotis. As expected, an increase in stiffness and strength is observed for FC and PI cases compared with BF due to the presence of the elastic cladding panels.

In Figure 4(right) the activation of the plastic hinges is shown

for the three configurations at two different values of top drift; 0.2% and 0.4% respectively. FC presents extensive formation of plastic hinges at the second/third floor levels, while the absence of claddings at the ground floor in the PI case results in a higher shear demand at the ground floor level which can lead, as expected, to a soft-storey mechanism at that level.

For all the multi-storey frames studied (5-10-15 storeys), the effects of claddings for both the FC and PI cases are investigated and summarise in Table 2 comparing the initial stiffness increment with the BF stiffness.

The initial stiffness ratio between the system with claddings ( $K_x$ ) and the bare frame ( $K_{BF}$ ) is higher, especially as the height of the frame decreases, underlining the positive contribution of the claddings. In particular, the 5 storey case presents a large increase compared with the other configurations, especially for the FC configuration. This can likely be attributed to the fact that the 5 storey frame has not been designed as a 5 storey frame but has been derived from the 10 storey frame. The consequence of this is that low frame height compared to the frame width (length of the base) means the frame is may behave like a squat frame.

##### 4.2 Time-history analysis

Time-history analyses have been performed investigating how the variables considered (panel distribution, building

Building Configuration	5 Storeys		10 Storeys		15 Storeys	
	Full Cladding	Pilotis	Full Cladding	Pilotis	Full Cladding	Pilotis
Increase in initial stiffness respect to the bare frame $\frac{(K_x - K_{BF})}{K_{BF}}$	+702 %	+217 %	+49 %	+38 %	+34 %	+23 %

Table 2. Pushover analysis – stiffness increment compared with Bare Frame case



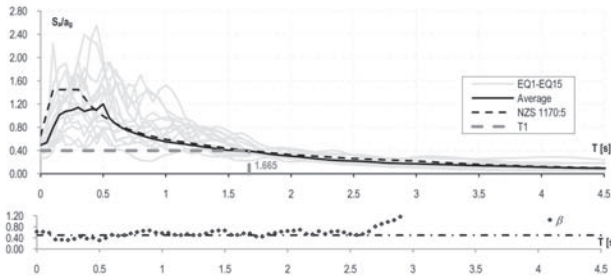


Figure 5. Scaled spectra to  $S_a=0.4g$  at the fundamental period  $T_1$  and lognormal coefficient of variation  $\beta$

height) can affect the response of the building. A suite of fifteen recorded and scaled natural accelerograms have been used (Pampanin et al. [15]). The records have been scaled according to NZS1170:0 [16] and NZS1170:5 [12], considering  $S_a=0.4g$  (Wellington, soil type C) as shown in Figure 5. A period range of interest has been defined between  $T_{min}$  and  $T_{max}$  where  $T_{min}=0.4T_1$  and  $T_{max}=1.3T_1$ ,  $T_1$  is the fundamental period of the structure equal to 1.665s (mean of the fundamental periods of every system studied in the parametric analysis).

The lognormal coefficient of variation is plotted in order to show the dispersion across the spectrum. Because its value is around 0.45 provided that the period is less than about 2.6s, the scaled suite is satisfactory (Figure 5). According to FEMA-302 [17], two earthquake intensity levels have been considered in the numerical analyses, subjecting the structure to two corresponding response spectra: the Design Basis Earthquake (DBE) ground shaking (probability of exceedance of 10% in 50 years) and the Maximum Considered Earthquake (MCE) ground shaking (probability of exceedance of 2% in 50 years). Referring to the performance objectives matrix (SEAOC [4]), the Basic Safety Objective is attained when a structure achieves both the Life Safety Performance level under the DBE level and the Collapse Prevention Performance level under the MCE level.

	Full Cladding		Pilotis	
	DBE $\theta_{max}$ [%]	MCE $\theta_{max}$ [%]	DBE $\theta_{max}$ [%]	MCE $\theta_{max}$ [%]
5 storeys	1.70 (1st floor)	2.49 (2nd floor)	1.67 (2nd floor)	2.56 (2nd floor)
10 storeys	1.56 (2nd floor)	2.40 (2nd floor)	1.62 (2nd floor)	2.55 (2nd floor)
15 storeys	1.26 (2nd-3rd floor)	2.02 (2nd floor)	1.38 (2nd floor)	2.05 (2nd floor)

Table 3. Median of the maximum drift of the tie-back connection  $\theta_{max}$  for the FC and PI cases under DBE and MCE intensity

In Figure 6 the results related only to the 10 storey case are shown. Figure 6(left) presents the maximum interstorey drift for BF, FC and PI. In correspondence of the second floor the highest values of drift are concentrated for all the three configurations analysed. This result is reflected in Figure 6(middle) and Figure 6(right) where the maximum and the median drift are plotted for every floor of the tie-back connections. In relation to the damage limit states presented in Figure 2. The claddings of the PI case are particularly affected by the earthquake, revealing the possibility of reaching at least in one case a maximum drift which can lead to the failure of the system.

Table 3 represents a summary of the results related to the connections obtained from the time-history analyses. Regardless of the number of storeys or the configuration type, the highest connections drifts are always localised at the second floor of the building. These results give a clear indication that the level of damage to claddings can be high, even for a DBE.

### 5. SECTION B: risk assessment analysis for cladding systems

In order to understand the probability of damage of some of the cladding connections analyzed in the previous sec-

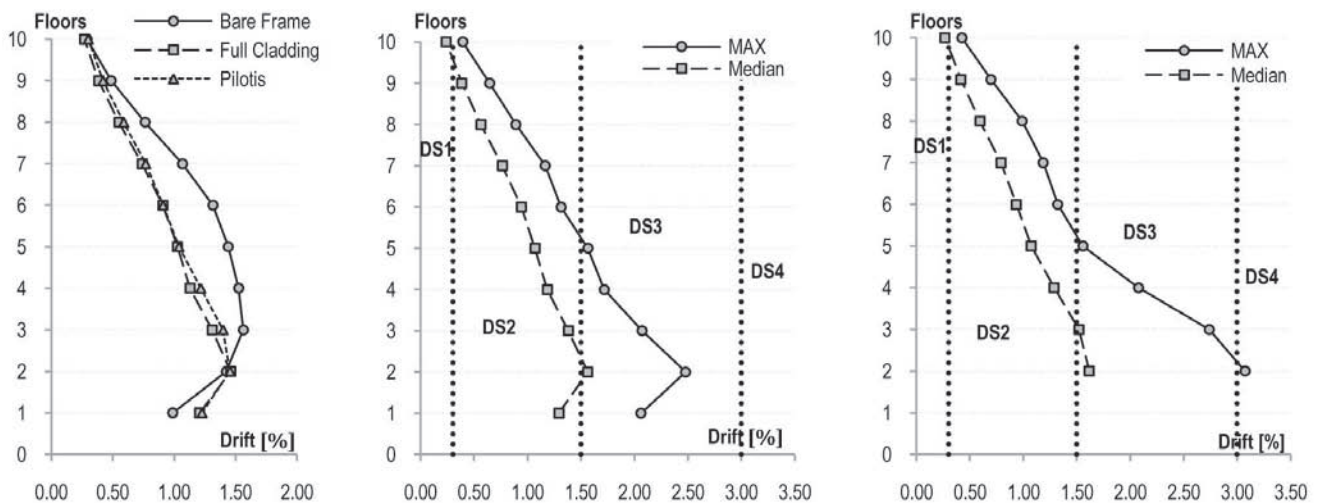


Figure 6. Maximum interstorey drift of the building (left), maximum and median drift of the cladding connections per storey (FC – middle, PI – right) for Design Basis Earthquake (DBE) intensity

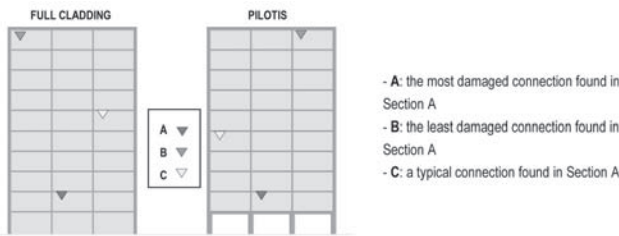


Figure 7. Cladding connections monitored for the risk assessment analysis

tion, a seismic risk assessment is presented. The performance of the cladding system under seismic load can be estimated using the Incremental Dynamic Analysis (IDA) procedure proposed by Vamvatsikos and Cornell [7]. IDA allows the evaluation of various outcomes for given hazard intensity levels, such as the Design Basis Earthquake (DBE) or the Maximum Considered Earthquake (MCE) already described in the last section. The 15 accelerograms presented previously are scaled from 0.1g to 1g with a step of 0.1g in relation to their spectral acceleration ( $S_a$ ).  $S_a$  has been considered as the Intensity Measure (IM) as opposed to Peak Ground Acceleration (PGA) because it has been observed from past researchers to be more appropriate (Shome and Cornell [18]). In total, 150 analyses have been performed for every connection analysed, considering the

maximum relative displacement between the frame and the cladding (cladding connection drift) as the Engineering Demand Parameter (EDP). The damage limit state of the tie-back connections defined in Figure 2 has been defined as the Damage Measure (DM). Three connections are herein considered for the 10 storeys building already presented with two different cladding panels distributions (FC and PI). The choice of the connections is related to the consideration from the analyses in Section A, as described in Figure 7.

### 5.1 Derivation of fragility curves

The results of the IDA for the cases defined above are used to find the probability of reaching/overcoming each damage limit state as a function of the IM. Because non-structural elements are dependent on not only their own performance but the performance of the primary structure, the fragility curves have been prescribed to take into account of the occurrence global collapse using Eq. 1. This concept has been widely described by Jalayer [19] and is commonly referred to as "total probability".

$$P[EDP_i > edp/S_{a_i}] = P[EDP_i > edp/NC, S_{a_i}] \cdot P[NC/S_{a_i}] + P[EDP_i > edp/C, S_{a_i}] \cdot P[C/S_{a_i}] \quad \text{Eq. 1}$$

Where  $edp$  and  $EDP$  are the Engineering Demand Parameters (damage limit state obtained from the analysis),  $S_a$  is the Spectral Acceleration.  $NC$  represents 'No Collapse' while  $C$  is 'Collapse'. For this study the condition of  $C$  (collapse) has been represented by FEMA recommended drift limit for 'Collapse Prevention' of a concrete frame of 4% drift (FEMA 356 [20]). This therefore assumes that the structure either collapses or is damaged beyond repair and will need to be demolished if it reaches a drift of 4% or greater. Figure 8 shows the contribution of the irreparability of the building condition.

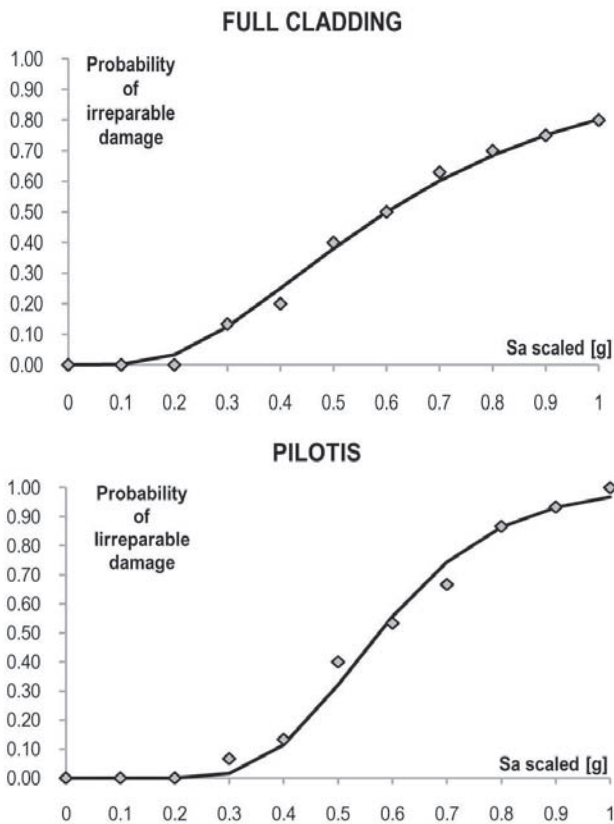


Figure 8. Lognormal probability of occurrence collapse/irreparability of the FC and PI buildings

This condition becomes particularly significant from 0.4g onwards when the probability overcomes 10-15%. At 0.6g half of the models are considered to be irreparably damaged for both building types. At 1.0g, the probability of the buildings overcoming the irreparability limit is around 80% and 95% for FC and PI respectively. Fragility curves for the connections can be derived based on these considerations. The graphs related to the connections A and B of the FC case are shown in Figure 9 using a lognormal cumulative distribution for their representation.

As expected, Figure 9 shows that the position of the connection up the building has a large influence on the probability of damage. Connection A has a higher probability of damage compared with Connection B. For example at 0.6g, Connection A has a 57% probability of being in DS4, while Connection B this probability is only 32%. The comparison between Connection A and B highlights how the failure of the connections over the 8th floor is largely attributed to the irreparable damage of the building rather than to the failure of the actual connections.

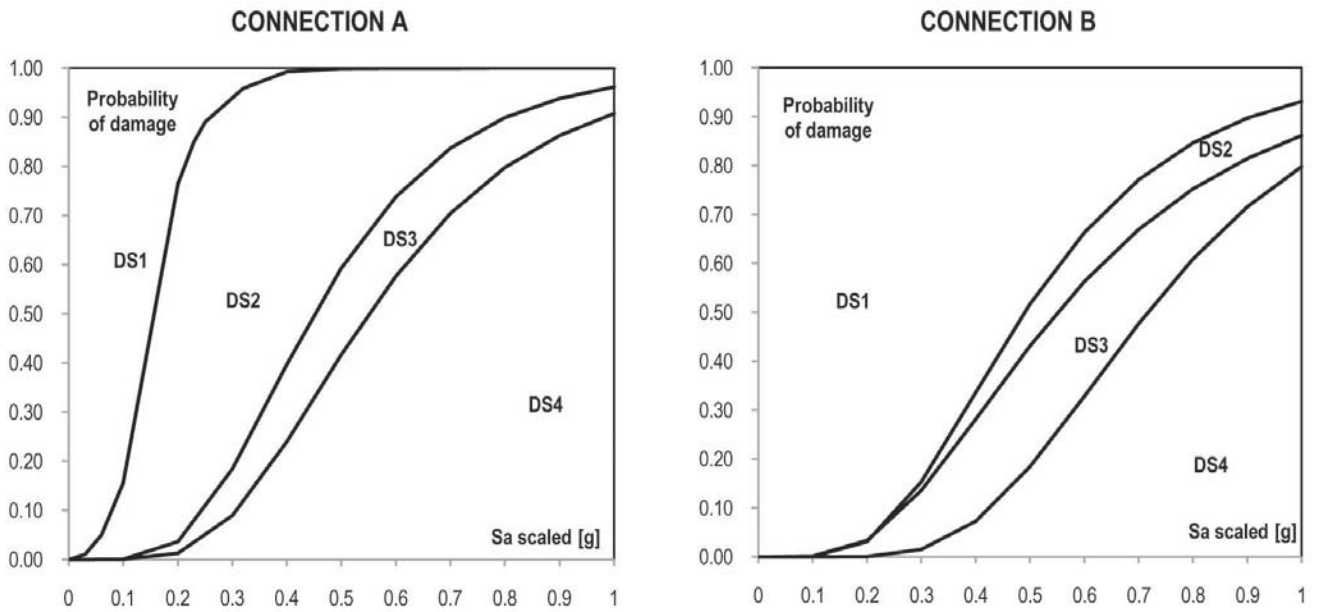


Figure 9. Fragility curves of the connections A and B (FC case)

### 5.2 Quantitative risk assessment

In order to determine damage probabilities of the cladding system in relation to annual frequency, the seismic performance predicted through IDA is required to be combined with the consensus probabilistic seismic hazard map applicable to the location. Fragility curves are herein re-plotted by changing the horizontal axis from the Intensity Measure IM to the annual probability  $p_a$  or return period in years, using the following seismic hazard relationship as a function of  $p_a$  (Maniyar et al. [21]):

$$P_a = q \sqrt{\frac{S_a(T=475)}{S_a(T=Tr)}} \cdot \frac{1}{475} \quad \text{Eq.2}$$

Where  $S_a(T=475)$  and  $S_a(T=Tr)$  are the Spectra

Acceleration at the natural period of an earthquake with respectively return period of 475 years and with return period  $T_r$  (the target  $S_a$ ). The parameter  $q$  is dependent of the local seismicity (0.333 for New Zealand).

Using this relationship it is possible to obtain the probability of the defined damage states not being exceeded for earthquake size of various annual probabilities. Based on the annual probability or return period of the earthquakes (in particular, DBE and MCE), Figure 10 shows the likelihood of the induced damage being within the limits of the four possible damage states for the connections A and B (FC case).

The information shown in Figure 10 can be translated into tabular form as shown in Table 4. The table shows the probability of the damage states not being exceeded (a)

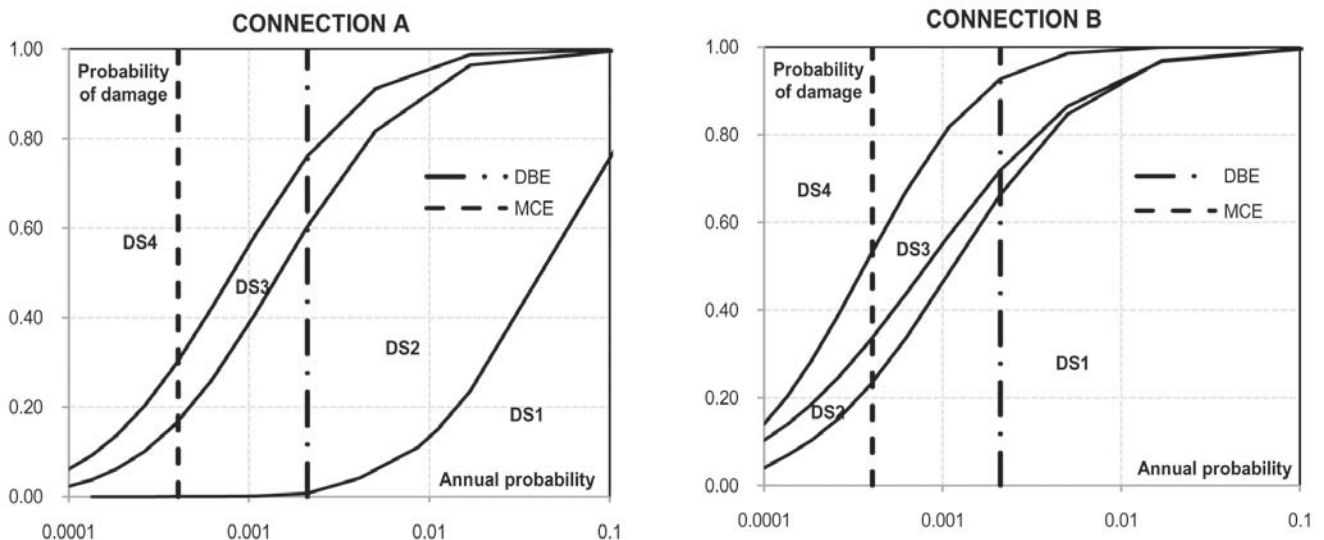


Figure 10. Quantitative risk assessment of connection A and B (FC case)

Connection	Damage Not Being Exceeded (a)					Being in A Given Damage Limit State (b)				
	$P_a$	P[DS1]	P[DS2]	P[DS3]	P[DS4]	$P_a$	P[DS1]	P[DS2]	P[DS3]	P[DS4]
<b>A</b>	DBE	1%	60%	76%	100%	DBE	1%	60%	16%	24%
	MCE	0%	17%	30%	100%	MCE	0%	17%	13%	70%
	$P_a$					$P_a$				
<b>B</b>	DBE	66%	72%	93%	100%	DBE	66%	5%	21%	7%
	MCE	23%	34%	53%	100%	MCE	23%	10%	20%	47%
	$P_a$					$P_a$				

Table 4. Probability of damage not being exceeded and of being in a given damage limit state for connection A and B (FC case) with earthquake of DBE and MCE intensity

	Full Cladding						Pilotis					
	A		B		C		A		B		C	
	DBE	MCE	DBE	MCE	DBE	MCE	DBE	MCE	DBE	MCE	DBE	MCE
<b>DS1</b>	1%	0%	66%	23%	0%	0%	0%	0%	64%	16%	0%	0%
<b>DS2</b>	60%	17%	5%	10%	65%	28%	64%	16%	11%	9%	75%	24%
<b>DS3</b>	16%	13%	21%	20%	19%	20%	11%	9%	10%	9%	11%	7%
<b>DS4</b>	24%	70%	7%	47%	15%	52%	25%	76%	15%	66%	14%	69%

Table 5. Probability of experience the same damage limit states in proportion of large number of cladding connections with same characteristics in similar buildings

and of being in a given damage state (b) for both the connections A and B after DBE and MCE intensity earthquakes. For example, in case (a) if an earthquake of annual frequency equal to DBE strikes, the probability of DS1 not being exceeded is 1% for the connection A, while 66% for the connection B. This highlights how connection B has a very high probability to not being damaged (DS1 = 66%) compared with A which will almost certainly be damaged (>DS1 = 99%).

In case (b), if for example an earthquake with annual frequency equal to MCE strikes, there is a 0% probability that the damage state will be in DS1 for the connection A while for the connection B there is a 23% probability. The probability of being in DS2 is respectively 17% and 10% and so on. Thus, if the intensity of the earthquake is MCE there is the certainty that connection A will be at least damaged in minor/moderate way (DS2). Considering the two configurations (FC and PI) and all the connections monitored, it is possible to present a summary table (Table 5) where all the results are interpreted in terms of the proportion of a large number of cladding connections with the same characteristics in similar buildings likely to undergo different levels of damage in a seismic event of given intensity.

Each column adds to unity so each connection must be in a given damage state. If for example it is desired to know the probability of being in DS2 for a population of 1000 similar buildings (FC case) subjected to an earthquake with DBE intensity, about 600, 50 and 650 (connections A, B and C respectively) are likely to be in DS2. The same reasoning can be made for another population of 1000 buildings (PI case) with the same conditions just described. This time 640, 110, 750 (connections A, B and C respectively) are likely to be in DS2.

### Conclusions

The seismic behaviour of a typical newly designed reinforced concrete multi-storey frame building has been analysed by means of non-linear static and dynamic analyses with the inclusion of common typologies of cladding systems. Results confirm the high influence of cladding systems upon the seismic performance of multi-storey buildings. An increase of between 40 and 50% in initial stiffness is observed for both cladding configurations compared to the bare-frame. A higher strength is also observed for both cases. The pilotis case exhibits a soft-storey mechanism as expected, but in general the maximum inter-storey drifts are concentrated on the first three floors. This trend does not appear to be dependent upon the number of floors or the distribution of claddings. The stiffness ratio between the claddings and the structure is higher, especially as the height of the frame decreases, underlining the positive contribution of the claddings.

Based on the results collected in the first section, a seismic risk assessment analysis was also presented in the form of fragility functions. These were based on damage limit states for cladding connections related to the differential displacement between the structure and the cladding. This revealed the significant variation in possible levels of cladding damage throughout a building. The level of damage in the connections is similar for the first 8 and 6 floors for the Full Cladding and the Pilotis case, respectively. Hereafter, the failure of the upper connections is largely attributed to the irreparable damage of the building rather than to the failure of the actual connections. According to the fragility curves presented, the main differences are observed in damage states DS1 and DS2, which is in relation to the differential damage up the height of the building. For example for a



DBE level earthquake, the probability of an upper level connection being damaged is 66%, compared with a lower level connection which has only a 1% probability of not being damaged.

The use of a 2D model meant representing out-of-plane failure due to high accelerations was not considered. Therefore the analyses only took into account drift related damage and failure of cladding panels. In order to expand upon these results, analyses which include the sensitivity to both drift and acceleration are suggested.

### Author Affiliation

Riccardo Diaferia<sup>1</sup>, Andrew Baird<sup>2</sup>, Stefano Pampanin<sup>3</sup> and Alessandro Palermo<sup>4</sup>

<sup>1</sup>Master Student, Department of Building Environment and Science Technology, Politecnico di Milano, Milan, Italy, riccardo.diaferia@mail.polimi.it

<sup>2</sup>PhD Student, Department of Civil and Natural Resources Engineering, University of Canterbury, Christchurch, New Zealand, andrew.baird@pg.canterbury.ac.nz

<sup>3</sup>Associate Professor (Reader), Department of Civil and Natural Resources Engineering, University of Canterbury, Christchurch, New Zealand, stefano.pampanin@canterbury.ac.nz

<sup>4</sup>Senior Lecturer, Department of Civil and Natural Resources Engineering, University of Canterbury, Christchurch, New Zealand, alessandro.palermo@canterbury.ac.nz

### References

- [1] Baird A., Diaferia R., Palermo A. and Pampanin S., Numerical modelling and preliminary experimental testing outcomes for the design of seismic resistant facades, SEWC 2011, Como, Italy, 4-6 April 2011.
- [2] McMullin K., Wong Y., Choi C. and Chan K., Seismic performance thresholds of precast concrete cladding connections, 13th World Conference on Earthquake Engineering, Vancouver, Canada, 2004.
- [3] Priestley M.J.N., Performance Based Seismic Design, 12th World Conference on Earthquake Engineering, Auckland, New Zealand, 2000.
- [4] SEAOC Vision 2000 Committee, Performance-based seismic engineering, Sacramento, California: Structural Engineers Associate of California, 1995.
- [5] Taghavi S. and Miranda E., Response Assessment of Nonstructural Building Elements, PEER Report, University of California, Berkeley, 2003, 96 pp.
- [6] Cornell C.A., Jalayer F., Hamburger R.O. and Foutch D.A., Probabilistic Basis for 2000 SAC Federal Emergency Management Agency Steel Moment Frame Guidelines, ASCE Journal of Structural Engineering, pp 526-533, April 2002.
- [7] Vamvatsikos D. and Cornell C.A., Incremental dynamic analysis, Earthquake Engineering and Structural Dynamics, 31(3), p. 491-514, 2002.
- [8] Stojadinovic B., Hunt J.P., Seismic performance assessment and probabilistic repair cost analysis of precast concrete cladding systems for multi-storey buildings, PEER Report, University of California, Berkeley, 2010, 364 pp.
- [9] New Zealand Concrete Society, Examples of Concrete Structural Design to New Zealand Standards 3101, editors: Bull D.K. and Brunson D., New Zealand, 1998.
- [10] Standards New Zealand, NZS 3101, Concrete Structures Standard - Part 1, Wellington, NZ, 1995.
- [11] Standards New Zealand, NZS 1170.1, Structural Design Actions - Part 1, Wellington, NZ, 2002.
- [12] Standards New Zealand, NZS 1170.5, Structural Design Actions - Part 5, Wellington, NZ, 2004.
- [13] Carr, A., Ruaumoko Programme for Inelastic Dynamic Analysis - User Manual, Department of Civil Engineering, University of Canterbury, New Zealand 2010.
- [14] Otani S., Sake A., "A Computer Program for Inelastic Response of R/C Frames to Earthquakes". Report UILU-ENG-74-2029, Civil Engineering, 1974.
- [15] Pampanin S., Christopoulos C. and Priestley M.J.N., Residual deformations in the performance-based seismic assessment of frame structures, IUSS Press, Pavia, Italy, 2002.
- [16] Standards New Zealand, NZS 1170.0, Structural Design Actions - Part 0, Wellington, NZ, 2002.
- [17] NEHRP, Recommended Provisions for Seismic Regulations for New Buildings and Other Structures - Part 1 - Provisions (FEMA 302), Federal Emergency Management Agency, Washington D.C., 1997.
- [18] Shome N. and Cornell C.A., Probabilistic seismic demand analysis of nonlinear structures, Report N. RMS-35, Stanford University, Stanford, CA, 1999.
- [19] Jalayer F., Direct probabilistic seismic analysis: Implementing non-linear dynamic assessments, Ph.D. Thesis, Stanford University, 2003.
- [20] FEMA 356, Prestandard and Commentary for the Seismic Rehabilitation of Building. FEMA, 2000.
- [21] Maniyar M., Khare R.K. and Dhakal R.P., Probabilistic Seismic Performance Evaluation of Non Seismic RC Frame buildings, Structural Engineering and Mechanics, N 33(6), 2009.

# Testing of Recycled Aggregate Concrete by Non-Destructive Tests

**M. Chakradhara Rao<sup>1</sup>,  
S.K. Bhattacharyya<sup>2</sup> and S.V. Barai<sup>3</sup>**

## Abstract

In the present paper an attempt was made to evaluate the properties of recycled aggregate concrete using non-destructive tests. Also, an attempt was made to correlate the compressive strength and density of recycled aggregate concrete (RAC) with rebound hammer and ultrasonic pulse velocity in this study. In the present investigation the recycled coarse aggregate (RCA) is obtained from three different demolished old structures viz: two RCC culverts of different sources and a RCC slab of an old residential building. From each source of RCA three recycled aggregate concrete mixes were prepared with 25%, 50% and 100%. In order to assess the performance of RAC in comparison with normal concrete, two normal concrete mixes prepared with 100% natural coarse aggregate. All mixes were designed for M25 grade of concrete with free water to cement (w/c) ratio of 0.43. It was observed that irrespective of the source of RCA, the compressive strength and density of recycled aggregate concrete is lower than the normal concrete. In addition, it was observed that the pulse velocity and rebound number increased with the increase in strength and density.

## Key words

Recycled aggregate concrete (RAC), Compressive strength, Density, rebound number, Ultrasonic pulse velocity (UPV)

## 1. Introduction

The new zoning bye-laws, legitimization of squatter settlements and increase in the urban population due to industrial development have led to the demolition of structures in the larger cities. Insufficient capacity of old road bridges for present and future growing traffic and modernization of highway bridges needs the demolition of old bridges too. Also, structures are destroyed due to either natural disasters such as earthquakes, cyclones etc. or man-made disasters. Hence, the entire world is facing the problem of handling the waste material generated from the demolition. The Central Pollution Control Board (CPCB) of India had estimated the total solid waste generation as 48 million tonnes for the year 2001 out of which 12 - 14.7 million tonnes from the construction industry itself and by 2010 this value was

predicted to be around 24 million tonnes (TIFAC Ed 2000). Further, there is a large requirement of raw materials in the construction sector in India. Projections for building material requirement of the housing sector indicate a shortage of aggregates to the extent of about 55,000 million cubic meters. For achieving the target for road development up to 2010, an estimated 750 million cubic meters of coarse aggregate as sub-base material shall be required (TIFAC Ed 2000). Recycling of aggregate material from the construction and demolition waste may reduce the demand-supply gap in both these sectors. The recycling technology not only solves the problem of waste disposal, but reduces the cost and preserves environment also. In addition, the recycling and proper management of construction and demolition waste gives better opportunities to handle the other kinds of waste, as less land is used for dumping of the construction and demolition waste.

The estimation of concrete strength in existing structures using non-destructive tests is of considerable interest of field engineers. Several national and international standards recognized the various methods of non-destructive tests as suitable (BS 6089 (1981)). Most of the non-destructive test methods are suitable to estimate the other properties of concrete than compressive strength. Among various test methods, the rebound hammer and ultrasonic pulse velocity tests are the most commonly used non-destructive test methods to estimate the compressive strength. Hence, in the present investigation, an attempt is made to correlate the strength, density, rebound number and pulse velocity of recycled aggregate concrete made with different source of recycled coarse aggregate.

## 2. Literature review

The research on the use of construction and demolition waste as an aggregate in the production of concrete has started since early 1950. The RILEM Technical committee 37 DRC published a state-of-the-art report on recycled concrete as an aggregate for concrete covering the period 1945 - 1977 (Nixon 1978). The author concluded that the past researchers examined the basic properties of concrete made with recycled concrete as coarse aggregate and most of the researchers found a good agreement on the behaviour of the concrete, made with recycled aggregate.

However, during this period most of the researchers have used the laboratory tested specimens as recycled aggregate in the production of concrete. Again in the year 1986, the second state-of-the-art-report on the developments between 1945 - 1985 on recycled aggregates and recycled aggregate concrete has been published by Hansen (1986). During this period, most of the researchers examined the influence of recycled aggregate on various properties of concrete and their utilization in non structural applications. After 1980 till 2000 there was not much progress in the field of recycled aggregate concrete. In the recent times, most of the countries have identified the disposal of construction and demolition waste as a serious problem. The researchers have started exploring on both aspects of field and laboratory waste concrete as aggregate in the production of concrete. Countries like UK, China, Japan, Germany, Hong Kong, etc., have published some guidelines and specifications on the use of recycled aggregates and its use in concrete. Most of the researchers have found that the properties of RAC made with different percentages of RCA are relatively weaker than those of normal concrete made with natural aggregate (Bairagi et al. 1993; Rao 2005; Kou and Poon 2008, Padmini et al. 2009). However, Etxeberria et al. (2007), Rao et al. (2010) suggested 25% of RCA may be used in the production of concrete. Few attempts have been made on the correlation of strength and in-situ test results of recycled aggregate concrete. Ravindrajah et al. (1987) observed that the recycled aggregate influence the strength of concrete cured under water. It was also reported that for the same value of pulse velocity, the strength of recycled aggregate concrete is more than that of normal concrete.

### 3. Experimental programme

#### 3.1 Materials

Ordinary Portland Cement (OPC) of 43 grade conforming to Bureau of India Standard Specifications of IS: 8112 (1989) with specific gravity 3.14 is used in this study. The locally available natural sand and 20 mm maximum size natural coarse aggregate available from the local quarries conforming to the grading requirements of IS: 383 (1970) are used. The recycled coarse aggregates are obtained from three different demolished structures: two different demolished old RCC culverts of different locations and a RCC slab of an old residential building. The recycled coarse aggregate obtained from the three sources are designated as RCA-S1, RCA-S2 and RCA-S3 respectively. The important properties of both natural and recycled coarse aggregates are presented in Table 1.

Property	Coarse aggregate			
	Natural	RCA-S1	RCA-S2	RCA-S3
Specific gravity (SSD)	2.75	2.51	2.47	2.417
Water absorption (%)	1.129	3.92	3.009	3.934
Density (kg/l)	1.581	1.413	1.34	1.35

Table 1. Properties of coarse aggregate

#### 3.2 Concrete Mixes

Three recycled aggregate concrete mixes are prepared with 100% RCA obtained from each source. These mixes are designated as MM-RAC, MK-RAC and MV-RAC respectively. In all the mixes, the first letter represents the mix, the second letter represents the source of RCA and RAC indicate the recycled aggregate concrete. In order to assess the performance of recycled aggregate concrete in comparison with normal concrete, two normal concrete mixes were prepared with 100% natural coarse aggregate and these are designated as M1-RAC0 and M2-RAC0 respectively. One corresponding to the RAC made with RCA obtained from the sources 1 and 2, and the other corresponding to the RAC with source 3 RCA. The cement used in the test is OPC 43 grade manufactured by Ultratech Cement Co., India. While testing, some variation in the chemical composition is observed and the same are indicated in Table 2. Cement 1 is used for the RAC made with sources 1 and 2 RCA and corresponding normal concrete and cement 2 is used in RAC made with source 3 RCA and in corresponding normal concrete. In all mixes the locally available natural sand used as fine aggregate. All mixes were designed for M25 grade of concrete in accordance with BIS (IS: 10262-1982). In all mixes, the free water-cement ratio was kept constant at 0.43 and slump was maintained in the range of 50-60 mm by adding Sika Viscocrete R-550 (l) superplasticiser. The details of all mixes are presented in Table 2.

Series No.	Mix designation	Cement (kg)	Natural FA (kg)	Natural CA (kg)	RCA (kg)	Super plasticizer*
1	M1-RAC0	401	574	1261	0	0.05
	MM-RAC25			911	303	0.05
	MM-RAC50			585	585	0.175
	MM-R100			0	1119	0.225
2	M1-RAC0			1261	0	0.05
	MK-RAC25			930	310	0.05
	MK-RAC50			601	601	0.175
	MK-RAC100			0	1114	0.225
3	M2-RAC0			1261	0	0.05
	MV-RAC25			931	310	0.05
	MV-RAC50			592	592	0.175
	MV-RAC100			0	1078	0.225

Table 2. Details of mix proportions (kg per cubic meter of concrete)

### 4. Results and Discussion

#### 4.1 Properties of Recycled Coarse Aggregate

- From Table 1 it is observed that the specific gravity (SSD) of recycled coarse aggregate is less than that of natural aggregate. The specific gravity of recycled coarse aggregate is in the range of 2.23 to 2.6 reported in the literature. The specific gravity of RCA obtained from the sources 2 (RCA-S2) and 3 (RCA-S3) are little lower than those obtained from source 1 (RCA-S1). This may be

due to fact that the recycled coarse aggregates obtained from these sources have 4% - 5% particles finer than 4.75 mm. This may be attributed to the adherence of relatively higher quantity of old cement mortar to the recycled aggregate. Due to lower specific gravity of recycled coarse aggregates, there is a reduction in the amount of recycled coarse aggregate to be used in the recycled aggregate concrete.

- Table 1 shows the density of RCA obtained from all the three sources are 10.6%, 15.2% and 14.6% respectively lower than that of natural coarse aggregate. This is mainly due to the old cement mortar which is adhered to recycled coarse aggregate is light and porous in nature. There is a little difference among the bulk density of recycled coarse aggregates obtained from the three different sources. This is obvious that the bulk density of recycled coarse aggregate mainly depends on the cement content attached which in turn depends on the quality of source concrete.
- The water absorption of natural coarse aggregate is 1.121%. This value is expected for natural gravel. It is worth noting that irrespective of source, the water absorption of recycled coarse aggregate is higher than that of the natural coarse aggregate. This is expected due to porous and high absorption capacity of old mortar adhered to the aggregate in recycled aggregate. The absorption capacity of the recycled coarse aggregate is 2.7 to 3.5 times higher than that of natural aggregate.

## 4.2 Properties of Recycled Aggregate Concrete

### 4.2.1 Compressive strength

The compressive strength test is conducted on 150 mm cubes at 28 days of curing in accordance with the guidelines of IS 516 (1959). The variation in 28 day compressive strength of recycled aggregate concrete made with different percentages of RCA obtained from all the three sources are presented in Fig. 1.

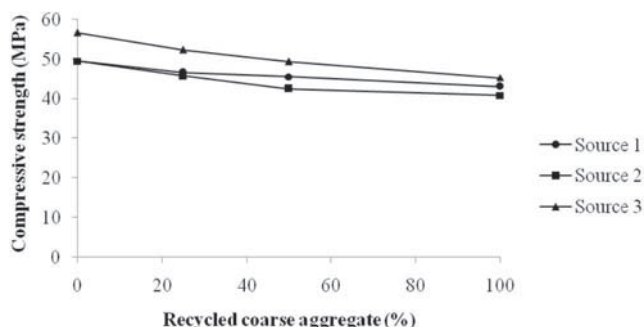


Figure 1. Compressive strength variation with percentage of RAC

It is observed that irrespective of the source of RCA the compressive strength of RAC decreased with the increase in percentage of recycled coarse aggregate. Nevertheless, all recycled concrete mixes have achieved the target

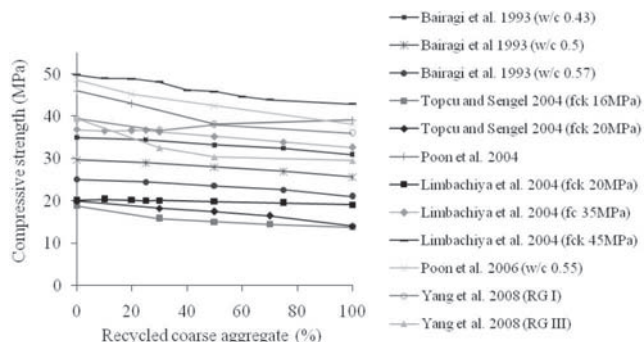


Figure 2. Variation in compressive strength with different percentage of RCA reported by different researchers

strength after 28 days of curing. The variation in compressive strength of RAC for different content of RCA reported by different researchers is presented in Fig. 2

It shows that the present test results are similar to the results reported in the literature. The reduction in compressive strength of RAC at 25%, 50% and 100% RCA obtained from sources 1, 2 and 3 are 5.7%, 7.8%, 12.9%; 7.5%, 14.1%, 17.5% and 11.3%, 14.7%, 17.6% respectively compared to normal concrete. These reductions in strength indicate that 25% RCA content does not influence much on compressive strength of concrete.

### 4.2.2 Density

The density test on both normal and recycled aggregate concrete are conducted in accordance with the guidelines of ASTM C 642-06. The test results of density of normal concrete and recycled aggregate concrete for different RCA values obtained from all the three sources are presented in

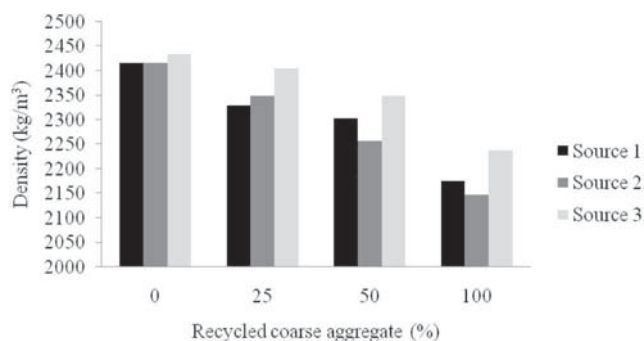


Figure 3. Density of recycled aggregate concrete made with RCA obtained from all the three sources

Fig. 3. Presented values are the average of three samples.

Fig. 3 reveals that in all the Sources of mixes the density of RAC decreased with the increase in coarse aggregate replacement percentage. The decrease in density may be due to fact that the density of recycled coarse aggregates are 1.12, 1.18 and 1.17 times lower in Sources 1, 2 and 3 than that of natural coarse aggregate. This may be attributed to the adherence of light and porous nature of old



cement mortar to the recycled aggregates. The density of RAC made with 25% to 100% RCA obtained from Sources 1 and 2 are in the range of 2329 kg/m<sup>3</sup> to 2175 kg/m<sup>3</sup> and 2349 kg/m<sup>3</sup> to 2148 kg/m<sup>3</sup> respectively against 2415 kg/m<sup>3</sup> for normal concrete. Similarly, the density of RAC made with 25 to 100% RCA obtained from Source 3 is in the range of 2405 kg/m<sup>3</sup> to 2238 kg/m<sup>3</sup> against 2435 kg/m<sup>3</sup> for normal concrete. In general the density of normal concrete made with natural aggregate is in the range of 2200 - 2600 kg/m<sup>3</sup> (Neville 2006). The density of RAC made with Source 3 RCA is relatively higher than that of RAC made with other Sources of RCA. As discussed earlier, more particles (5%) finer than 4.75 mm in Source 3 RCA, the density of the mixes may increase relatively. The reduction in density of recycled aggregate concrete made with RCA obtained from sources 1, 2 and 3 are in the range of 3.6 to 10%, 2.7 to 11.1% and 1.2 to 8.1% respectively compared to the concrete with natural coarse aggregate. This reduction may be advantage where dead weight is a problem and where light weight concrete is required. In concrete structures the self-weight contribution is a major portion of the total load on the structure. Therefore, by using RAC of low density with reasonable strength, smaller sections may be adopted thereby the foundation size can be reduced.

#### 4.2.3 Non-Destructive Test Results

The non-destructive tests are useful for the assessment of homogeneity and quality of concrete. Though there are many tests available, in the present study only rebound hammer test and ultrasonic pulse velocity tests are used. Three samples are used for each test and the mean values are presented. On each sample the pulse velocity, rebound number tests are conducted.

##### (a) Ultrasonic pulse velocity

The test results of ultrasonic pulse velocity and compressive strength of RAC made with different percentages of recycled coarse aggregate obtained from all the three Sources are shown in Table 3.

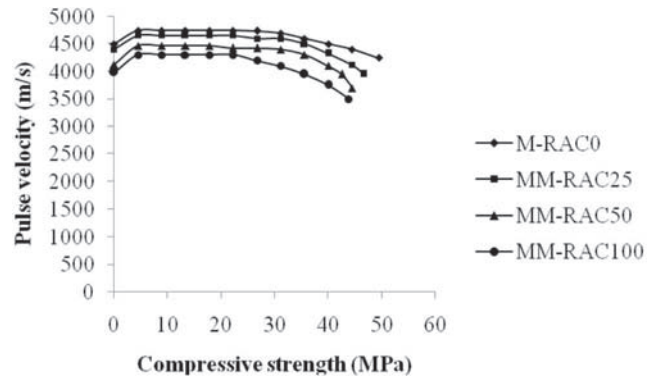


Figure 4. Ultrasonic pulse velocity variation under stress for RAC with Source 1 RCA

It is observed that irrespective of the Source of RCA the ultrasonic pulse velocity of recycled aggregate concrete decreased with the increase in recycled coarse aggregate percentage. This may be due to the change in porosity of recycled coarse aggregates and the presence of more number of micro cracks in recycled aggregates. The recycled aggregates generally consist of strong natural aggregates with more porous cement mortar attached to them. Similar result is reported in the literature (Ravindrarajah et al. 1987). Compared to normal concrete, there is a reduction of 1.9 to 9.4% in UPV in RAC with 25 - 100% RCA obtained from Source 1. Similarly, the reduction in UPV in RAC with 25 - 100% RCA obtained from Sources 2 and 3 are 1.9 - 10% and 5.5 - 10.8% respectively compared to the corresponding normal concrete. In addition, it is observed that the pulse velocity of RAC for all the percentages of RCA obtained from all Sources are in the range of 4.181 km/s to 4.66 km/s and the same for normal concrete is 4.69 to 4.75 km/s. This indicates the uniformity of concrete mixes. According to IS: 13311-1992 (Part 1), the quality of concrete graded as excellent and good when the pulse velocity is more than 4.5 km/s and 3.5 to 4.5 km/s respectively.

The variation in pulse velocity under compressive stress for

Source of RCA	Mix designation	RCA (%)	Ultrasonic pulse velocity (km/s)	Rebound number
Normal concrete	M1-RAC0	0	4.748	26.47
Source 1: RCC culvert near Medinipur	MM-RAC25	25	4.658	19.48
	MM-RAC50	50	4.464	16.23
	MM-RAC100	100	4.3	17.68
Source 2: RCC culvert near Kharagpur	MK-RAC25	25	4.66	16.68
	MK-RAC50	50	4.358	15.2
	MK-RAC100	100	4.275	13.2
Source 3: RCC slab of an old residential building near Vizianagaram	M2-RAC0	0	4.69	31.6
	MV-RAC25	25	4.43	29.46
	MV-RAC50	50	4.43	29.04
	MV-RAC100	100	4.181	27.95

Table 3. Ultrasonic pulse velocity, rebound number and compressive strength of both normal and recycled aggregate concrete

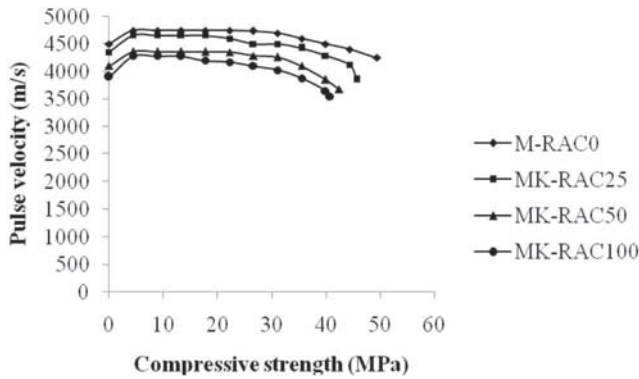


Figure 5. Ultrasonic pulse velocity variation under stress for RAC with Source 2 RCA

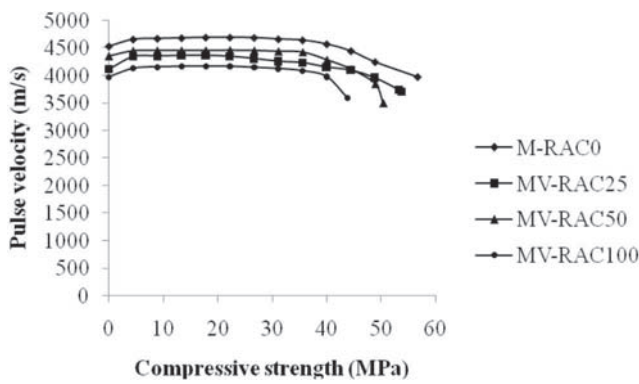


Figure 6. Ultrasonic pulse velocity variation under stress for RAC with Source 3 RCA

RAC made with different percentages of RCA obtained from all the three sources is presented in Figs. 4 - 6 respectively.

It is observed that the variation in pulse velocity with stress is almost similar in both normal concrete and recycled aggregate concrete with all sources of RCA. Further, it reveals that the pulse velocity increases with the increase in strength up to 4-5 MPa and then it is constant with further increase in stress up to 30 to 35 MPa and thereafter starts decrease with further increase in stress up to failure. The initial increase in velocity may be due to restructuring of the internal microcracks in the material. As the load increases these microcracks gets widened and the velocity is reduced. At the time of failure the drop in velocity is higher in case of RAC with higher percentage of RCA (50 - 100%) when compared to normal concrete and RAC with lower percentage of RCA.

**(b) Relationship between compressive strength, density and pulse velocity**

The compressive strength of concrete is one of the prime properties of structural concrete. Hence, the strength and pulse velocity relation is obtained from the experimental results. The compressive strength and density is a function of pulse velocity for RAC with all percentages of RCA obtained from all the Sources is presented in Fig. 7.

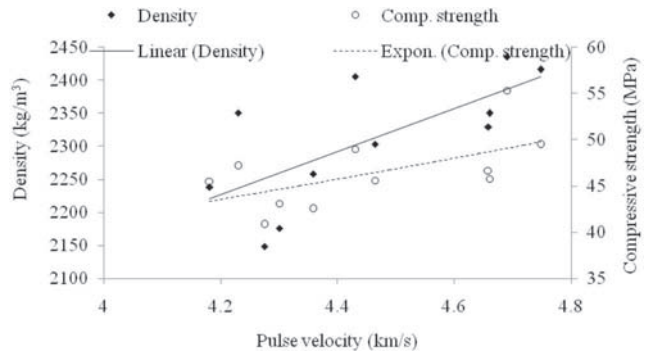


Figure 7. Compressive strength and density are as function of pulse velocity

It is observed that both compressive strength and density are decreased with the decrease in pulse velocity. A regression analysis between compressive strength and pulse velocity and density and pulse velocity are performed to obtain a correlation coefficient equal to 0.6 and 0.7 by using exponential and linear models respectively which are the best fitted curves for the relationships under study. The obtained relationships are indicated in Eqn.1 for compressive strength ( $f_{ck}$ ) and pulse velocity ( $V$ ) and Eqn.2 for density (?) and pulse velocity ( $V$ ).

Compressive strength  $f_{ck} = 15.66 \times e^{0.243XV}$  ( $R^2 = 0.36$ ) (1)  
 Density  $\rho = 325.7 \times V + 858.6$  ( $R^2 = 0.5$ ) (2)

Where  $f_{ck}$  is in MPa,  $\rho$  is in  $kg/m^3$  and  $V$  is in  $km/s$ .

**(c) Rebound number**

The rebound hammer test is conducted as per the procedure given in BIS (IS: 13311-1992 (Part 2)). It is classified as hardness test and it is based on the principle that the rebound of an elastic mass depends on the surface hardness against which the mass impinges. It measures only the surface zone properties. The test results of rebound hammer for both normal concrete and recycled aggregate concrete made with different percentages of recycled coarse aggregate obtained from all the Sources are vide Table 2. It is observed that the rebound number decreases as the recycled coarse aggregate percentage increases. In addition, it is observed that there is a large difference in rebound number between normal concrete and recycled aggregate concrete made with all percentages of recycled coarse aggregate. The rebound number for normal concrete is 26 to 31, whereas, the same for RAC with 25 to 100% RCA obtained from Source 1 is in the range of 20 to 16 and for RAC with same percentages of RCA from Sources 2 and 3 are 17 to 13 and 27 to 29 respectively. This may be due to the more porous nature of recycled aggregates due to weak cement paste that is adhered to them.

**(d) Relationship between compressive strength and rebound number**

Fig. 8 shows the compressive strength is a function of rebound number for RAC with all percentages of RCA obtained from all Sources.

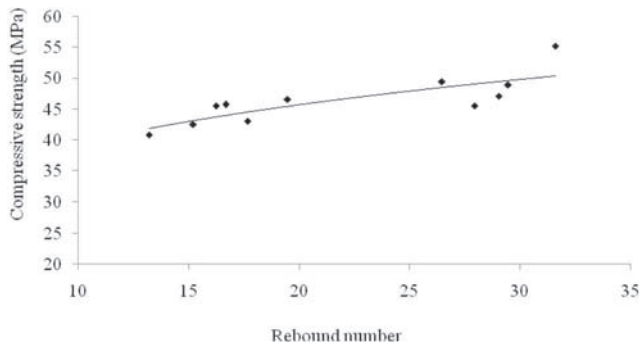


Figure 8. Compressive strength is a function of rebound number

A regression analysis between compressive strength and rebound number is carried out to obtain a correlation coefficient equal to 0.67 by using a power model which is the best fitted for the relationships under study. The obtained relationship is indicated in Eqn.3.

$$\text{Compressive strength } f_{ck} = 24.16 \times N^{0.213} \quad (R^2 = 0.67) \quad (3)$$

Where  $f_{ck}$  is in MPa and N is a number.

It reveals that the compressive strength decreased with the decrease in rebound number.

## 5. Closing Remarks

Compressive strength, density, rebound number and pulse velocity of both normal and recycled aggregate concrete with different percentage of recycled coarse aggregate obtained from three different sources are studied. Based on the test results the following conclusions may be drawn.

The compressive strength and density of recycled aggregate concrete are relatively lower than those of corresponding normal concrete. However, inclusion of 25% RCA in RAC does not affect significantly the properties of concrete. The pulse velocity and rebound number of RAC are decreased with the increase in RCA content. Nevertheless, the results of pulse velocity of RAC indicate the quality of concrete is good. The stress level in concrete influences the pulse velocity of both normal and recycled aggregate concrete. The compressive strength and density are related with pulse velocity using exponential and linear best fit curves respectively. However, more data is required to make the exact relationship among these properties.

## Acknowledgements

The authors would like to thank the University Grants Commission (UGC), Government of India for their financial support. The authors also thank the staff of structural Engineering laboratory of Civil Engineering Department, IIT Kharagpur for extending their cooperation in conducting the experiments. The authors acknowledge the supplier of Sika Viscocrete Superplasticiser, SIKA India Pvt. Ltd., Kolkata.

## Author Affiliation

M. Chakradhara Rao<sup>1</sup>, S.K. Bhattacharyya<sup>2</sup> and S.V.Barai<sup>3</sup>

<sup>1</sup>Civil Engineering Department, Gitam Institute of Technology, GITAM University, Visakhapatnam, Andhra Pradesh - 530 045, India

<sup>2</sup>Central Building Research Institute, Roorkee, Uttarakhand-247 667, India

<sup>3</sup>Civil Engineering Department, Indian Institute of Technology, Kharagpur - 721302, India Email: skbarai@civil.iitkgp.ernet.in

## References

- A. Rao. (2005). M.Tech. Thesis submitted to Indian Institute of Technology, Kanpur, India.
- A.K. Padmini, K. Ramamurthy and M.S. Mathews. (2009). "Influence of parent concrete on the properties of recycled aggregate concrete." *Construction and Building Materials*, 23, 829 - 836.
- A.M. Neville. (2006). *Properties of Concrete*. Pearson Education Ltd.
- C.S. Poon, S.C. Kou, and D. Chan. (2006). "Influence of steam curing on hardened properties of recycled aggregate concrete". *Magazine of Concrete Research*, 58, 289-299.
- C.S. Poon, Z.H. Shui, L. Lam, H. Fok, and S.C. Kou. (2004). "Influence of moisture states of natural and recycled aggregates on the slump and compressive strength of concrete". *Cement and Concrete Research*, 34, 31-36.
- I.B. Topcu, and S. Sengel. (2004). "Properties of concretes produced with waste concrete aggregate". *Cement and Concrete Research*, 34, 1307-1312.
- K.H. Yang, H.S. Chung, and A.F. Ashour. (2008). "Influence of replacement level of recycled aggregate on concrete properties". *ACI Materials Journal*, 105, 289-296.
- M. Chakradhara Rao, S.K. Bhattacharyya, and S.V. Barai. (2011). "Influence of field recycled coarse aggregate on the properties of concrete". *Materials and Structures*, 44, 205 - 220.
- M. Etxeberria, E. Vazquez, A. Mari, and M. Barra. (2007). "Influence of amount of recycled coarse aggregates and production process on properties of recycled aggregate concrete." *Cement and Concrete Research*, 37, 735 - 742.
- M.C. Limbachiya, A. Koulouris, J.J. Roberts, and A.N. Fried. (2004). "Performance of recycled aggregate concrete". *RILEM Int. symp. on environment-Conscious materials and system for sustainable development*, 127-136

- N.K. Bairagi, R. Kishore, and V.K. Pareek. (1993). "Behaviour of concrete with different proportions of natural and recycled aggregates." *Resources Conservation and Recycling*, 9, 109 - 126.
  - R. Ravindrarajah, Y.H. Loo, and C.T. Tam. (1988). "Strength evaluation of recycled aggregate concrete by in-situ tests." *Materials and Structures*, 21, 289 - 295.
  - S.C. Kou, and C.S. Poon. (2008). "Mechanical properties of 5-year-old concrete prepared with recycled aggregates obtained from three different sources." *Magazine of Concrete Research*, 60, 57 - 64.
  - T.C. Hansen. (1986). "Recycled aggregates and recycled aggregate concrete second state of the art report developments 1945 - 1985." RILEM TECHNICAL COMMITTEE - 37 - DRC. *Materials and Structures (RILEM)*, 19, 201 - 246.
  - TIFAC. Ed., (2005). *Utilisation of waste from construction industry*, Department of Science and Technology, New Delhi.
-



# The Spanish Fortress in l'Aquila: Emergency Actions, Investigations and Monitoring

F. Casarin<sup>1</sup>, F. Lorenzoni<sup>2</sup>, L. Cantini<sup>2</sup>, S. Munda<sup>3</sup>, L. Binda<sup>4</sup>,  
C. Modena<sup>5</sup>, R. Ciabattoni<sup>6</sup> and C. Cacace<sup>6</sup>

<sup>1</sup>Dr. Eng., Department of Structural and Transportation Engineering, University of Padova; casarin@dic.unipd.it

<sup>2</sup>Dr. Eng., Department of Structural Engineering, Politecnico di Milano; cantini@stru.polimi.it

<sup>3</sup>Full Professor, Department of Structural Engineering, Politecnico di Milano; binda@stru.polimi.it

<sup>4</sup>Full Professor, Department of Structural and Transportation Engineering, University of Padova; modena@dic.unipd.it

<sup>5</sup>Eng., Department of Structural and Transportation Engineering, University of Padova; lorenzoni@dic.unipd.it

<sup>6</sup>Istituto Superiore per la Conservazione ed il Restauro, Rome

## Summary

The earthquake occurred on the 6th of April 2009 in the Abruzzo Region of Italy seriously hit the Cultural Heritage (C.H.) patrimony with major destructive effects on l'Aquila, a city of 70,000 inhabitants with the size and the historical and strategic importance of the capital of the Region. The emergency activities to protect the C.H. have been developed following two parallel levels: (i) damage survey and (ii) design and implementation of temporary safety measures. The organization of emergency actions was managed by a centralized structure, the so-called Function 15 "Protection of Cultural Heritage" directed by a Special Commissioner. The structure coordinated the on-site surveys of protected buildings and the design and implementation of temporary safety measures. Several Italian Universities during and after these first emergency actions were invited by the Commissioner to work on selected Case Histories: the aim was on the one hand to provide a first interpretation of the observed damages and on the other hand to define some guidelines for a higher level of investigation.

In this paper the case study of the Spanish Fortress in L'Aquila supervised by the authors is reported with the description of the earthquake dam-

ages and the emergency intervention derived from the "Palaces template" [Ref. 1]. The emergency interventions were carried out in order to avoid progressive damages due to the following several aftershocks. The authors decided together with the officers of MiBAC (Ministry of C.H.) in L'Aquila to proceed with further on site investigations and monitoring. A series of non destructive and minor destructive testing were performed in the Spanish Fortress by the research groups of the Politecnico di Milano and the University of Padova in order to characterize and evaluate quantitatively and qualitatively the state of damage of the masonry structures (walls and pillars) and to identify the structural response of the most damaged wings of the building. The experimental campaigns included: (i) sonic pulse velocity tests, radar tests and thermography, (ii) single and double flat jack tests, (iii) dynamic identification tests. The ND tests were mainly aimed at defining the state of damage of the heavy pillars and of the transversal bearing walls on the ground floor and at designing the most effective strengthening interventions. Furthermore a permanent static and dynamic monitoring system was installed by the ISCR (Rome) and the University of Padova respectively in order to control the dynamic character-

istics of the fortress, constantly verify the damage pattern of the structure and provide a step-by-step monitoring procedure during each phase of restoration.

## Keywords

Cultural Heritage Buildings, Earthquake, ND Investigation Techniques, Monitoring.

## Theme

Tests – earthquake – masonry

## 1. Historical notes

The Spanish Fortress of L'Aquila (Figure 1 and Figure 2) is one of the most impressive Renaissance castles in Central and Southern Italy. In the 15th century L'Aquila became the second most powerful city in the Kingdom of Naples, under the Spanish domination. In 1528 Viceroy Filiberto d'Orange ordered to build a fortress in the highest North spot of the city, according to the project of a famous Spanish architect, Don Pirro Aloisio Escrivà. The construction started in 1534; Escrivà designed a giant fortress, composed by four bastions connected through heavy walls, 60 meters long, with a thickness of 30 m at the bottom and 5 m at the top. All around the fortress there was a ditch (never filled with water) 23 meters wide



Figure 1: Aerial view of the Spanish fortress of L'Aquila, before the earthquake

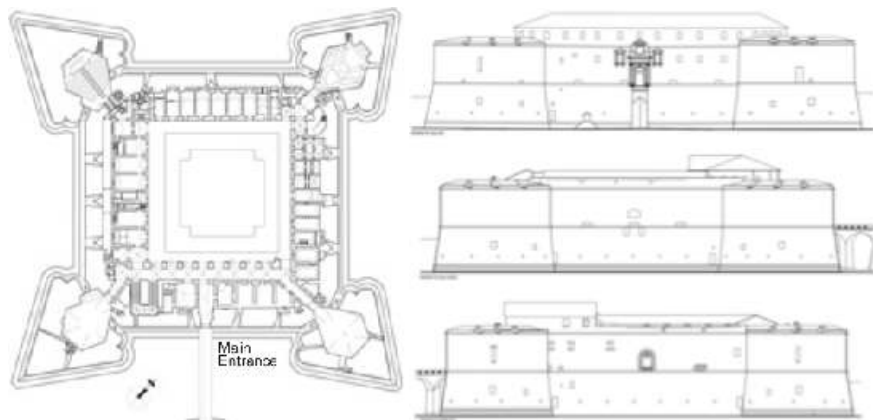


Figure 2: Geometric survey of the building: plan view (on the left) and elevations (on the right)

and 14 meters deep, aimed at defending the foundations from the enemy artillery. The Fortress, which was built not to defend the city, but to control it (many cannons pointed to the city) and to be a completely self-sufficient structure, was never used in battles. Its cannons, always ready to fire, were silent throughout the centuries: the only victim was the city itself, whose decline began with the construction of the fortress and went on under the Spanish domination. Between 1949 and 1951 the castle was restored, and chosen as the seat of the National Museum of Abruzzo.

## 2. Damage description

The Spanish fortress was seriously damaged by the earthquake of the 6th of April 2009. The most relevant damages and collapses involved especially the upper floors of the Fortress. According to the damage survey template for palaces used in the technical inspections [Ref. 1], overturning and

flexural mechanisms on the external walls, shear damage in the external and internal walls, damages to vaults and arches, local collapses of floors and vaults, correspond to the most worrying observations. The damages shown by the building were remarkable both for intensity and distribution, and were considered so serious to be likely menacing the overall stability of some large parts of the building.



The South-East wing (Figure 3) of the fortress underwent the most significant structural problems. On the external front it can be noted the overturning of the upper masonry walls; several collapses took place at the second floor together with a considerable separation of the floors from the longitudinal walls.

In the internal front of the same side the pillars of the porch arcade show crushing failure mechanisms. The seismic event damaged the walls of the first floor and produced a longitudinal crack in the barrel vault of the arcade. The crack is also visible on the floor surface above, meaning that it interests the entire thickness of the floor. There are also many shear cracks on the transverse bearing walls (Figure 4).

In the South-West wing it can be noted an overturning mechanism of the two facades, cracks on vaults and shear cracks on the transverse walls. Moreover, on the first and second floor the separation between external perimeter walls and internal walls and floors are clearly evident.

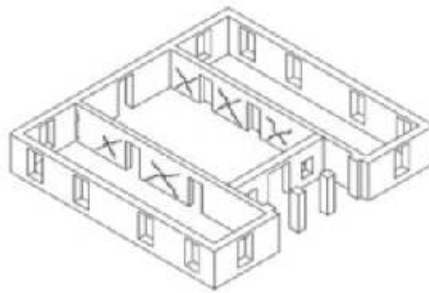
The two facade of the North-West part showed a greater resistance to the overturning mechanism; there are no large detachments of the floors from the perimeter walls. In fact in this area of the fortress a system of tie rods connecting the perimeter walls had been inserted before the earthquake. This intervention was effective and avoided collapses and irreversible damages to the structure. However, the transverse



Figure 3: Out-of-plane overturning of the upper part of the main façade (South-East side)



Figure 4: Severe shear cracks and collapses in the internal walls of the South-East wing



walls are seriously damaged and on the second floor some parts of masonry walls and floor slabs collapsed.

The North-East wing is affected by a slight overturning mechanism of the two façades. There are some shear cracks on masonry walls but the most evident damages are localized on the upper floors.

### 3. Emergency provisional structures

The design of temporary interventions for the safety of an historical building starts from the damage survey and from the identification of the collapse mechanisms activated from the seismic action [Ref. 2].

According to the observed damage pattern, provisional strengthening interventions were applied to the South-East and South-West wings of the fortress, where the heaviest damages were observed. Different teams of specialized people from the National Fire Brigades (SAF-Speleo-Alpino-Fluviali) carried out the strengthening interventions, which did not rely upon external propping structures, also considered the massive dimensions of the fortress. The structural stability was provided by relying on the remaining strength of the resisting elements, e.g. by connecting the internal and external façades of the damages wings by means of stainless steel cables, in order to avoid the observed overturning mechanisms evolution, especially taking into account that non negligible aftershocks occurred for several months. In the South-East wing it was necessary to rebuild the roof, by using hollow section steel trusses and a light

covering structure made of wood. The substitution of the original wooden structure of the roof with a heavy and stiff reinforced concrete structure, without any strengthening interventions on the underlying masonry walls, caused the collapse of the upper part of the façade (Figure 3). In the South-West wing steel frames were positioned in contrast to the external and internal façades before tensioning the cables (Figure 5).

### 4. On site preliminary experimental investigations

A series of non destructive (NDT) and

minor destructive (MDT) testing were performed in the Spanish Fortress by the research groups of the Politecnico of Milan and the University of Padova in order to characterize and evaluate the state of damage of the masonry structures (walls and pillars) quantitatively and qualitatively and to identify the structural response of the most damaged wings of the palace (especially the South-East one).

The experimental campaigns included: (i) Sonic pulse velocity tests; (ii) Radar tests; (iii) Thermographic tests; (iv) Single and double flat jack tests; (v) Dynamic identification tests.

The ND tests were mainly aimed at understanding of the reasons for the high damage of the heavy pillars and of the transversal walls at the ground floor. Furthermore a permanent static and dynamic monitoring system has been installed in order to control the dynamic characteristics of the fortress. Figure 6 shows the plan of the investigated walls and pillars and the position of the tests at the first floor of the castle.



Figure 5: Provisional interventions carried out on SE and SW wings: connection of the internal and external façades by means of steel cables and steel frames against the façades.

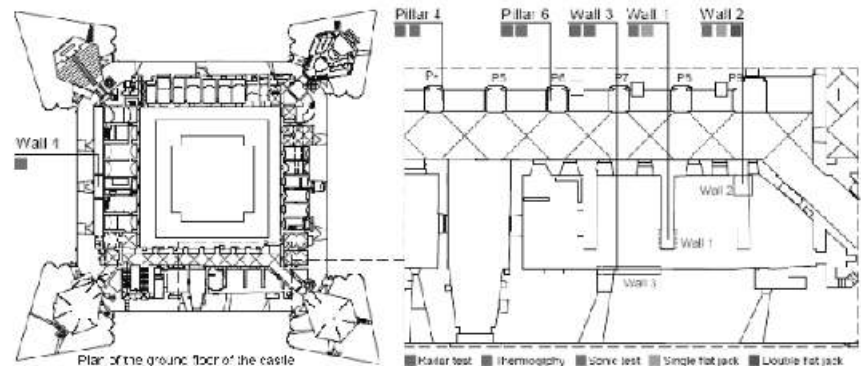


Figure 6: Plan of the Spanish fortress: position of the tests at the ground floor of the SE wing



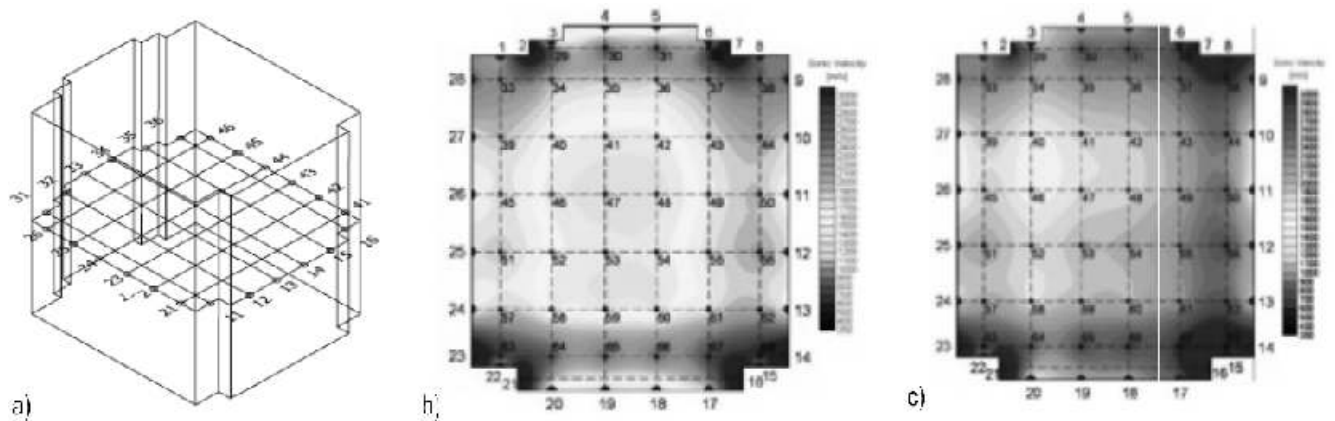


Figure 7: Grid of acquisition (a) and sonic tomographies of the damaged (b) and the undamaged (c) pillar

### 4.1. Sonic pulse velocity tests

The sonic tests belong to the category of non-destructive techniques and are properly applied in order to obtain information for the characterization and the qualitative description of masonry [Ref. 3].

On September 2009 the research groups of the University of Padova and the Politecnico of Milan carried out sonic tests in the Spanish fortress: three sonic tomographies were performed. This technique, especially useful for the diagnosis of isolated elements such as pillars, detects the variation of the density of the masonry. Two pillars (4 and 6), located on the inner side of the South-East wing and a vertical section of a thick masonry wall (wall 4) in the South-West area were tested (Figure 6).

It was decided to perform sonic tests both on a damaged and on an undamaged pillar, in order to attempt a quantitative comparison between the tests results. Tomography, which is based on a combination of sonic acquisitions over several directions in the same material section, can give the distribution of densities in the masonry section [Ref. 4]. For the application of a simple and rough "tomographic survey" it is necessary to acquire data on a regular grid of points (Figure 7a).

The obtained results allow detecting clearly that the crack on the damaged pillar affects the entire thickness of it. In fact for all the acquisitions that cross it

geometrically, there is a clear decrease of speed. Combining the acquisitions on the pillar's faces it is possible to define and analyze the mapping of speeds in the investigated section, whose value is indicated by different colors. The obtained average speeds vary from 900 m/s to 2000 m/s and can identify the areas of the section where the main crack is located (Figure 7b).

The sonic tests on the undamaged pillar was performed in the same manner as the previous one. The test results (with speeds of about 2000 m/s) demonstrate that masonry is in a good state of conservation. The outer parts of the pillar are made with materials of higher quality than the inner part. It is evident that average speeds, in the perimeter parts, are always much higher, with a variation ranging from 2000 m/s to 3300 m/s (Fig.20). A third more complex tomography involved the vertical section of a masonry wall in the South-West wing of the fortress (Wall 4). The aim was to collect qualitative data of masonry in this part of the castle that was heavily damaged by the earth-

quake. In this case a vertical grid of acquisition was determined on the section and six points with their counterparts on the other side of the masonry wall were fixed. The recorded speed values are roughly homogeneous through the section with an average value of 2223 m/s. (Figure 8)

### 4.2. Radar tests

On pillar N.6 radar tests were carried out using a high frequency antenna (1GHz) in reflection, in order to detect the morphology of the section and the details of the masonry leaves and of damaged areas. Pillar N.6 was chosen on purpose since information were previously given by sonic tests and simple tomography (see section above).

In Figure 9 some of the results through radargrams are reported. More in details the profiles 1,3,4,7 are represented. It is possible to state that all the profiles represent very clearly the thickness and dimension of the regular stones of the external leaf of the pillar (red lines in the figure). The first three profiles show the presence of internal

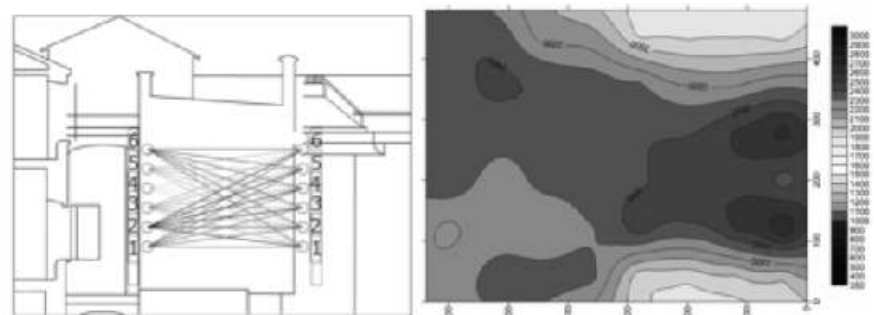


Figure 8: Grid of acquisition and tomography on the vertical section of the masonry wall



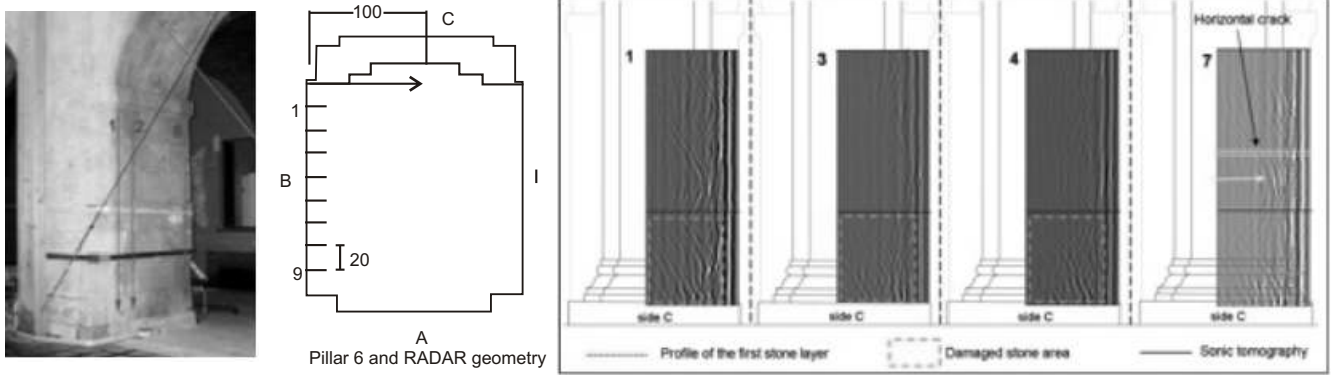


Figure 9: Radar test site (left) and some results on the pillar N.6

cracks and damages at the bottom of the pillar (up to 100 cm of height) caused by the out of plane action of the earthquake, whereas the fourth profile shows a lower damage at the bottom (up to 30cm). Furthermore the horizontal crack present in the pillar is very well shown by this profile and also the multiple vertical cracks in the stone at the bottom of the pillars (yellow arrow).

### 4.3. Thermographic tests

Thermographic tests were performed to achieve information about the masonry texture, which was hidden by a thick plaster layer.

The knowledge of the disposition of bricks or stones and of their shape is important to identify the most representative areas where to place local tests, such as single and double flat jack tests which can give information on the masonry properties. After heating for more than 1 hour the surface of the walls, active thermography revealed

the presence of a non-homogeneous masonry texture under the plaster of wall 1, wall 2 and wall 3. The peculiar presence of bricks and of large stones at the springs of the vault arches was also detected by active thermography on wall 2 (Figure 10).

The yellow and blue colored area at the basis of the vault was identified as a discontinuity in the stone masonry. Performing a contained removal of the plaster on that area, brick masonry was detected.

Underneath the spring of the vault large blocks of rather regularly cut stones were found forming a sort of built-in stronger column collecting the higher stresses coming from the vault spring.

### 4.4. Flat jack tests

Thanks to the results coming from active thermography tests, two areas of the walls having different character-

istic were identified. On these two areas other diagnostic tests were carried on: sonic tests to reach indications about the morphology of the masonry sections. Single flat jack tests on wall 1 were carried out to verify the state of stress and its distribution.

On both side of wall 1, single flat jack tests were performed to control the suspected presence of concentration and eccentricity in the distribution of stresses in the masonry structure. Tests were performed under the corbel of the vault and the resulting states of stress were different: the estimated stress on the east side of the wall is equal to  $2.47 \text{ N/mm}^2$ , while on the opposite side is equal to  $1.82 \text{ N/mm}^2$ .

The flat jack test revealed a rather high state of stress on both sides of the wall, with a maximum value under the vault corbel. These values will be also verified by the structural modeling in order to understand the reasons of such high

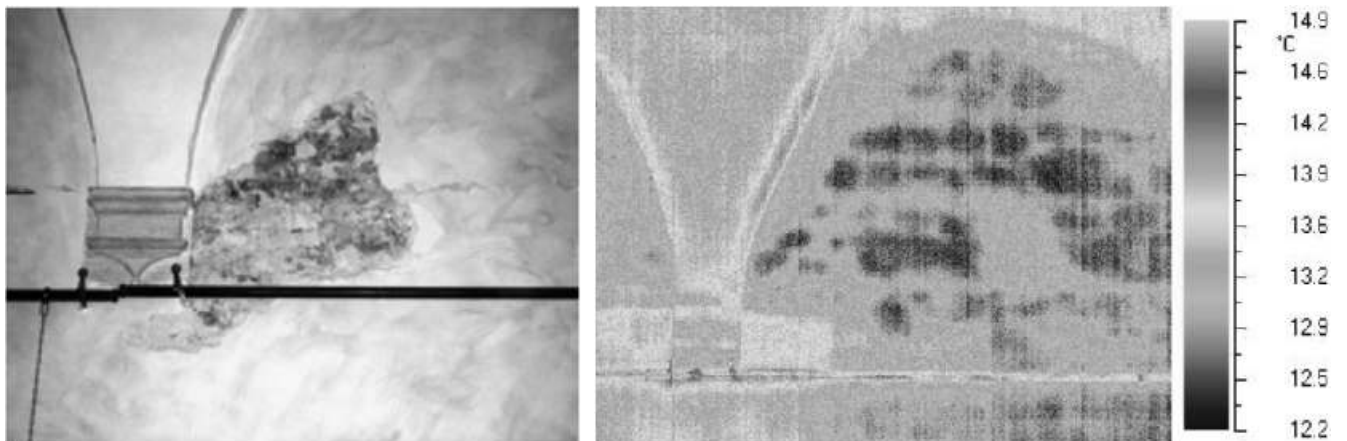


Figure 10: Active thermography on wall 2

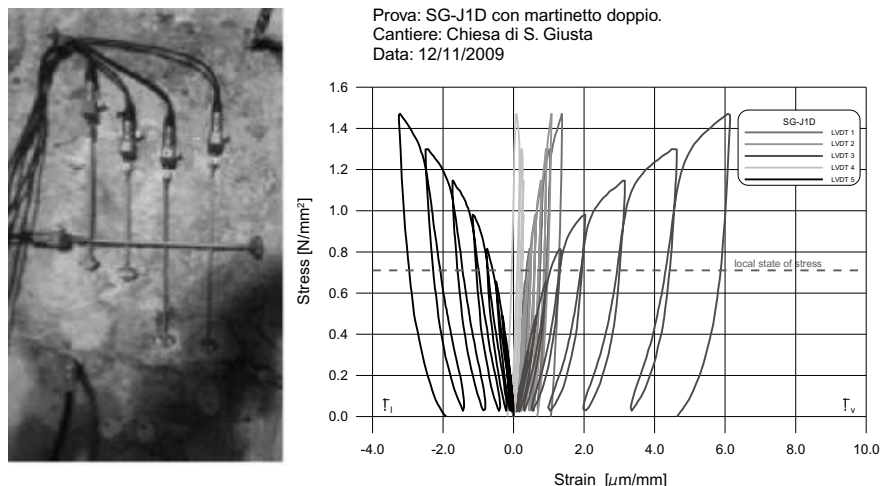


Fig. 11. Stress-Strain graph obtained from the double flat jack test on wall 2.

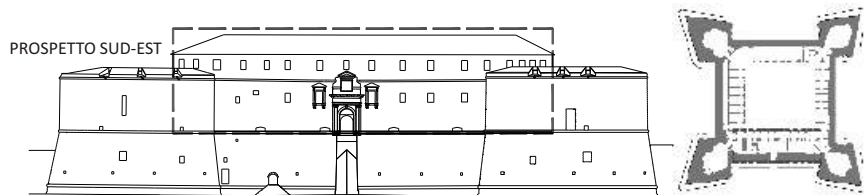


Figure 12: The South-East wing of the Spanish fortress where dynamic identification tests were performed

concentration of stresses, which can only be partially explained without calculation.

It was decided to carry out also a double flat jack test (Figure 11), to study the elastic characteristic of the masonry, that in this position presented one of the most regular textures of the entire wall. Nevertheless here the masonry seems to be rather weak; in fact the maximum value reached in compression was 1.47 N/mm<sup>2</sup> (and already under large deformations out of the elastic range). The average value of the elastic modulus was 1,654 N/mm<sup>2</sup>.

#### 4.5. Dynamic identification tests

Among the different methods of non-destructive tests (NDT) for the characterization of the historical masonry buildings, dynamic investigations have proven to be a particularly effective tool [Ref. 5].

Dynamic identification tests are aimed at determining the modal response of the structure; the results are directly related to the physical and structural parameters of the construction, such as the geometry (distribution of masses), the stiffness and the boundary conditions.

On September 8<sup>th</sup> and 9<sup>th</sup>, 2009 dynamic identification tests have been performed in the South-East wing of the Spanish fortress (Figure 12). The investigations consisted in the measurement of environmental vibrations (excitation source: wind, traffic, etc.) in several points of the structure. Tests were aimed at identifying the dynamic behavior of this part of the building (natural frequencies and mode shapes) at the present state - i.e. following the severe state of damage caused by the earthquake and subsequent emergency provisional interventions. In order to maximize the amplitude of the signals, the accelerometers - in the considered setups - were positioned on the upper floors of the building (first and second floor).

Five configuration setups were performed with 27 points of acquisition. For each setup no more than eight sensors were used, including two fixed reference sensors, arranged in two directions (X and Y) parallel to the ground and perpendicular to each other (channels 1 and 2 at the second floor) (Figure 13). The records concentrated mainly on the perimeter walls, as the aim was to investigate any dissimilar dynamic behavior of the two facades due to the heavy state of damage of the structure.

The identification of the modal parameters (natural frequencies and associated mode shapes) was obtained by means of identification techniques of the output signals (Operational modal analysis) [Ref. 6].

Data from different setup tests were



Figure 13: Accelerometers on walls and the acquisition system

Mode	Frequency (Hz)	Comment
FDD Mode 1	2.35	First out-of-plane bending mode
FDD Mode 2	4.18	Second out-of-plane bending mode
FDD Mode 3	5.20	Third out-of-plane bending mode
FDD Mode 4	8.82	Local mode

Table 1: Identified mode shapes and natural frequencies

together analyzed. The analysis of the results clearly identify the first out of-plane bending mode, corresponding to the frequency of 2.93 Hz, a bending mode of higher order and another bending mode with amplification in the center of the facade (Table 1). The identification of the global vibration mode of the structure indicates that the building, in spite of the high level of damage and the disconnection of the perimeter masonry walls, has still a unitary dynamic response, probably thanks to the provisional emergency system of steel cables. It was also identified a local mode, at the frequency of 8.72 Hz, which only involves the sensors placed on the masonry walls toward the courtyard. Most likely this value indicates a structural disconnection of this part from the rest of the building.

In order to better understand the results of the dynamic experimental identification campaign, it will be interesting to correlate in the future the outcomes of the dynamic tests with the results of an appropriate Finite Element Model.

### 5. Monitoring

Monitoring is being more and more taken into account in the study of C.H. structures, as a key activity in order to increase the knowledge on their structural behavior and to have a deeper insight on their conditions. This knowledge allows to carry out with more confidence a strengthening intervention if needed, but also to prevent the execution of intrusive repair works, if they are not justified by an experimentally demonstrated worsening of the conditions of the structure [Ref. 7].

In December 2009 a dynamic monitoring system was installed in the Fortress, following a first investigation campaign carried out in September, includ-

ing dynamic identification tests. The system complements a static monitoring system installed in the first months after the earthquake by the ISCR (Istituto Superiore per la Conservazione ed il Restauro – National Conservation and Restoration Institute) of Rome, devoted to the control of the crack pattern evolution and of the environmental parameters (Figure 14).

An acquisition unit connected to eight high sensitivity piezoelectric accelerometers composes the dynamic sys-

tem. The central unit, located at the second floor of the fortress, in the South-East wing, is provided with a Wi-Fi router for remote data transmission.

A couple of reference sensors is fixed at the base of the structure for the record of the ground acceleration both in operational conditions and during seismic events. The positioning of the acceleration sensors on the elevation of the S-East was decided as a result of the structural dynamic identification. According to the predominant motion direction, sensors were fixed orthogonally to the façade, following vertical and horizontal lines, on the internal and external façades, with an increased number of sensors at the second level (Figure 15).

Dynamic data are collected both at

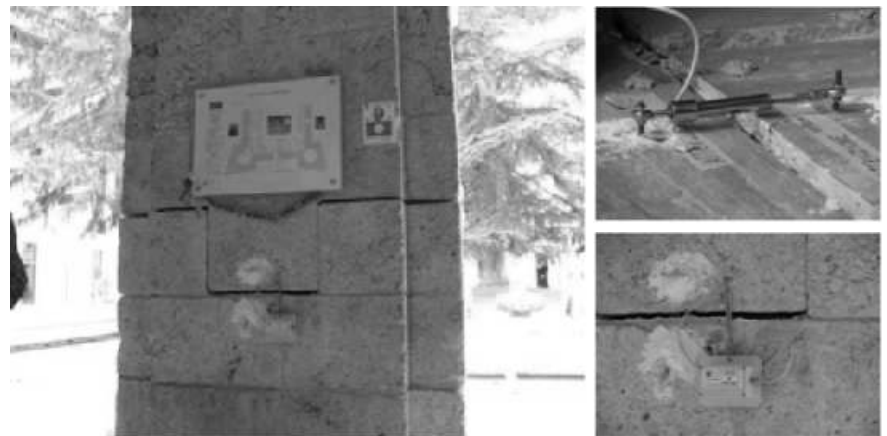


Figure 14 The static monitoring system installed by ISCR: displacement transducers on the cracks.



Figure 15: The Spanish fortress: left - localization of the acceleration transducers; right – base acceleration transducers (CH1, 2) and acquisition unit.



fixed time intervals ("long" acquisition, corresponding to 131'072 points, or to 21'51" of record at a sampling frequency of 100 SPS, each 1-24 hours) to allow successive dynamic identification of the structure with different environmental conditions, and on a trigger basis (shorter records, 3'35" at a sampling frequency of 100 SPS), when the signal, on one of the acceleration channels, gets over the predefined threshold (meaningful event, e.g. earthquake).

Results of the monitoring give then indication on the evolution of the dynamic response of the monument with varied environmental conditions.

From the observation of the initial results, it seems to exist a correlation between natural frequencies and environmental parameters, as frequencies tend to increase with the temperature. The prosecution of the monitoring activities will allow for a more precise evaluation.

### Conclusions

The authors presented here the case study of the Spanish Fortress, called "the Castle" in L'Aquila. This monument suffered rather heavy damages during the earthquake in 2009 and the following aftershocks, but thanks to the damage survey and the emergency provisional structures, is now under study for the future design for repair and conservation. The Palace template filled up for the building soon after the earthquake was a reliable tool for the first detection of the failure mecha-

nisms and of their causes and the design of the emergency provisional structures allowed to stop the progression of damage in the most vulnerable part of the building (SE and NW wings). As a consequence it was possible to design the preliminary on site investigation and the further control of the structure. An investigation methodology based on the geometrical, crack pattern survey and investigation by minor and non destructive testing, was applied to the most damaged wing of the Fortress. The data collected from sonic, thermographic radar and flat jack tests allowed to study the local damage situation on pillars and damaged masonry walls and to characterise the masonry quality.

Dynamic identification tests allowed defining the vibration modes of the SE wing as a global behaviour of the structure under the environmental conditions.

The investigation carried out allowed designing and installing a static and dynamic monitoring of the structure. The combined use of dynamic identification procedures and "local" controls (besides the monitoring of the environmental parameters), providing quantitative information on local conditions of structural elements (e.g. cracks opening), can be an important asset in the effort of attaining a deeper degree of awareness on the "real" structural functioning of the monuments.

### References

[1] Model B-DP PCM-DPC MiBAC 2006 –

Scheda per il rilievo del danno ai beni culturali – Palazzi. Source: [www.protezionecivile.it](http://www.protezionecivile.it)

- [2] Bellizzi M., Colozza R., Dolce M. (2001). Le opere provvisorie nell'emergenza sismica. Atti del X Convegno ANIDIS "L'ingegneria Sismica in Italia", Potenza-Matera 9-13 settembre 2001.
- [3] Binda L., Saisi A., Zanzi L. (2003) "Sonic tomography and flat jack tests as complementary investigation procedures for the stone pillars of the temple of S.Nicola' L'Arena (Italy)", *NDT&E International Journal*, 36, pp. 215-227.
- [4] da Porto F., Valluzzi M.R., Modena C. (2003). Use of sonic tomography for the diagnosis and the control of intervention in historic masonry buildings. *International Symposium Non-destructive testing in Civil Engineering NDT-CE*. 16-19 Sept. 2003. (pp. CD-ROM).
- [5] Modena C., Franchetti P., Zonta D., Menga R., Pizzigalli E., Ravasio F., Muti M., Meloni R. and Bordone G. (2001) Static and Dynamic Analyses of Maniace Castle in Siracusa-Sicily, Proc. 3rd Int. Seminar on Structural Analysis of Historical Constructions, Guimarães, Portugal
- [6] Brincker, R., Zhang, L., and Andersen P. (2000). Modal Identification from Ambient Responses using Frequency Domain Decomposition. Proc. 18th International Modal Analysis Conference, 7-10 February 2000, San Antonio, TX
- [7] Casarin F., Valluzzi M.R., da Porto F., Modena C. (2008), Structural monitoring for the evaluation of the dynamic response of historical monuments, RILEM Symposium on On Site Assessment of Concrete, Masonry and Timber Structures - SACoMaTiS 2008, eds. L. Binda, M. di Prisco, R. Felicetti, ISBN 978- 2-35158-061-5, pages 787 – 796, Publisher RILEM Publications SARL



## Japan finishes 'Sky Tree' - World's Tallest Communications Tower

Construction of the Tokyo Sky Tree, the world's tallest communications tower and second-highest building, finished recently, two months late because of the quake and tsunami that struck Japan last March. Construction of the tower, near the popular Asakusa traditional district on Tokyo's eastern side, began in July 2008.

The Tokyo Sky Tree tops the 600-metre Canton Tower in China's Guangzhou and the 553-metre CN Tower in downtown Toronto. It is the world's second-tallest manmade structure, beaten only by the 828-metre Burj Khalifa in Dubai. Some 580,000 workers were engaged in the construction, which cost 65 billion yen (\$806 million) for the tower alone.

The Tokyo Sky Tree is expected to overshadow landmarks in the capital's upscale western parts, including the 333-metre Tokyo Tower, which was built in 1958 and became a byword in Japan for the country's rapid post-war growth. It hosts two observation decks -- at 350 metres and 450 metres above ground -- as well as restaurants and office space and sits at a former freight shunting yard along the Sumida river.



## Shanghai to Put More Limits on Skyscraper Foundation Pits

SHANGHAI will restrict the construction of large foundation pits for new building projects in an effort to reduce land subsidence hazards, city construction officials said recently. Projects that involve building deep and large foundation pits inside the Outer Ring Road will be closely restudied by the watchdogs for their potential influence on the underground environment, while new approvals will be restricted.

The decision came after a 10-meter-long road crack emerged in the Lujiazui area, the city's financial zone, earlier this month. The incident made headlines and stirred concerns among local residents, prompting talk about whether high-rise construction fever should be cooled. Not surprisingly, officials later concluded that the crack was the "result of the foundation ditch construction" of the Shanghai Tower project, which will be China's highest skyscraper, at 632 meters, upon completion by 2014.

Subsidence takes place when groundwater is pumped out, which happens for pit construction for the foundations



of high-rises. The higher the building, the deeper and larger the foundation pit must be dug. Many locals have called for a slowdown in the construction of high-rises and more efforts to control land slippage in downtown areas, especially in Lujiazui, famous for its skyscrapers.

## New online calculator estimates carbon benefits of wood buildings

WoodWorks, a cooperative venture of major North American wood associations, recently launched an online tool that estimates the carbon benefits of wood buildings. Released as a complement to the online cost calculator estimates the amount of carbon stored in a building's wood products (which was absorbed by the trees while growing) and the greenhouse gas emissions avoided by not using steel or concrete. The calculator is available at [www.woodworks.org](http://www.woodworks.org).

The new WoodWorks tool allows users to calculate the carbon benefits of wood buildings in one of two ways:

If wood product information is known (such as the volume of lumber, panels, engineered wood products, decking, siding and roofing), the carbon calculator will provide a detailed estimate related to that specific building. The more detailed the information, the better the results.

If product information is unknown, users can select from a list of common building types and receive an estimate based on typical wood use.

In addition to the carbon calculator, WoodWorks recently released a cost calculator that estimates the savings of using wood building materials.

## Kingdom Tower Project in Jeddah Gets Final Go-ahead



A Jeddah-based project to build the tallest tower in the world has been given the go-ahead after it received its final license, Chairman of Kingdom Holding Company (KHC) Prince Alwaleed bin Talal confirmed. The SR4.6 billion Kingdom Tower, which will stand over 1,000 meters tall, is the centerpiece and the first construction phase of Kingdom City, Jeddah Economic Company's (JEC) new urban development covering more than 5.3 million square meters of land in the north of Jeddah overlooking the Red Sea and Obhur Creek. Work on the project began on Jan. 1.

The vision of constructing the tallest tower in the world in Jeddah belongs to Prince Alwaleed bin Talal, who was closely involved in the selection of the scheme currently under design. The tower's height is remarkable, obviously, but the building's iconic status will not depend solely on that. Its form is brilliantly sculpted, making it quite simply the most beautiful building in the world of any height.

## Pakistan's Tallest Building to be Built in Karachi



Ocean Towers, formerly known as Sofitel Towers, is 393 feet high and will house a shopping mall, food courts, corporate offices and a business club. The 28-floor skyscraper has bypassed the 381-foot tall MCB Tower on Il Chundrigar road as the tallest building in the country. The towers were initially supposed to house the Sofitel chain of hotels, but they withdrew because of the violence in Karachi. The managing partner of the project, Abdul Rehman Naqi, said that a popular supermarket chain in the city would be the first store in the towers and would open its doors to the public, hopefully by May 25, 2012

## London to Host World's First Rotating Tower

Looking to grab the global spotlight ahead of the 2012 Summer Olympic Games, London is putting a spin on modern architecture with the world's first rotating tower. The 80-story skyscraper will boast independently-rotating floors that can be orchestrated to give the building a fluid, changing look architect David Fisher hopes will usher in a new era of architectural design.

Dynamic Architecture, the firm behind the unique design, was initially planning for the first project to take place in Dubai, but because of financial concerns and other factors the team decided to focus instead on the London project.

While the status of the Dubai project



remains ambiguous, the firm is optimistic that work will begin when the regional economy has recovered. Construction of the London tower should begin sometime this year,

according to a representative of the architecture group, as the firm hopes the project will 'serve as a landmark' during the media frenzy of the Olympic Games this summer.

## Final touches being given to London's amazing 1,000ft glass skyscraper

Perched precariously on narrow steel bars 1,000ft above the ground, their high-visibility jackets mere pinpricks of colour against the grey London sky, construction workers are putting the final touches to Europe's tallest building.

After three years of work and 12 years after the project was conceived the last few floors of The Shard are taking shape. Workers are now constructing a spire of steel and glass, which will sit atop 72 floors of offices, hotel rooms and viewing galleries. It will bring The Shard's final height to 1,017ft some 230ft higher than the tallest building at Canary Wharf.

The final pieces of this 3D jigsaw are being hoisted into place by Britain's highest crane, attached to the outside of the building's 55th floor. After the 500 tons of steel skeleton needed for this section, the crane is now bringing up the glass 'skin', designed to reflect sunlight so that the tower will change its appearance with the seasons and time of day.

More than 14 acres of triple-glazed panels will eventually cover the building. They are fitted from the



inside, but construction still requires the most fearless of the 1,600 workers to attach themselves to girders with safety harnesses. They also have to brave the elements as they work round the clock on the site: temperatures here are several degrees lower than on the streets below and high winds sometimes make it unsafe to work.

But the courageous are rewarded with

views of the capital that will be unique until the 72nd-floor observation deck opens in February 2013. The £400 million structure by London Bridge is due to be finished this June, a month before the Olympics. Billed as a 'vertical city', it will comprise offices up to floor 28, then three floors of restaurants; a five-star 19-storey hotel of 200 rooms; ten apartments over 12 floors each seven times larger than a semi-detached house and likely to fetch tens of millions of pounds each; and, finally, the observatory and spire.

Designed by Italian Renzo Piano to resemble an iceberg emerging from the Thames, The Shard has not been without controversy. English Heritage has expressed fears about the 'major and detrimental' impact on views of St Paul's Cathedral, the Tower of London and the Palace of Westminster.

The workers building The Shard come from all over the world, although two-thirds are British. A fifth are from other EU nations, while Brazil, Albania and Australia are also well represented.



## North Korean Skyscraper to Open, Only Two Decades Late

North Korea has been toiling over its most luxurious hotel since 1988 and 23 years later, the project is nearly finished. The 105-story Ryugyong Hotel is set to partially open for business this spring.

The original goal of the Ryugyong Hotel was to outdo South Korea. As Seoul prepared to host the 1988 Summer Olympics, the capital city revamped its skyline with construction of new high rises, boasting a 63-story; gold-embellished building that reigned as the highest in Asia. With the financial support of the Soviet Union, North Korea aimed at erecting the Ryugyong, a hotel meant to be almost 200 feet higher than Seoul's newest addition. But the Soviet Union collapsed, leaving North Korea short of funds and raw materials.



## Environment Group Moves to Block UK Skyscraper Plans



An environmental campaign group has added its voice to calls for plans to be dropped for an 18-storey skyscraper in the heart of Dalston. Open Dalston is objecting to proposals from Rothas Ltd to build flats next to Dalston Kingsland Station in Kingsland High Street.

The project involves bulldozing the Peacocks store and building two blocks, one rising more than 50 metres. Neighbours fear the scheme, opposite Ridley Road Market, would plunge their homes into darkness. Campaigners have sent their objection to Hackney Council and to the Greater London Authority calling for the plans to be rejected.

The development has 130 flats with two separate entrances for “private” and “affordable” homes. One seven-storey block facing

High Street has 17 lower cost affordable flats, and the 18-storey block behind would have 113 luxury apartments. In a letter to the GLA, Open Dalston said: “The proposal amounts to overdevelopment which, whilst it extracts huge development value from the site, it does so to the detriment of the surrounding area.”

A spokesman for Rothas Ltd said: “We are committed to bringing forward a scheme which celebrates the unique character of Dalston, drawing particular inspiration from local initiatives such as the Eastern Curve Garden and local charity Bootstraps. “Sustainability is central to our design. The proposals will include extensive green terraces, inspired by the work being undertaken locally and also the rooftop farms started by local communities in Brooklyn, New York.”

## Ultra-high-speed Elevator for Skyscraper

Mitsubishi Electric Corp announced the overview of its ultra-high-speed elevator developed for the 632-meter Shanghai Tower under construction in Shanghai, China.

For the traction motor of the elevator, Mitsubishi Electric employed a parallel drive system that uses two three-phase winding coils for each motor and controls the two three-phases with two control panels. By using two compact control panels, the company enabled to design the layout of a machinery room more freely while increasing output power. The operation of the elevator is scheduled to begin in 2014.

To realize the world's fastest speed of 1,080m per minute, Mitsubishi Electric used new technologies for higher safety, lifting height and comfort as well as for the motor for the winch. Specifically, to enhance safety, the company employed a two-tiered brake (the company's former product has a one-tiered brake) for emergency stop and used fine ceramic with a heat resistance of up to about 1,000°C for the brake shoe.





The buffer (shock absorber) at the bottom of the elevator shaft is comprised of three tiers (the former product has a one-tiered butter) and has a stroke of 7.3 meters, which is about 30% shorter than the stroke of the former product's buffer.

For the "sflex-rope," a rope for the winch, Mitsubishi Electric employed a new structure so that it can hold a greater weight of a longer rope. The company improved the density of the rope by using a concentric-layered steel wire and filled the gap between the layers with plastic.

As a result, the company increased breaking load by 85% while increasing mass per unit length only by 18%. The new rope is less extensible. So, when people get in the elevator, it does not shake vertically much. This time, Mitsubishi Electric newly developed a control cable that is 20% lighter than the one used for the former product.

For the comfort, the new elevator is equipped with the "active roller guide," which detects vibration and applies anti-phase vibration to it so that the vibration of the car is reduced. While two units of the active roller guide are installed in the bottom of the former product, Mitsubishi Electric added two more to the upper side of the new elevator because a different type of vibration is applied to the new product when it is moving at an ultra-high speed. As a result, vibration was reduced to about 1/3 that of the former product.

Furthermore, the new elevator is equipped with a streamlined aerodynamic car cover that reduces air resistance as well as an air pressure control device consisting of an air blower, a duct and a box for switching between air intake and emission. As a result, rapid changes in atmospheric pressure can be prevented, reducing passengers' feeling of fullness in the ear.

## Last Aerial Dish from London's Iconic BT Tower is Removed

For nearly half a century it has been a landmark on the London skyline. But there was something not quite right of late about the building most of us still know as the Post Office Tower.

Gradually, the mushroom-shaped dishes that stuck out like blisters on its already skinny waistline have been removed. And although the 620ft tower has been the focus of architectural division since before its foundations were laid in 1961, a new, slim version has reappeared. Gone are the 31 huge dishes that once used microwave signals to beam TV programmes to a grateful nation.

They have long been superseded by advances in fibre optic technology. It means that for the first time in five decades, the tower looks the same as it did in the early 1960s, before the miracle of microwave communication was complete. The building has sparked much debate since it opened in October 1965, the same month the Beatles collected their MBEs. Some described it as a monstrosity, not least because of its cluster of protrusions.

Since early this year, however, four engineers have been cutting off the carbuncles, dangling 500ft up to detach all 31 of the long defunct dishes. Once free of their rusting bolts, each 12ft wide dish was lowered by an in-house crane to the 28th floor of the 36 storey building, cut into sections and sent down to street level.

Here's a problem though. The crane is stationed on the 31st floor and can't reach the ground. So how did they do it? Simple. Someone put the bits into one of the tower's passenger lifts and pressed the button marked 'G'.

'This was a mammoth job on a scale that BT has never seen before,' said head engineer Mark West. 'These are huge dishes floating above people's heads in a busy area. It took a long time because we have to be so careful now with health and safety.'

The GPO (General Post Office) Tower overtook St Paul's Cathedral during 1962 as the tallest building in London. That title was briefly snatched away by the newly constructed Millbank Tower, which took less time to build but regained by the GPO Tower when completed, and held until the emergence of the Nat West Tower in 1980.

Since then, the likes of Canary Wharf and the soon-to-be-completed Shard have stolen its towering glory. Perhaps surprisingly, few seemed to notice the tower's slimming-down process over the last few months. And the future? 'It will remain a fully functioning, 24/7 building,' said a BT spokesman. 'Ninety per cent of what we see on TV, including Premiership football, comes through the BT Tower.'



Sixties icon: The tower takes shape in 1964



Bristling: The famous dishes in 2009



Slimmed down: The thinner tower in 2011

## Vancouver Architect Plans Wood Skyscraper



A Vancouver architect is the latest designer to promote the use of wood in the construction of tall buildings. Michael Green's design calls for a 30-story tower, based on laminated composite wood. Mass timber products using layers of wood fused together at right angles are strong enough to handle load-bearing infrastructure, walls and floors. "We think we can go higher than 30 stories," Mr. Green told the CNN. "We stopped exploring wood around 100 years ago (with the advent of steel and concrete); now we're looking at a whole new system using mass timber products." Cutting down trees doesn't sound like the most environmentally sensitive approach, the reporter notes. But Mr. Green argued that using wood from sustainable forests and the carbon dioxide savings make wood an eco-choice.

There seems to be something of a pro-wood advocacy movement in the tall building community these days. Last week the Canadian Wood Council released a detailed study suggesting a wood-based structural system "represents the first significant challenge to concrete and steel structures since their inception in tall building design more than a century ago."

Courtesy: CNN

## Major Changes for Wilshire Grand Project: Two-tower Effort now Envisioned as One

Korean Air is considering major changes to its USD1 billion plan to replace the aged Wilshire Grand Hotel.

Instead of building a 45-story tower with 560 hotel rooms and a second-phase, 60-story office complex, the company is looking at erecting a single tower with 900 hotel rooms and a diminished office component. The pending changes come as Korean Air has parted ways with office giant Thomas Properties Group, which handled the project's entitlements and was widely expected to serve as the project developer, according to coverage in the Los Angeles Downtown News.

While specifications for the single tower are still under study, it would be closer in height to the approved phase two office building, architect Chris Martin told the paper. That structure was most recently imagined as a 60-story tower, but the entitlements would allow for a building of 1,250 feet in height, or 75-80 stories, he said.

If Korean Air built the tower as tall as its approvals allow, it would surpass U.S. Bank Tower as the tallest building west of the Mississippi River.



## Malmo's Turning Torso Landmark Put up for Sale

Swedish housing cooperative HSB has announced that it plans to sell the Turning Torso skyscraper in Malmo, one of the city's most prominent landmarks and a symbol of its recent regeneration process. HSB Malmo has no plans to move from its head office in the landmark tower and plans to maintain its base there, the company said in a statement.

"Through the sale, HSB Malmo gains the resources to invest in 1,000 rental apartments which will either be built or acquired in the next few years," HSB's board announced in a statement recently. The 190-meter-tall Turning Torso is the tallest building in Scandinavia and was designed by the Spanish architect Santiago Calatrava. It was completed in 2005.

The property was valued in 2008 at around 2 billion kronor (USD300



million), HSB announced in 2004 that it was considering an offer to sell the property, but decided to retain ownership.

**2012**

**Global Thinking in Structural Engineering: Recent Achievements**

7 - 9 May, Sharm El-Sheikh, Egypt - IABSE Conference  
www.iabse.org

**IASS Annual Symposium IASS-APCS 2012:**

21 - 24 May, Seoul, Korea  
The IASS-APCS 2012 symposium will be held in Seoul, Korea and the submission of papers will be soon open at <http://www.iass2012.org>.

**SSCS 2012: International Conference on Numerical Modeling Strategies for Sustainable Concrete Structures**

29 May - 1 June, Aix-en-Provence, France  
www.sscs2012.com

**fib Symposium: Concrete Structures for a Sustainable Community**

11 - 14 June, Royal Institute of Technology (KTH), Stockholm, Sweden  
www.fibstockholm2012.se

**Bond in Concrete: Bond, Anchorage, Detailing**

17 - 20 June, University of Brescia, Brescia, Italy  
www.bondinconcrete2012.org

**9th fib International PhD Symposium in Civil Engineering**

22 - 25 July, KIT Karlsruhe, Germany Karlsruhe, Germany  
<http://fib-phd.imb.kit.edu/>

**Innovative and Sustainable Infrastructures - Toward Human Urbanism**

19 - 21 September, Seoul, Korea - 18th IABSE Congress (Annual Meetings precede Congress)  
www.iabse.org

**8th RILEM International Symposium on Fibre Reinforced Concrete: Challenges and Opportunities**

19 - 21 September, University of Minho Guimaraes, Portugal  
www.befib2012.civil.uminho.pt

**ASCE 6th Congress on Forensic Engineering**

31 October - 3 November, San Francisco, USA (Co-sponsored by IABSE)  
www.asce.org/event

**International Conference on Sustainable Development of Critical Infrastructure**

15 November, Shanghai, China - IC-SDCI (Co-sponsored by IABSE)  
www.wfeo.net

**2013**

**ISFGE 2013 Fourth International Seminar on Forensic Geotechnical Engineering**

10 - 12 January, 2013, Bengaluru, India.  
Email: [isfge2013@gmail.com](mailto:isfge2013@gmail.com)

**Int. Conf. on Advances in SPIN 2013 Johannesburg, S. Africa Cement and Concrete Technology in Africa (ACCTA 2013)**

28 - 30 January  
www.spin.bam.de/en

**UKIERI Concrete Congress Innovations in Concrete Construction**

5 - 8 March, Dr B R Ambedkar National Institute of Technology, P.O. REC, Jalandhar - 144 011 (Punjab) India  
Email: [spsingh@nitj.ac.in](mailto:spsingh@nitj.ac.in), [uccnitj@gmail.com](mailto:uccnitj@gmail.com)  
www.ukiericoncretecongress.com

**fib Symposium: Engineering a Concrete Future: Technology, Modeling and Construction**

20 - 24 April, Group Israel, Tel-Aviv, Israel  
www.fib2013tel-aviv.co.il

**IABSE Conference Assessment, Upgrading and Refurbishment of Infrastructures**

6 - 8 May, Rotterdam, The Netherlands IABSE  
www.iabse.org

**1st International Conference on Concrete Sustainability**

27 - 29 May, JCI Tokyo, Japan  
www.jci-iccs13.jp

**ICSA 2013 2nd International Conference on Structures and Architecture 2013**

24 - 26 July, Convention Centre, Campus of Azurém, University of Minho Guimarães, Portugal  
www.icsa2013.com

**2013 IASS The 2013 IASS Annual Symposium with the theme "Beyond the Limit of Man"**

23 - 27 September, Wroclaw, Poland  
www.iass-structures.org

**26th IABSE Symposium: Long Span Bridge and Roof Structures - Development, Design and Implementation**

24 - 27 September, Kolkata, India (Annual Meetings precede Symposium)  
www.iabse.org

**2nd International Symposium on UHPFRC**

2 - 4 October, AFGC Marseille, France  
www.afgc.asso.fr

**SEWC 2013 Symposium International Symposium on Innovative Architecture-Structure interaction towards Sustainable Development with Green environment**

25-27 November, OCF Plot No.2, Pocket 9, Sector-B Vasant Kunj, New Delhi-110070.

Contact Point: IFP Qatar Ltd.  
Tel.: +90 11 26194486  
Fax: +91 11 46023053  
Email: [scmehrotra@mehroconsultants.com](mailto:scmehrotra@mehroconsultants.com)

**2014**

**4th International fib Congress fib group India**

10-14 February, Mumbai, India and Exhibition



ANNOUNCEMENT

# SEWC 2013 SYMPOSIUM

International Symposium on Innovative Architecture-Structure interaction  
towards Sustainable Development with Green environment

25-27 November, 2013, New Delhi

Address for Communication

OCF Plot No.2, Pocket 9, Sector-B Vasant Kunj, Tel.: +90 11 26194486

Contact Point: IFP Qatar Ltd.

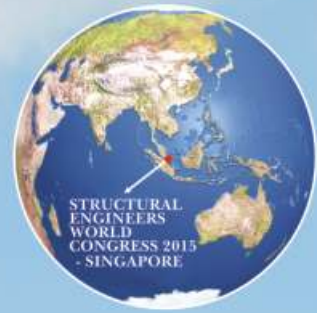
Fax: +91 11 46023053 Email: scmehrotra@mehroconsultants.com

## GLIMPSES FROM THE PAST: SEWC COLLOQUIUM 2010, BENGALURU



<http://www.sewc-worldwide.org>





# SEWC 2015 Singapore

The City of Iconic Structures Beckons Structural Engineers

The 5th Structural Engineers World Congress (SEWC), which is dedicated to the art, science, and practice of structural engineering, is slated to be held in Singapore in 2015. The event holds special significance as it marks an occasion where the conference is being held in a city, which is renowned for its prowess in structural engineering and its iconic buildings. The event would be conducted by the Association of Consulting Engineers, Singapore (ACES) and the Prestressed and Precast Concrete Society of Singapore (PPCS).

The World Congress held every four years, aims to cover major aspects pertaining to technical, and professional practice issues. The congress focuses on the needs and the contemporary issues of the structural engineering profession worldwide and highlights the profession's interface with the society. It also re-iterates the impact of the structural engineering profession on the society reflected by excellent public image, standing, and credibility of structural engineers. SEWC 2015 presents excellent opportunities for structural engineering professionals to interact with each other and to learn more about what is happening in the World of Structural Engineering.

## Jointly Organized by



ACES



Prestressed and  
Precast Society

## Supported By



BCA



SECB



# THE ENGINEER'S CHOICE ...AND HERE'S WHY.

## ABOUT ULTRATECH CEMENT

- India's largest exporter of cement and clinker
- Aditya Birla Group, of which UltraTech cement is a part, has 11 integrated plants 11 split grinding units and 5 bulk terminals, including 1 in Sri Lanka
- Annual capacity: 48.8 Mn Tn

## TYPES OF CEMENT MANUFACTURED

- Ordinary Portland cement – OPC43, OPC53
- Portland Pozzolana Cement
- Portland slag Cement

## VALUE ADDED SERVICES

- Mobile Concrete Lab Services
- Mason/Site Supervisor Training Programs
- Field visits by Qualified Civil Engineers
- Educating Home Builders on good construction practices
- Non-destructive testing of concrete

## ADVANTAGES

- Multiple Techno-economic benefits
- Quicker form removal and handling
- Comfortable working time and reduced risks
- Good cohesion, workability and reduced bleeding
- Enhanced durability even in aggressive environment and severe climatic conditions, coastal regions and industrial areas
- Quicker construction
- Low heat of hydration that prevent thermal cracks
- High credibility and safety



Toll Free No. - 1800 425 2525



# Don't let leakages leave you high & dry.

- Cement-based, high adhesive strength
- Single solution for all types of leakages
- Withstanding capacity of 7 bar pressure
- Better compatibility with cementitious surface



UltraTech Cement Ltd. (Building Products Division)

Ground Floor, 'B' Wing, Ahura Center, Mahakali Caves Road, MIDC, Andheri - East, Mumbai - 400 093.

Email: [ultratech.npd@adityabirla.com](mailto:ultratech.npd@adityabirla.com) | [www.ultratechbuildingproducts.com](http://www.ultratechbuildingproducts.com) | For enquiries, call: 9702074444 / 8652201009



International  
**JOURNAL of  
SEWC**  
— Structural Engineers World Congress —